1970

An Oblique Rotator Model For The Magnetic And Spectrum Variable Hd 173650

John Buchanan Rice

AN OBLIQUE ROTATOR MODEL FOR THE MAGNETIC AND SPECTRUM VARIABLE HD 173650

by

John Buchanan Rice

Department of Astronomy

Submitted in partial fulfillment of the requirements for the degree of Doctor of Philosophy

Faculty of Graduate Studies

The University of Western Ontario

London Canada

July 1969

ABSTRACT

The star HD173650 is shown to be a typical magnetic and spectrum variable with light, radial velocity and line strength variations of period $9^{d}.9748$. Line identification and curve of growth studies are completed from 14 spectrograms at various phases of the star's cycle. An oblique rotator model is formed for the star, a model which is consistent with the line profiles and which accurately reproduces the spectrum and magnetic variations. It is proposed that the construction of this model for a typical spectrum variable provides support for the adequacy of the oblique rotator hypothesis to explain the spectrum variables in general.

ACKNOWLEDGMENT

I would like to express my thanks to my supervisor, Dr. W. H. Wehlau and to my advisory committee Dr. D. F. Gray and Mr. J. Moorhead for their advice and assistance in the preparation of the thesis. I wish also to thank Dr. K. O. Wright of the Dominion Astrophysical Observatory for his advice and for generously allowing me observing time at the 48 inch telescope.

To my wife, Barbara, for her encouragement, assistance and for typing the first drafts of the thesis and to Mrs. Hilda Shaw for typing the final draft, I express very grateful thanks for these efforts.

TABLE OF CONTENTS

LIST OF TABLES

LIST OF FIGURES

CHAPTER I

THE SPECTRUM VARIABLE A_p STARS

Introduction

In recent years considerable effort has been devoted to the study of peculiar A stars in general and to the spectrum variables in particular. At present, opinion would appear to favour a binary origin for the peculiar A stars and an oblique rotator model to explain the spectral, light and magnetic variations commonly observed in these stars. The purpose of this thesis is to test the adequacy of the oblique rotator model to reproduce the observed properties of an A_p star by examining a representative spectrum variable in some detail. The resultant model will yield a description of the characteristics of the surface of the star which must be explained by any proposed theory of peculiar A stars. The star chosen for this analysis is the magnetic variable HD173650 whose spectrum, light and radial velocity variations have been observed in order to obtain the distribution of light and line strengths over the surface of the star that would be required by the oblique rotator model.

The first section of the thesis will be a review of the phenomena commonly observed in the spectrum variable A_p stars and of the oblique rotator model.

Observations

a) Equivalent Width Variations

The peculiar A stars as a group exhibit abnormal line strengths, particularly the lines of Cr, Mn, Sr and the rare earths. These abnormally strong lines are the ones that usually vary in the spectrum variables, a class that constitutes a quarter of all peculiar A stars. Maximum line strength is frequently twice the minimum value but much larger variations are often observed. Typically, all of the lines vary in phase or antiphase with the light and magnetic variations. Otherwise the lines can be divided into two groups; one is the metals such as Cr and Ti and the other is the rare earths and these two groups vary in anti-phase with one another, one group being in phase with the magnetic variations. There is as yet no rule to govern which lines vary in phase with the magnetic or light variations and which do not. It should be noted that the lines of two different ionization levels such as CrI and CrII vary in phase with each other.

b) Line Width vs. Period Relationship

One of the most significant observations is the period-line width relation. The relation is in the sense that the shorter the period the greater the line width. Using Babcock's (1958) parameter, w, to express the line width, where w is an estimate from the Zeeman spectrograms of the half width of weaker lines, the extrema of the variation are from HD124224 with a period of $0.^{d}5$ and a w of 4.0

to HD188041 with a probable period of 26^d and a w of 0.11. A listing of stars demonstrating this correlation is given by Deutsch (1958).

c) Light and Colour Variations

It would appear that all of the spectrum variables exhibit light and colour variations, normally of the order of only a few hundredths of a magnitude (Abt and Golson 1962). The period of the light variation is the same as the magnetic and spectrum variations when these can be well determined, and the U, B and V curves are normally in phase with one another. The star 53 Cam is a pathological case since, according to Preston (1968), the U and V curves are in antiphase and the B variation is weak.

d) Magnetic Field Variations

The spectrum variables all exhibit strong magnetic fields as measured with a Zeeman analyser designed to measure the line of sight component of the magnetic field. In all cases where the spectrum exhibits variations the magnetic field also varies, in many cases switching polarity. Wherever a period is determined for the magnetic variations, it is in agreement with the spectrum and photoelectric period. In those cases where a magnetic variation is classified as irregular, the suspicion is that the irregularity is due to insufficient data and not to a true irregularity. The principal observational work on the magnetic field has been done by Babcock, and his catalogue (Babcock 1958) is the principal reference for magnetic stars.

Babcock noted that in some stars, at a time when the longitudinal magnetic field was observed to be nearly zero, a given line appeared to be wider when viewed in circularly polarized light of one sense than when viewed in the circularly polarized light of the opposite sense. This effect is known as the crossover effect. An explanation of the effect was presented by Babcock and, in its simplest form, is as follows.

Suppose two distinct regions on the stellar surface contribute to the line showing the effect and that these regions have local fields, which we will assume for simplicity to be longitudinal, giving Zeeman displacements H_1 and H_2. Suppose further that there is a velocity difference between these regions causing a Doppler displacement of ΔV between the zero field positions of the line contributions from these two regions. Let us also assume for the simplest case that each of the σ components is a single line.

The separation between the dextrogyrate lines (which in the case of the stellar spectrum is the width of the resultant dextrogyrate line) is

$$\Delta \lambda_R = \Delta V - \tfrac{1}{2} H_2 + \tfrac{1}{2} H_1$$

For the levogyrate case,

$$\Delta \lambda_L = \Delta V - \tfrac{1}{2} H_1 + \tfrac{1}{2} H_2$$

so that the difference in the widths of the lines in the spectrum is

$$\Delta W = \Delta\lambda_L - \Delta\lambda_R = H_2 - H_1$$

The case for H_1 a negative field is shown in figure I,1.

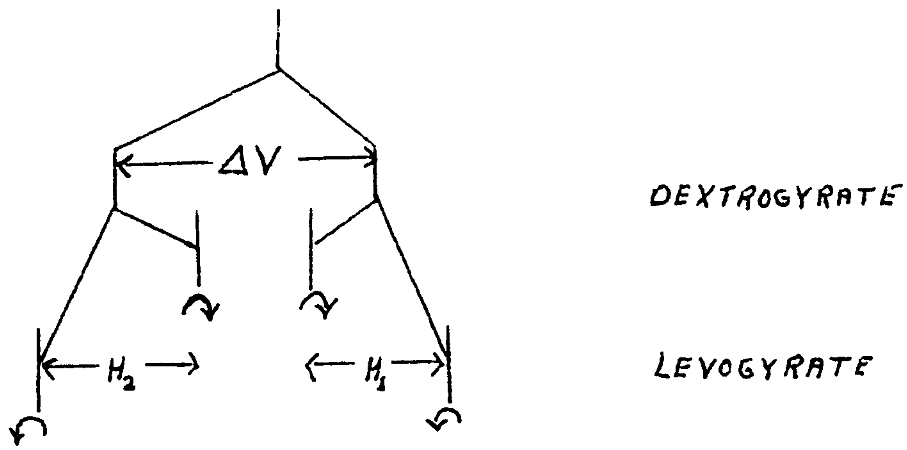

Figure I,1 - H_1 is a negative field and H_2 is positive

e) Radial Velocity Observations

Those lines in the spectrum variables which show a strong variation in strength also frequently display radial velocity variability. Again, the period of the variation is the same as the light and spectral period with maximum velocity following maximum line strength by 0.25 in phase. In some cases the radial velocity curve is complicated such as in 56 Ari where there is a double peak to the variation.

f) Binary and Rotational Velocity Observations

When the first attempts were made to measure the Zeeman splitting of stellar lines it seemed natural to look for magnetic fields where physically one would expect to find the greatest fields, in the more rapidly rotating stars, the

A stars. Since only sharp line stars could be measured for magnetic fields and since spectral peculiarities are most easily spotted in sharp line stars, researchers were inclined to wonder whether the magnetic and spectral observations were characteristic of a much larger percentage of the A stars and that the identified group of A_p stars were only those whose rotational axis tended to be in the line of sight. Slettebak (1954) in a survey of rotational velocities accomplished by measuring the line widths on spectral plates with a visual comparator, confirmed the bias in line widths associated with the A_p and Am stars. He found the results of table I,1.

Table I,1

Class	$V_e \sin i$
B8 - A2V	139 km/sec
A_p	41 km/sec
Am	40 km/sec

As for the occurance of binaries in the A_p stars, it appears, according to the Jascheks (1958), that the occurance of spectroscopic binaries is about 16% whereas in normal stars it is about 43% for those with $\langle V_e \sin i \rangle < 75$ km/sec. The frequency of visual binaries seems to be about 25% in both cases. For the Am stars, according to Abt (1967), the observations indicate that spectroscopic binaries comprise the whole class.

While the evidence in the form of the frequency of spectroscopic binaries in the A_p stars seems to favour the "pole on" hypothesis, Abt points out that the orbital elements of many of the spectroscopic binary A_p stars do not point to this conclusion.

It should be noted that for the one spectrum variable that is a member of a close binary system, the orbital period is the same as the period of spectral, light, and magnetic variation. This striking case is the very close system HD98088 where the separation of the two components is only ten stellar radii. Since in close binaries one suspects the rotational and orbital period to be synchronous, this phenomenon would suggest that the magnetic and spectral variations are due to variable features over the surface of the star.

Models

The Oblique Rotator

Basically, the oblique rotator can be visualized as a star with the predominant magnetic field direction being inclined to the rotational axis and the rotational axis in its turn inclined to the line of sight. In order to produce the observed variations in equivalent widths, light and radial velocities, it is proposed that there is a change in line strengths and brightness with position on the surface of the star. The distribution of line strengths and brightness one presumes to be symmetric about the magnetic axis to a greater or lesser degree. This model is particularly successful in explaining Deutsch's (1956) observation of the period-line width correlation. The model can also explain conveniently the rapid switching of magnetic polarities without encountering difficulties because of the large decay times one would expect to have for magnetic fields imbedded in stars. The crossover effect, as explained earlier, finds in the oblique rotator, a physical model that naturally provides circumstances corresponding to the conditions proposed by Babcock as the probable source of the phenomenon. The most significant point is that in those stars where there is a pronounced radial velocity variation associated with only certain lines in the spectrum, this model predicts a variation of the right amplitude without requiring a radial oscillation of the star that is completely ruled out by the small amplitude of the light and colour variations and by the absence of a radial velocity variation in all lines. Furthermore this model predicts the general observation that the most pronounced V_r variation is associated with the lines of most pronounced line strength variation. This situation is particularly true of the star that is the subject of this research as will be shown later.

The objections to the oblique rotator hinge mostly on assumptions that one needs rapid rotation to generate large magnetic fields and that if the magnetic field causes a concentration of line strength to one magnetic pole it should do the same at the other so that the period of the spectrum variation would be, in most stars, half the magnetic period. Before progress can be made on the second objection, which becomes a discussion of the mechanism by which the magnetic field strengthens or weakens the lines, one requires knowledge of the distribution of magnetic field strength and line strength over the surface of the star. I propose to approach this problem in this thesis. Until now, only one attempt has been made to produce a model of a peculiar A star that predicts all the observations for a given star (Deutsch 1958) and the results were not entirely satisfactory.

The oblique rotator is not the only model proposed to explain the spectrum variables, but it is the most favoured. A survey paper covering several other models and giving references can be found as the introductory chapter to The Magnetic and Related Stars (Preston 1967) and one might also refer to Steinitz (1964).

CHAPTER II

THE SPECTRUM VARIABLE HD173650

The star HD173650, $\alpha = 18^h 41^m.3$, $\delta = +21° 53'$ (1900) has been a major topic in three papers to date. Babcock (1958) obtained all the magnetic observations taken on this star over the period from 1948 to 1956. Along with the magnetic field observations, there is a tabulation of the radial velocities derived from the measures taken for the Zeeman analysis. The notes to the star include the observations that SiII and SrII lines are the most prominent and that lines of MnII, CrI, CrII, EuII, GdII and the line λ 4200 are also seen. The lines of SrII have a well marked variation in intensity and "the majority of the lines of the metals, including EuII, vary with SrII". The range in variation for He was from -540 gauss to +700 gauss.

Wehlau (1962) determined a light period of approximately $10^d.1$ and showed that the blue and yellow variation was in phase. It was shown that a group of magnetic observations taken by Babcock (1958) over a short period of time also indicated periodicity of $10^d.1$.

Jaschek and Garcia (1966) published a line identification list for HD173650 and one other λ 4200 star. Visual estimates of line strength are given as well as the measured wavelength of each identified line.

CHAPTER III

THE SPECTRUM AND EQUIVALENT WIDTHS

Fourteen plates of HD173650 were obtained at the Dominion Astrophysical Observatory, 9 plates in the summer of 1966 and 5 in the summer of 1967. Table III,1 gives the plate numbers, J.D., and phase computed from a $9^{d}.9748$ period and zero phase corresponding to minimum light at J.D. 2,437,121.6. Each plate was taken using the 32"2 camera which gives a dispersion of about 6.5 A/mm.

TABLE III,1

Plate	Date	Phase	Plate	Date	Phase
2700	2,439,357.702	0.174	2771	2,439,390.740	0.487
2705	9,358.701	0.274	2775	9,398.744	0.289
2717	9,362.804	0.686	2783	9,402.692	0.685
2737	9,372.692	0.677	3271	9,693.778	0.867
2742	9,374.710	0.880	3278	9,697.815	0.272
2748 weak	9,382.730	0.684	3280	9,698.831	0.373
2749	9,387.686	0.180	3287	9,703.778	0.869
			3316	9,713.867	0.881

The plates were traced on the microphotometer at D.A.O. using a calibration curve derived from calibration strips on the plates. These strips are arranged so that each step of increasing density corresponds to an increase in the log of the intensity of 0.2. Each plate was run in two sections - one from λ3700 to λ4250 and the other from λ4250 to λ4800 - with each section calibrated separately.

The output of the microphotometer then corresponds to the log of the stellar intensity at each wavelength. The continuum was drawn on the log I trace, and a device referred to as an intensitometer was used to produce mechanically the corresponding intensity curve with a constant five-inch continuum.

The line identification was accomplished by picking out the major lines, and then identifying the lines as given by Jaschek and Garcia by measuring their positions from the prominent features, using rulers calibrated according to the comparison spectrum on the plates. The rulers were then laid on the traces and adjusted so as to give the best fit for several of the lines given by Jaschek and Garcia and the very weak lines were then assigned a wavelength according to their positions. A judgement was then made as to the possible element or elements that could be responsible for the spectral feature and the tenative identification and its laboratory wavelength were written on the trace.

Two traces at line strength maximum were overlapped on a light table and apparently unblended lines were sketched on the trace of plate 2783. Sketches of the profiles in the regions $\lambda 3800$ to $\lambda 4250$ and $\lambda 4250$ to $\lambda 4700$ were made on separate sheets of paper and seven mean profiles were drawn up for each of these two regions. The two sets of profiles were measured with a planimeter for area and the equivalent widths were computed assuming the dispersion at $\lambda 4000$ for the profiles pertaining to the blue end of the traces and the dispersion at $\lambda 4450$ for those pertaining to the red end.

A correction for the variation in dispersion in each of the two regions was applied later, on the IBM 7040 computer, to the equivalent widths estimated with the mean profiles.

The estimate of the strengths of all lines identified on the traces were made by overlaying the mean profiles on the lines of the trace and making a judgement based primarily on area as to where the lines fell in the range of mean profiles. The equivalent widths were assigned by interpolating in the values of the equivalent widths of the mean profiles.

Table III,2 gives the line identifications and equivalent widths for all lines used in the curve of growth analysis. The mean profiles are reproduced in figure VII,1. The sources of the log gf values are listed separately in the bibliography in order of preference with the most preferred sources listed first.

TABLE III,2

LAMBDA	ELEM	MUL	EP	LOGGF	EQUIVALENT WIDTHS MILLIANGS AT PHASE 685	677	686	880	180	274	289	174	487	869	881	867	272	373
3849.36	CR I	138	3.00	0.63	68	49	51	39	54	30	1	9	80	37	51	1	20	34
3941.49	CR I	23	1.03	-0.82	61	51	51	1	29	37	1	9	49	49	35	2	1	74
3991.67	CR I	38	2.53	0.24	82	54	1	45	28	45	1	1	48	33	33	30	50	60
4076.06	CR I	279	4.08	0.55	63	29	31	48	28	28	1	29	54	24	41	51	8	28
4190.16	CR I	84	2.86	-0.15	76	56	50	39	44	42	56	23	44	47	1	50	27	45
4254.35	CR I	1	0.00	-0.27	196	169	169	115	161	104	96	90	150	120	122	133	115	124
4274.80	CR I	1	0.00	-0.09	103	96	89	64	55	55	49	32	85	38	62	65	38	72
4289.72	CR I	1	0.00	-0.58	87	92	72	52	36	58	85	60	92	63	60	68	40	58
4325.07	CR I	104	2.95	0.11	46	53	25	81	71	23	49	34	64	32	11	63	27	55
4375.33	CR I	103	2.97	0.19	61	38	31	27	74	17	1	17	47	8	37	1	15	56
4430.49	CR I	234	3.54	0.02	101	86	67	36	1	38	56	1	57	35	36	38	32	60
4514.53	CR I	95	2.90	-0.23	47	92	54	1	1	47	1	1	73	18	57	34	35	34
4530.75	CR I	33	2.53	0.43	38	37	1	9	1	1	1	1	1	12	1	1	35	18
4652.16	CR I	21	1.00	-0.79	57	28	61	1	28	72	1	1	29	19	35	26	19	43
3814.00	CR II	628	-1.20	1.80	152	121	174	120	89	87	98	126	0	115	102	1	136	163
3865.59	CR II	167	5.30	-0.66	107	184	148	114	162	119	96	114	65	115	119	119	145	152
3866.01	CR II	130	4.90	-1.98	89	75	41	57	81	34	21	46	28	33	46	33	21	53
3866.54	CR II	130	4.92	-1.96	111	83	56	76	74	57	48	1	21	48	47	52	57	53
3905.64	CR II	167	5.31	-0.87	90	213	162	157	207	127	117	125	112	151	156	162	163	141
3911.32	CR II	129	4.92	-2.13	111	97	51	75	72	40	49	31	31	48	77	78	59	63
3979.51	CR II	183	5.65	-0.69	107	136	97	94	97	55	57	54	1	94	87	94	68	90
4003.33	CR II	194	6.46	-0.78	94	114	77	1	50	40	51	70	1	85	54	80	33	59
4012.50	CR II	183	5.64	-0.47	90	279	211	176	162	155	119	155	1	176	149	159	121	116
4017.96	CR II	166	5.31	-2.26	180	72	65	84	40	46	37	72	1	55	49	29	25	42
4038.03	CR II	194	6.46	-0.61	105	143	109	123	61	104	50	91	32	106	1	83	57	75

TABLE III,2

LAMBDA	ELEM	MUL.	EP	LOGGF	EQUIVALENT WIDTHS MILLIANGS							AT PHASE						
					685	677	686	880	180	274	289	174	487	869	881	867	272	373
4048.02	CR II	182	5.65	-1.48	71	50	25	51	20	39	32	33	1	25	1	29	29	30
4049.14	CR II	193	6.46	-0.91	93	64	57	78	57	54	71	1	15	49	1	51	33	39
4051.97	CR II	19	3.09	-2.08	114	103	78	112	83	78	83	53	54	77	1	93	36	78
4053.45	CR II	19	3.09	-2.30	200	122	68	99	64	45	33	74	46	47	1	60	36	67
4054.11	CR II	19	3.09	-2.13	151	133	87	117	78	64	74	78	55	82	1	79	54	54
4056.07	CR II	182	5.64	-1.47	40	78	54	51	45	29	36	33	40	42	1	30	50	49
4070.90	CR II	193	6.46	-0.85	106	91	95	108	91	64	82	83	55	86	88	68	55	73
4082.30	CR II	165	5.30	-1.13	111	80	86	109	38	70	61	69	46	58	54	70	53	60
4086.14	CR II	26	3.70	-2.22	133	83	64	98	83	81	53	78	48	58	81	80	52	55
4088.90	CR II	19	3.09	-3.43	67	58	59	51	65	58	40	36	32	45	56	56	37	50
4111.01	CR II	18	3.09	-1.86	121	138	113	87	101	63	72	95	59	70	83	72	65	95
4111.01	CR II	26	3.74	-1.86	110	138	113	87	101	63	72	95	59	70	83	72	65	95
4112.59	CR II	18	3.09	-2.96	190	56	58	59	66	51	58	53	43	33	52	56	39	46
4113.24	CR II	18	3.09	-2.58	149	58	63	54	62	61	1	34	24	56	62	63	62	62
4132.41	CR II	26	3.74	-2.16	147	159	115	148	51	86	78	82	83	90	77	144	71	81
4145.77	CR II	162	5.30	-1.10	120	121	102	116	116	63	86	81	63	99	79	86	105	59
4151.00	CR II	163	5.31	-2.29	107	77	56	74	33	31	42	74	42	50	1	54	48	74
4172.60	CR II	18	3.09	-2.25	110	102	81	106	77	39	53	81	45	68	59	60	47	60
4179.43	CR II	26	3.81	-1.09	121	164	140	146	115	101	98	106	39	110	80	98	80	77
4195.41	CR II	161	5.30	-1.73	140	134	129	119	119	62	85	101	50	106	79	94	75	56
4207.35	CR II	26	3.81	-1.75	149	118	93	105	75	57	76	70	61	70	72	83	45	59
4209.02	CR II	162	5.30	-1.47	150	83	76	108	78	53	70	72	28	75	62	70	45	69
4209.84	CR II	180	5.65	-1.60	111	75	69	51	47	54	30	44	45	73	70	54	14	49
4217.07	CR II	18	3.09	-2.38	83	111	76	91	51	48	51	50	28	79	54	66	51	52
4222.00	CR II	180	5.64	-1.25	60	78	76	77	57	28	64	62	36	51	51	34	36	42

TABLE III,2

LAMBDA	ELEM	MUL	EP	LOGGF	EQUIVALENT WIDTHS MILLIANGS AT PHASE 685	677	686	880	180	274	289	174	487	869	881	867	272	373
4224.85	CR II	162	5.31	-1.27	80	116	93	86	70	64	1	78	54	86	76	75	78	75
4229.81	CR II	26	3.81	-2.79	190	63	79	36	47	1	1	39	34	74	45	31	34	31
4242.38	CR II	31	3.85	-1.02	117	193	161	186	116	116	111	131	111	146	142	137	106	111
4252.62	CR II	31	3.84	-1.85	120	171	154	158	121	1	94	1	1	146	107	111	77	80
4256.16	CR II	192	6.46	-1.51	111	96	108	93	41	49	32	68	59	92	45	90	62	49
4261.92	CR II	31	3.85	-1.21	107	209	216	175	123	169	124	124	117	172	139	158	114	137
4268.93	CR II	192	6.46	-1.51	89	76	82	79	43	63	36	61	49	34	39	59	39	59
4269.28	CR II	31	3.84	-2.06	80	93	130	89	93	99	36	75	82	69	86	75	61	86
4275.57	CR II	31	3.84	-1.33	90	130	130	123	89	106	64	110	89	92	91	86	68	96
4284.21	CR II	31	3.84	-1.64	50	129	129	123	110	116	85	95	89	90	112	123	75	120
4306.94	CR II	587	-1.80	1.05	81	91	83	81	45	65	62	65	0	61	95	44	41	42
4539.62	CR II	39	4.02	-1.98	111	102	121	102	117	117	83	44	62	87	115	123	66	117
4555.02	CR II	44	4.05	-1.44	133	140	134	123	128	158	91	78	83	106	117	113	87	128
4558.66	CR II	44	4.06	-0.31	193	272	272	262	243	272	243	163	176	222	265	261	182	265
4565.78	CR II	39	4.02	-1.91	60	116	109	113	101	87	101	72	46	63	91	101	61	140
4588.22	CR II	44	4.05	-0.65	107	213	210	167	168	220	213	139	121	157	141	165	133	255
4592.09	CR II	44	4.06	-1.37	120	143	153	100	94	112	124	110	62	116	158	127	83	119
4616.64	CR II	44	4.05	-1.51	80	180	160	163	144	139	128	118	99	116	1	128	114	152
4618.83	CR II	44	4.06	-0.98	90	224	186	155	144	128	170	116	120	152	1	168	128	157
4634.11	CR II	44	4.05	-1.19	50	165	159	120	127	152	108	97	114	158	138	116	127	122
3819.67	EU II	1	0.00	0.02	86	54	71	35	36	1	1	10	68	30	29	1	55	46
3907.10	EU II	5	0.21	0.03	48	31	45	35	25	1	21	19	42	10	32	45	28	34
3930.50	EU II	5	0.21	0.09	113	72	124	37	28	15	31	34	51	54	46	79	1	18
4129.73	EU II	1	0.00	-0.31	99	82	103	86	37	51	60	14	83	53	37	105	63	37
4205.05	EU II	1	0.00	-0.08	134	118	118	64	44	39	55	51	85	75	51	78	23	38

TABLE III,2

LAMBDA	ELEM	MUL	EP	LOGGF	EQUIVALENT WIDTHS MILLIANGS							AT PHASE						
					685	677	686	880	180	274	289	174	487	869	881	867	272	373
3787.88	FE I	21	1.01	-0.44	80	52	33	70	54	33	65	43	66	57	34	1	1	52
3806.70	FE I	607	3.25	0.67	70	53	1	38	35	1	33	1	53	36	54	1	49	71
3812.96	FE I	22	0.95	-0.66	79	41	47	88	51	37	48	47	58	37	49	1	88	87
3815.84	FE I	45	1.48	0.56	110	64	40	98	83	51	57	55	115	77	75	1	82	82
3820.43	FE I	20	0.86	0.43	91	83	74	95	108	47	84	73	101	81	70	1	97	90
3821.18	FE I	608	3.25	0.73	31	44	31	53	53	1	49	32	49	22	31	1	56	74
3825.88	FE I	20	0.91	0.29	129	92	85	88	73	84	90	68	95	87	63	1	70	97
3843.26	FE I	528	3.03	0.55	32	48	39	1	26	47	1	19	27	20	22	1	41	12
3846.80	FE I	664	3.24	0.66	49	1	47	19	32	29	54	32	32	41	27	1	11	39
3849.97	FE I	20	1.01	-0.43	83	49	60	57	58	38	52	21	76	55	48	1	60	57
3856.37	FE I	4	0.05	-1.15	51	29	31	41	51	26	35	1	49	28	5	37	35	29
3859.91	FE I	4	0.00	-0.51	88	73	84	111	72	65	76	40	84	63	79	62	76	56
3867.22	FE I	488	3.00	0.05	65	38	40	78	28	34	31	1	40	28	49	30	46	43
3872.50	FE I	20	0.99	-0.63	66	46	100	129	68	44	49	72	68	54	5	43	28	26
3878.02	FE I	20	0.95	-0.50	58	51	54	71	54	31	36	49	61	60	33	54	59	53
3899.71	FE I	4	0.09	-1.33	57	50	21	46	32	1	1	37	44	54	29	34	24	25
3902.95	FE I	45	1.55	0.12	81	46	35	91	51	45	58	37	79	54	58	52	54	57
3903.90	FE I	429	2.98	-0.02	75	56	53	67	53	48	58	46	66	82	59	56	49	77
3907.94	FE I	280	2.75	-0.34	56	23	34	55	1	34	31	29	50	30	30	40	41	40
3920.26	FE I	4	0.12	-1.49	66	29	51	43	51	40	1	32	51	28	66	54	24	37
3922.91	FE I	4	0.05	-1.38	34	29	49	34	51	29	48	22	1	27	46	39	34	37
3927.92	FE I	4	0.11	-1.21	55	46	40	40	37	51	51	31	46	41	56	52	19	58
3948.78	FE I	604	3.25	0.42	82	51	56	28	46	32	1	25	34	26	53	32	20	46
3951.16	FE I	661	3.26	0.36	74	32	56	30	46	34	1	20	62	42	38	56	49	54
3952.60	FE I	278	2.68	-0.21	69	60	80	31	62	28	21	14	69	48	47	31	29	33

TABLE III,2

LAMBDA	ELEM	MUL	EP	LOGGF	EQUIVALENT WIDTHS MILLIANGS AT PHASE 685	677	686	880	180	274	289	174	487	869	881	867	272	373
3956.68	FE I	278	2.68	0.33	88	50	70	53	44	69	60	46	42	82	77	56	35	52
3981.77	FE I	278	2.72	-0.19	73	43	72	31	35	43	1	1	56	55	83	81	43	59
3983.96	FE I	277	2.72	0.11	123	85	125	85	54	65	60	1	90	66	50	59	95	76
4005.25	FE I	43	1.55	-0.06	105	57	1	72	79	46	50	1	58	55	49	60	77	57
4021.87	FE I	278	2.75	0.12	1	1	48	20	29	37	34	1	49	1	1	51	21	14
4029.64	FE I	556	3.25	-0.42	51	40	57	1	34	25	1	1	25	34	51	30	40	27
4045.81	FE I	43	1.48	0.72	154	108	118	117	122	104	96	80	108	101	1	113	78	74
4063.60	FE I	43	1.55	0.39	160	112	148	142	112	108	103	88	132	110	104	115	86	105
4071.74	FE I	43	1.60	0.36	64	73	76	77	90	57	77	58	54	74	79	68	53	33
4118.55	FE I	801	3.56	0.92	56	48	52	36	58	52	56	30	51	60	57	57	45	51
4132.06	FE I	43	1.60	-0.16	78	78	71	78	71	51	82	54	78	63	39	46	75	38
4143.42	FE I	523	3.03	0.62	63	51	56	78	34	28	50	34	47	60	1	54	24	34
4143.87	FE I	43	1.55	-0.12	95	63	82	78	54	54	50	39	75	54	1	56	51	45
4154.81	FE I	694	3.35	0.25	77	48	63	29	24	63	39	24	56	36	33	33	33	36
4156.80	FE I	354	2.82	0.14	39	10	33	29	20	1	1	23	48	34	53	14	16	19
4175.64	FE I	354	2.83	0.09	49	56	51	63	56	42	47	19	72	53	64	55	24	45
4184.90	FE I	355	2.82	0.01	62	32	27	62	23	56	28	14	39	26	49	35	35	28
4187.04	FE I	152	2.44	0.26	129	77	94	94	70	53	66	1	80	54	59	74	52	51
4187.80	FE I	152	2.41	0.23	111	85	81	90	77	56	85	33	106	104	70	94	62	55
4191.43	FE I	152	2.46	0.06	56	47	62	85	62	33	59	23	47	26	47	53	27	39
4198.31	FE I	152	2.39	0.13	123	104	105	109	93	78	1	80	119	108	59	106	70	85
4202.03	FE I	42	1.48	-0.29	81	70	66	56	27	45	70	64	73	53	31	66	50	51
4210.35	FE I	152	2.47	-0.23	49	44	53	19	28	1	1	39	1	45	53	35	23	39
4219.36	FE I	800	3.56	0.86	45	50	23	45	34	28	1	14	28	30	51	19	21	1
4225.46	FE I	693	3.40	0.13	39	55	39	57	23	1	28	28	45	5	42	1	28	24

TABLE III,2

LAMEDA	ELEM		MUL	EP	LOGGF	EQUIVALENT WIDTHS MILLIANGS							AT PHASE						
						685	677	686	880	180	274	289	174	487	869	881	867	272	373
4227.43	FE	I	693	3.32	1.00	94	76	74	73	48	1	53	28	70	67	73	61	61	61
4235.94	FE	I	152	2.41	0.33	67	69	63	50	34	42	39	31	50	63	45	50	50	23
4238.82	FE	I	693	3.38	0.40	127	108	77	74	60	70	77	47	86	81	80	57	60	89
4247.43	FE	I	693	3.35	0.39	82	72	77	39	1	28	50	1	70	50	33	46	29	33
4250.12	FE	I	152	2.46	0.22	94	80	50	57	1	57	1	1	1	77	46	74	1	54
4250.79	FE	I	42	1.55	-0.38	89	72	63	50	1	50	1	1	1	79	56	36	70	73
4260.48	FE	I	152	2.39	0.62	90	90	85	36	82	58	61	49	82	65	60	79	56	61
4271.16	FE	I	152	2.44	0.19	64	52	55	68	61	27	59	61	57	64	38	64	36	46
4271.76	FE	I	42	1.48	0.16	96	117	103	81	103	57	82	76	90	90	66	82	65	93
4294.13	FE	I	41	1.48	-0.71	81	60	81	64	60	55	64	39	57	59	89	62	38	60
4299.24	FE	I	152	2.41	0.16	48	39	64	36	81	32	38	36	32	27	60	13	26	1
4307.91	FE	I	42	1.55	0.22	169	128	128	132	147	102	110	101	149	88	140	94	87	91
4325.76	FE	I	42	1.60	0.24	182	186	173	143	183	126	136	92	183	94	103	100	102	165
4352.74	FE	I	71	2.21	-0.54	63	69	44	54	76	35	41	36	45	32	38	68	40	43
4383.55	FE	I	41	1.48	0.35	102	102	74	92	1	47	88	1	66	71	88	92	65	85
4404.75	FE	I	41	1.56	0.11	144	132	126	89	122	66	94	1	97	60	94	78	64	87
4415.12	FE	I	41	1.60	-0.09	86	58	46	49	55	23	30	1	39	32	46	15	55	47
4443.20	FE	I	350	2.85	-0.24	48	57	1	1	35	26	1	1	42	38	30	1	40	48
4447.72	FE	I	68	2.21	-0.48	103	67	57	48	45	1	52	1	48	37	57	45	25	35
4466.55	FE	I	350	2.82	0.20	64	64	81	17	48	1	18	1	81	45	44	38	10	37
4476.02	FE	I	350	2.83	0.21	38	45	35	1	73	12	20	1	48	31	42	35	28	24
4494.57	FE	I	68	2.19	-0.44	73	108	66	17	47	1	30	9	64	38	53	27	26	41
4525.14	FE	I	826	3.59	0.03	41	63	60	1	1	30	10	18	60	35	15	41	15	60
4528.62	FE	I	68	2.17	-0.25	62	63	63	54	1	24	1	1	18	32	34	24	43	38
3783.35	FE	II	14	2.27	-2.65	140	78	53	85	92	69	42	47	57	61	80	1	1	58

TABLE III,2

LAMBDA	ELEM	MUL	EP	LOGGF	EQUIVALENT WIDTHS MILLIANGS AT PHASE 685	677	686	880	180	274	289	174	487	869	881	867	272	373
3827.08	FE II	153	4.71	-1.80	107	79	61	34	38	57	40	50	33	49	58	1	39	41
3863.41	FE II	152	4.71	-1.72	71	114	60	63	1	57	46	31	1	49	34	42	79	57
3863.95	FE II	127	4.48	-1.58	150	96	60	84	1	65	51	37	46	64	81	51	72	61
3863.95	FE II	152	4.72	-1.47	40	96	60	84	1	65	51	37	46	64	81	51	72	61
3906.04	FE II	173	5.55	-1.39	93	136	104	105	98	82	53	83	78	100	56	69	84	79
3914.48	FE II	3	1.66	-3.09	140	79	59	49	114	59	55	34	46	49	83	74	69	59
3935.94	FE II	173	5.54	-0.96	106	156	113	118	112	92	79	92	68	114	113	108	76	100
3938.29	FE II	3	1.66	-3.40	163	104	51	83	61	68	62	74	32	65	82	82	46	73
3938.97	FE II	190	5.89	-1.39	90	135	75	108	96	78	78	68	47	81	99	81	54	78
3960.89	FE II	212	7.24	-0.51	111	75	47	55	40	34	37	59	16	40	24	39	65	35
4002.07	FE II	29	2.77	-3.17	150	77	50	1	48	58	37	45	1	50	61	52	54	40
4024.55	FE II	127	4.48	-1.95	120	129	109	113	87	82	68	82	1	81	91	85	78	74
4031.45	FE II	151	4.71	-2.51	120	64	57	75	50	57	29	48	1	55	46	48	48	23
4032.95	FE II	126	4.48	-1.59	89	134	113	144	83	113	83	82	1	110	1	102	104	74
4044.01	FE II	172	5.55	-1.43	86	78	50	61	49	61	48	34	35	36	1	33	39	32
4057.46	FE II	212	7.24	-0.30	89	103	78	78	53	57	57	67	55	84	1	57	60	54
4061.79	FE II	189	5.93	-0.82	171	78	67	80	55	57	45	45	34	28	51	76	47	54
4122.64	FE II	28	2.57	-2.73	131	133	112	114	119	132	81	89	82	97	117	112	84	78
4124.79	FE II	22	2.53	-3.15	129	103	75	82	54	57	39	35	28	61	82	52	58	24
4128.73	FE II	27	2.57	-2.76	190	78	95	108	103	87	67	115	61	121	78	87	95	74
4160.62	FE II	39	2.83	-3.51	131	60	50	24	24	28	39	24	1	50	70	33	39	20
4173.45	FE II	27	2.57	-2.01	149	178	157	191	164	140	140	152	114	157	152	123	115	110
4178.85	FE II	28	2.57	-2.00	79	151	140	119	130	130	110	110	52	115	112	115	81	75
4233.17	FE II	27	2.57	-1.43	121	282	239	263	263	207	216	216	166	280	207	205	216	207
4258.15	FE II	28	2.69	-2.59	107	143	159	124	99	93	96	56	82	121	114	124	93	118

TABLE III,2

LAMBDA	ELEM	MUL	EP	LOGGF	EQUIVALENT WIDTHS MILLIANGS							AT PHASE						
					685	677	686	880	180	274	289	174	487	869	881	867	272	373
4273.32	FE II	27	2.69	-2.27	217	114	111	96	96	92	49	117	85	87	91	112	80	96
4278.13	FE II	32	2.68	-3.15	21	95	85	92	82	89	49	89	60	65	67	83	64	90
4296.57	FE II	28	2.69	-2.36	50	116	122	116	102	135	81	101	89	72	93	87	86	92
4303.17	FE II	27	2.69	-2.00	147	169	166	160	145	168	109	121	118	92	119	66	100	98
4314.29	FE II	32	2.66	-2.81	50	120	105	124	75	128	75	87	83	76	90	93	62	79
4351.76	FE II	27	2.69	-1.76	110	148	154	141	138	148	102	87	104	98	109	128	108	180
4354.36	FE II	213	7.62	-0.34	143	40	39	54	39	40	38	1	35	28	43	62	30	30
4366.16	FE II	216	7.67	-0.66	90	36	15	36	27	27	1	1	26	1	31	1	34	1
4369.40	FE II	28	2.77	-2.83	81	90	115	58	103	61	47	53	74	62	68	53	72	77
4385.38	FE II	27	2.77	-2.02	133	158	129	135	88	1	95	102	1	85	106	113	92	123
4413.60	FE II	32	2.68	-3.00	115	86	61	43	36	34	27	35	1	26	39	35	27	61
4416.82	FE II	27	2.77	-2.09	83	162	138	119	101	125	82	111	1	87	92	79	72	111
4431.62	FE II	222	7.91	-0.71	93	54	42	35	24	74	12	38	1	22	61	30	25	24
4446.25	FE II	187	5.93	-1.70	50	60	1	77	1	60	27	58	1	57	45	28	38	35
4449.66	FE II	222	7.89	-0.79	106	48	85	67	48	1	38	30	1	56	57	25	36	48
4472.92	FE II	37	2.83	-2.76	150	114	84	89	73	102	66	42	1	66	84	89	36	91
4489.18	FE II	37	2.82	-2.23	150	148	163	123	122	140	109	116	91	91	118	118	87	122
4491.40	FE II	37	2.84	-2.09	40	116	116	102	87	95	77	84	69	62	93	91	62	87
4493.58	FE II	222	7.89	-0.11	114	69	116	62	47	80	53	47	34	41	38	59	56	87
4508.28	FE II	38	2.84	-1.76	50	155	161	122	128	1	116	108	90	94	101	113	107	125
4515.34	FE II	37	2.83	-1.91	103	165	218	166	178	1	115	127	108	100	159	161	111	165
4520.22	FEII	37	2.79	-1.87	150	142	142	110	124	1	101	83	86	83	92	93	92	118
4522.63	FE II	38	2.83	-1.51	90	178	211	142	178	1	121	121	115	115	130	133	113	136
4526.58	FE II	171	5.54	-1.57	107	57	62	26	23	1	25	10	34	38	58	56	35	57
4541.52	FE II	38	2.84	-2.29	80	136	129	95	102	129	81	69	59	88	110	117	65	110

TABLE III.2

LAMBDA	ELEM	MUL	EP	LOGGF	EQUIVALENT WIDTHS MILLIANGS AT PHASE													
					685	677	686	880	180	274	289	174	487	869	881	867	272	373
4555.89	FE II	37	2.82	-1.79	124	140	163	140	134	163	123	120	126	118	126	122	109	123
4576.33	FE II	38	2.83	-2.22	120	106	112	94	83	116	116	80	40	83	100	77	62	90
4580.05	FE II	26	2.57	-2.87	186	86	86	68	46	72	86	53	34	48	62	58	34	58
4582.83	FE II	37	2.83	-2.44	150	116	101	108	86	90	104	79	46	80	53	86	53	92
4583.83	FE II	38	2.79	-1.25	117	213	201	188	174	213	188	162	139	157	156	181	157	167
4598.53	FE II	219	7.77	-0.72	143	86	62	37	34	93	52	34	40	55	40	37	36	58
4620.51	FE II	38	2.82	-2.63	133	114	93	89	71	87	95	62	64	85	1	93	57	95
4625.91	FE II	186	5.93	-1.56	103	47	45	42	34	46	54	35	58	41	1	1	37	1
4628.82	FE II	219	7.81	-0.60	137	64	52	28	1	57	25	35	34	26	47	46	24	35
4629.33	FE II	37	2.79	-1.78	133	159	137	110	162	152	122	94	107	119	122	113	118	116
4635.33	FE II	186	5.93	-0.95	107	99	99	85	66	87	56	66	88	83	80	87	85	76
4652.28	FE II	219	7.85	-0.50	150	57	28	61	1	28	72	1	1	19	35	26	19	43
4656.97	FE II	43	2.88	-2.53	169	106	84	80	62	59	63	46	57	60	68	86	53	68
4666.75	FE II	37	2.82	-2.64	150	100	91	109	107	46	65	69	57	69	89	56	49	89
4670.17	FE II	25	2.57	-2.87	114	100	91	88	89	56	83	1	70	88	86	62	79	111
3850.69	GD II	2	0.08	-0.22	90	46	64	31	47	40	1	1	78	52	62	1	45	61
3852.45	GD II	2	0.03	-0.15	38	35	50	30	21	35	1	21	37	24	9	1	21	36
3957.67	GD II	19	0.60	-0.22	91	50	82	50	22	22	34	47	54	50	84	34	36	42
3994.16	GD II	49	0.52	-0.57	111	54	1	33	36	33	40	1	73	37	55	77	28	48
4037.33	GD II	49	0.66	-0.12	51	15	65	1	29	1	1	1	48	15	1	2	21	25
4073.20	GD II	34	0.43	-0.70	59	41	55	53	1	1	1	1	39	21	51	31	10	47
4085.56	GD II	50	0.73	-0.04	83	57	58	56	33	20	66	30	79	77	75	53	50	56
4212.00	GD II	15	0.42	-0.46	78	55	64	57	19	28	44	1	69	51	53	54	31	48
4229.80	GD II	117	1.61	-0.06	63	79	36	47	1	1	39	34	63	74	45	31	34	31
4251.73	GD II	15	0.38	-0.39	110	83	73	50	1	50	1	1	1	74	50	53	73	54

TABLE III,2

LAMBDA	ELEM	MUL	EP	LOGGF	EQUIVALENT WIDTHS MILLIANGS AT PHASE 685	677	686	880	180	274	.289	174	487	869	881	867	272	373
4406.67	GD II	103	1.42	-0.24	71	64	52	18	60	35	60	1	39	15	35	43	30	66
3917.32	MN II	691	-1.10	0.40	26	40	31	28	26	29	1	40	0	7	54	14	14	31
4174.31	MN II	2	1.80	-3.32	73	76	77	33	39	66	57	19	1	66	94	37	49	33
4206.37	MN II	7	5.37	-1.13	156	139	129	86	70	64	101	39	129	89	83	117	57	75
4251.74	MN II	618	-0.76	1.10	83	73	50	1	50	1	1	1	0	74	50	53	73	54
4253.02	MN II	7	5.36	-1.43	125	117	94	70	1	57	1	1	1	83	60	45	77	80
4259.20	MN II	7	5.37	-1.15	118	108	114	63	76	82	82	62	100	88	72	94	56	90
4283.77	MN II	6	5.35	-1.72	55	36	1	12	1	23	46	26	1	34	36	25	47	21
4292.24	MN II	6	5.36	-1.39	75	84	64	71	89	42	68	68	81	64	36	36	58	57
4365.22	MN II	657	-1.17	0.36	47	42	36	52	1	8	26	44	0	33	36	17	39	12
4478.64	MN II	664	-0.92	0.73	74	53	1	56	27	38	1	70	0	20	20	17	30	51
3853.66	SI II	1	6.83	-1.62	172	138	121	163	116	84	112	80	119	109	84	1	144	126
3856.02	SI II	1	6.83	-0.70	314	237	241	299	212	170	222	170	282	257	231	222	231	259
3862.59	SI II	1	6.83	-0.94	280	209	197	235	169	150	184	119	204	205	161	231	205	184
4128.05	SI II	3	9.79	0.59	390	323	342	313	285	285	269	218	304	275	269	285	256	218
4130.88	SI II	3	9.80	0.74	403	361	323	304	284	236	269	221	304	269	265	269	265	246
4077.71	SR II	1	0.00	0.18	332	283	293	159	191	159	166	155	283	195	199	202	159	193
4161.80	SR II	3	2.93	-0.36	94	77	81	63	45	60	48	33	77	77	51	47	36	51
4215.52	SR II	1	0.00	-0.11	284	240	262	155	132	112	128	112	213	175	181	201	122	147
4305.45	SR II	3	3.03	-0.08	90	91	91	62	60	1	20	34	65	58	66	51	55	26
3913.46	TI II	34	1.11	-0.24	97	66	72	109	72	66	32	31	79	47	77	82	51	67
3932.01	TI II	34	1.13	-1.37	37	10	58	29	14	1	1	29	26	1	29	34	1	26
4028.33	TI II	87	1.88	-0.65	57	40	55	1	29	22	30	1	49	48	32	44	21	8
4163.64	TI II	105	2.58	0.20	79	31	76	56	36	50	53	28	60	72	30	50	42	59
4171.90	TI II	105	2.59	0.13	151	136	146	130	102	110	120	94	151	129	81	123	91	57

TABLE III,2

LAMBDA	ELEM		MUL	EP	LOGGF	EQUIVALENT WIDTHS MILLIANGS							AT PHASE						
						685	677	686	880	180	274	289	174	487	869	881	867	272	373
4290.22	TI	II	41	1.16	-0.79	129	81	123	91	57	42	75	42	89	68	82	77	58	75
4300.05	TI	II	41	1.18	-0.46	105	116	106	98	116	84	95	67	128	76	95	76	84	64
4301.93	TI	II	41	1.16	-1.11	62	36	64	62	1	23	45	55	39	57	58	26	34	36
4312.86	TI	II	41	1.18	-1.06	126	89	105	113	126	75	68	75	94	78	117	39	75	65
4367.66	TI	II	104	2.58	-0.39	39	15	65	32	1	1	36	1	36	31	10	5	59	17
4386.86	TI	II	104	2.59	-0.46	69	36	43	36	1	1	10	1	41	10	28	27	33	50
4394.06	TI	II	51	1.22	-1.47	35	36	1	20	17	1	15	1	1	1	17	24	15	1
4399.77	TI	II	51	1.23	-1.06	57	53	52	8	47	17	47	1	35	32	34	28	25	41
4411.08	TI	II	115	3.08	-0.07	43	35	15	12	34	11	10	1	34	24	12	1	1	30
4417.72	TI	II	40	1.16	-1.18	49	26	29	35	26	1	55	1	61	25	51	26	12	53
4443.80	TI	II	19	1.08	-0.74	96	63	57	55	60	35	38	1	57	57	81	37	42	38
4450.49	TI	II	19	1.08	-1.41	64	40	35	42	60	38	26	1	39	45	57	31	36	38
4468.49	TI	II	31	1.13	-0.65	87	87	57	84	91	54	48	1	67	55	45	37	37	57
4488.32	TI	II	115	3.11	0.01	53	1	44	24	66	35	1	12	41	32	31	39	24	12
4501.27	TI	II	31	1.11	-0.79	119	115	90	84	1	80	47	66	107	90	80	76	64	96
4563.76	TI	II	50	1.22	-0.86	66	59	53	63	35	37	38	38	72	61	70	63	27	59
4571.97	TI	II	82	0.00	0.00	72	62	59	80	80	90	65	43	86	82	63	67	50	88

CHAPTER IV

THE UBV OBSERVATIONS

Photoelectric observations taken in 1960, 61, 64, 65 and 1967 have been used to determine a period of $9^{d}.9748$ for the star. The points for 1960, 1964 and 1967 are each sufficient to define a complete light curve. The observations given for 1967 were obtained at Kitt Peak by Dr. Edward Burke. A period of approximately $10^{d}.1$ had been established previously on the basis of the 1960 observations (Wehlau 1962). Figure IV,1 gives the relationships of the B, V, and B-V observations to phase computed using the $9^{d}.9748$ period and a zero phase date of JD 2437121.6. On the basis of the 1960 observations this date had appeared to be minimum light but the combined observations would indicate minimum light about 0.4 days later; maximum light six days later. Burke's observations, given only in the blue, were with respect to a different comparison star, HD 174261, and the scale for his observations is given on the inside of the ordinate axis for B. The two comparison stars for the University of Western Ontario observations were HD 175427 (AO) and HD 171948 (B9) with the former used to obtain ΔB and ΔV, in the sense of HD 173650 - HD 175427. Table IV,1 is a tabulation of all the photoelectric observations used to establish the period and the differential magnitudes are reported on the instrumental system.

The University of Western Ontario photometer contained, for the 1960 and 1961 observations, a 1P21 photomultiplier tube with blue filters Schott GG13 plus Corning 5030 and yellow filter Schott GG11. For the later observations the photomultiplier tube was changed to an E.M.I.6094A. The observing program required that the variable star be observed nine times per night and each comparison star five times per night. Once it had been established that the comparison stars were non-variable, the star HD 171948 was dropped and only the star HD 175427 was used as a comparison. The extinction coefficient was generally determined on a night by night basis by following one comparison star for an entire nights observing. The time of the observation was taken to be the mean heliocentric time for the five observations on the variable in one night.

Generally it will be noticed that the light curve is somewhat asymmetric with maximum light occuring later than mid-cycle by about $0^{d}.60$. The ΔB and ΔV curve show amplitudes of about $0^{m}.040$ and the $\Delta(B-V)$ plot indicates very little if any colour variation.

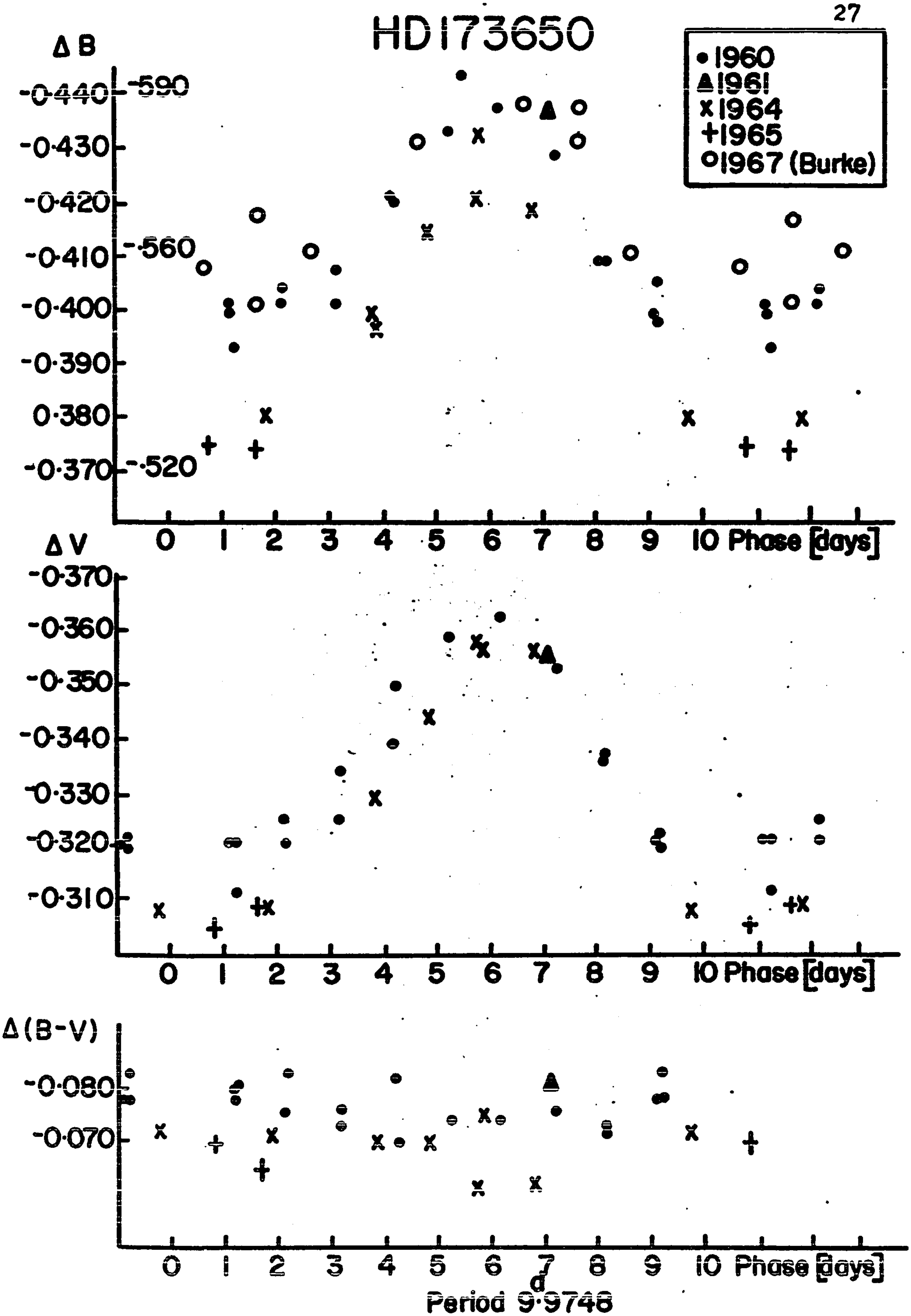
HD173650
• 1960
▲ 1961
x 1964
+ 1965
o 1967 (Burke)
Δ B
-0·440
-0·430
-0·420
-0·410
-0·400
-0·390
0·380
-0·370
-590
-560
-·520
0 1 2 3 4 5 6 7 8 9 10 Phase [days]
Δ V
-0·370
-0·360
-0·350
-0·340
-0·330
-0·320
-0·310
0 1 2 3 4 5 6 7 8 9 10 Phase [days]
Δ (B-V)
-0·080
-0·070
0 1 2 3 4 5 6 7 8 9 10 Phase [days]
Period 9·9748 d

FIGURE IV,1

TABLE IV,1

HD 173650

PHOTOELECTRIC OBSERVATIONS

	J.D.	B	V	(B-V)	ϕ
	7122.721	-.401	-0.321	-0.080	1.121
	123.707	-.401	- .325	- .076	2.107
	130.711	-.399	- .321	- .078	9.111
	139.685	-.409	- .336	- .073	8.110
	140.763	-.398	- .320	- .078	9.188
	146.788	-.433	- .359	- .074	5.238
	147.719	-.437	- .363	- .074	6.169
	155.751	-.420	- .350	- .070	4.227
1960	158.760	-.429	- .353	- .076	7.236
	162.762	-.393	- .312	- .081	1.263
	165.685	-.421	- .339	- .082	4.186
	172.667	-.399	- .321	- .078	1.193
	174.643	-.407	- .334	- .073	3.169
	180.622	-.405	- .322	- .083	9.148
	183.611	-.404	- .321	- .083	2.162
	184.576	-.401	- .325	- .076	3.127
	7189.585	-.409	- .337	- .072	8.136
1961	7487.729	-.436	- .355	- .081	7.033
	8543.786	-.420	-0.358	- .062	5.760
	557.729	-.380	- .308	- .072	9.728
	613.676	-.432	- .357	- .075	5.826
1964	621.699	-.396			3.875
	644.583	-.418	- .356	- .062	6.809
	651.600	-.399	- .329	- .070	3.851
	652.575	-.414	- .344	- .070	4.826
	8669.545	-.380	- .309	- .071	1.846
1965	8898.762	-.374	-0.309	-0.065	1.642
	957.780	-.375	- .305	- .070	0.811
* 1967	9636.954	-.551			1.697
	639.899	-.581			4.642
	641.932	-.588			6.675
	642.913	-.587			7.656

* The observations for 1967 were communicated by Burke.

J.D.	B	V	(B-V)	ϕ
655.889	-.558			0.682
656.865	-.567			1.658
657.827	-.561			2.620
662.869	-.581			7.662
663.837	-.560			8.630

CHAPTER V

THE RADIAL VELOCITIES

To the extent that the plates of this star would allow, the radial velocities of the various species of elements observed in the star were measured. The purpose was to determine whether a radial velocity variation consistent with the oblique rotator or any other model could be observed.

For this purpose approximately one hundred stellar lines were selected from among the lines identified on the traces made of the plates of the star. These lines were chosen so that they would be, as far as could be determined, unblended and sufficiently strong so that they could be measured fairly reliably on all plates. The optimum number of lines for each ionization level of each element necessary for this was set at 15 but in most cases this number of lines was much greater than could, in fact, be chosen. The list of lines selected for this purpose is in table V,1. The wavelengths given are from C. Moore's Multiplet Table. (C.Moore,1959)

The positions and rVs factors for each of the lines chosen were computed by linear interpolation in a table of wavelengths, positions and rVs factors (given for every 5 Angstroms) that was provided by Mr. M. Fletcher of the Dominion Astrophysical Observatory. The comparison lines used were selected from a table of comparison lines for the 3282 camera that was also provided by Fletcher.

TABLE V,1

Fe I	FeII	Cr I	CrII	Mn II	Ti II
3859.91	4173.45	3804.80	4003.33	3844.17	3900.55
4005.25	77.70	4254.35	4170.86	4136.91	13.46
45.81	78.86	74.80	72.60	74.31	4163.64
63.60	4205.48	4593.84	79.43	4206.38	84.33
4143.42}	58.16		4217.07	53.02	4290.22
.87}	73.32		24.85	59.20	4312.86
87.04	96.57		56.16	92.25	14.98
87.80	4314.29		61.92	4343.99	95.03
4227.43	4416.82		75.57	48.39	4501.27
71.76	89.18		4539.62	65.22	89.96
99.24	91.40		55.02	4478.64	
	4549.47		58.66		
4404.75	83.83		65.78		
4596.06			88.22		

Eu II	Zr I	Zr II	Si II	Gd II	Sr II	Ca II	Mg II
3819.67	4507.11	3818.78	3856.02	3850.69	4077.71	3933.65	4481.13}
4129.73		3934.80	62.59	4212.00	4161.80	68.47	.33}
4205.05		98.98	3954.51	4251.73	4215.52		
		4149.22	4075.45	4327.13	4305.45		
		61.20	76.78				
			4128.05				
			30.88				
			4190.74				
			[4200.75]				

The line measurement was performed on a Zeiss-Abbé comparator at the D.A.O. Each stellar line was measured twice in each direction on the plate and the average measure of each direction was used. The comparison lines were measured once on the upper one and once on the lower line and averaged as above in each direction. The standard reduction procedure of averaging the measures of each direction, drawing a correction curve to correct the measured positions to the ones that would correspond to the plate represented by the calculated values in the table, taking the displacement in position i.e. measured minus calculated and multiplying by the rVs factors to give the radial velocities for each line, was followed. The radial velocities of all the lines measured of a given species were recorded on separate sheets and averaged. The correction to the sun was computed for each plate and applied to each of the velocity values of the elements. The corresponding heliocentric values of the radial velocities were plotted against phase for each ionization state of each element observed.

The species of Eu II, Gd II and Zr II showed a rather convincing radial velocity variation with phase, particularly Zr II in view of the fact that five lines contributed to this mean. It would appear that Zr I, as opposed to Zr II, shows no apparent variation. This conclusion should be viewed with skepticism though since the values for Zr I are based on only one line. With only one line on which to make a conclusion the possibility of a mis-identification remains strong.

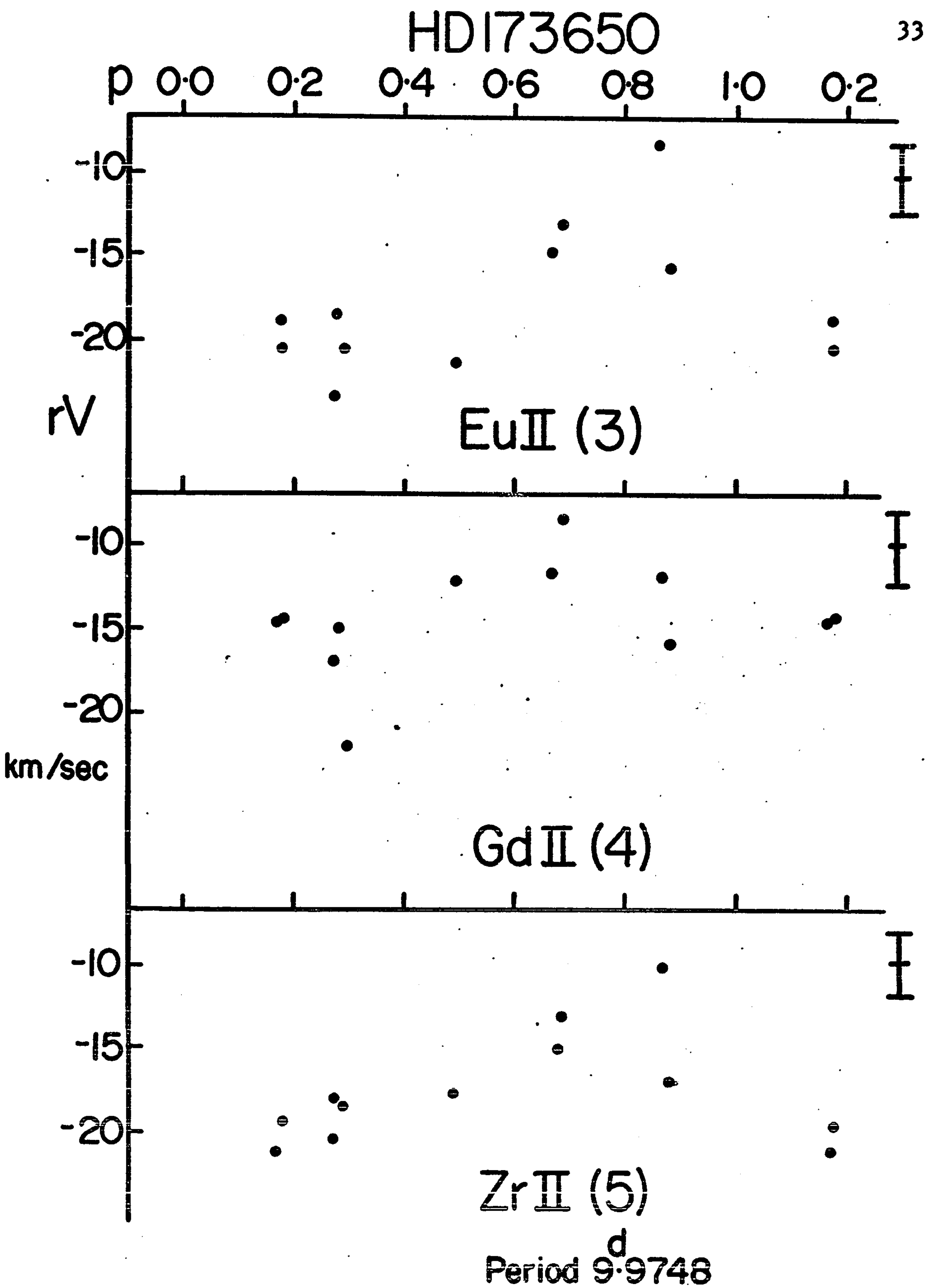
HD173650
p 0·0 0·2 0·4 0·6 0·8 1·0 0·2
-10
-15
-20
rV
km/sec
EuII (3)
GdII (4)
ZrII (5)
Period 9·9748 d

FIGURE V,1

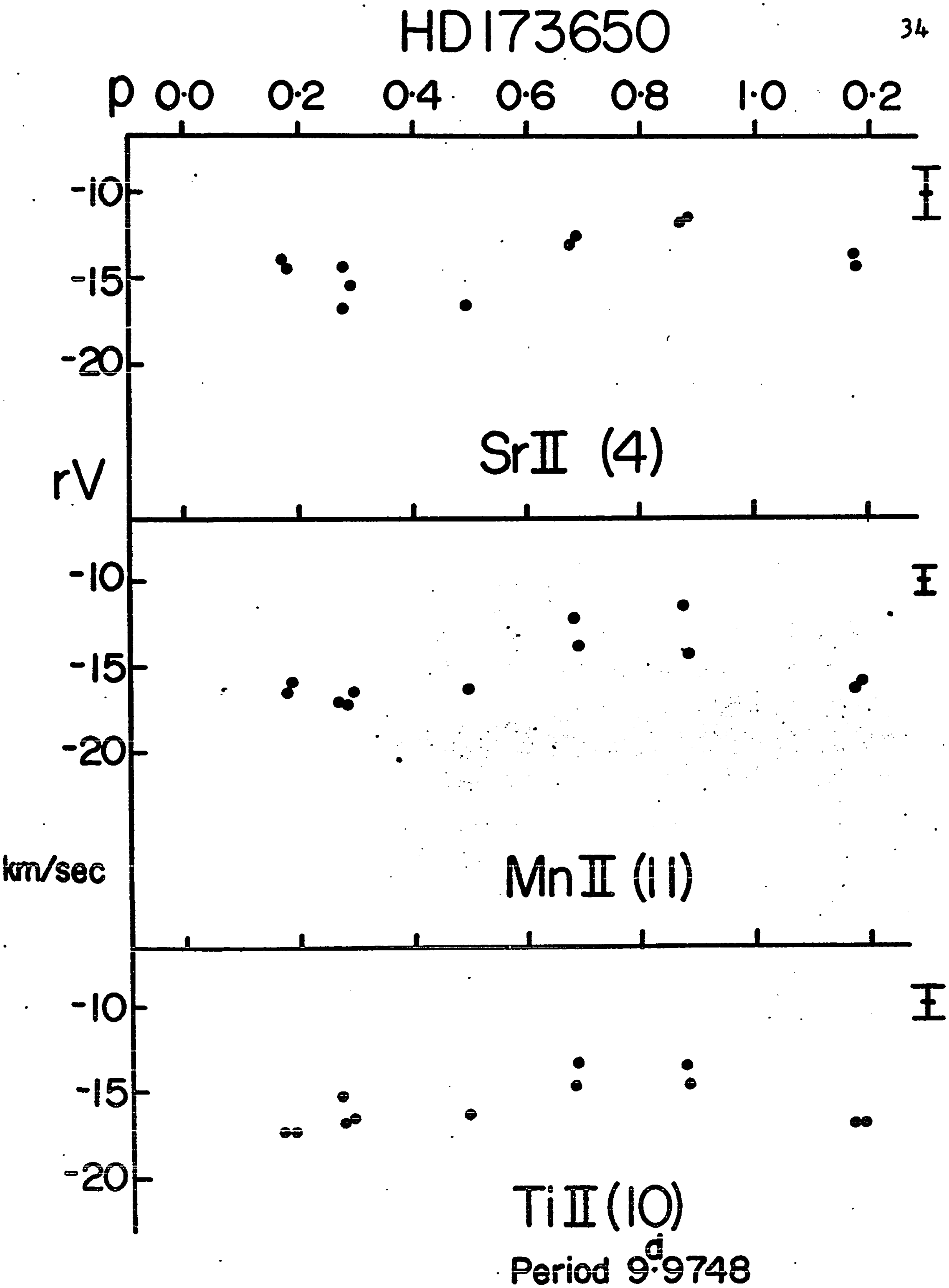
HD173650
p 0·0 0·2 0·4 0·6 0·8 1·0 0·2
-10
-15
-20
SrII (4)
rV
-10
-15
-20
km/sec
MnII (11)
-10
-15
-20
TiII (10)
Period 9d9748

FIGURE V,2

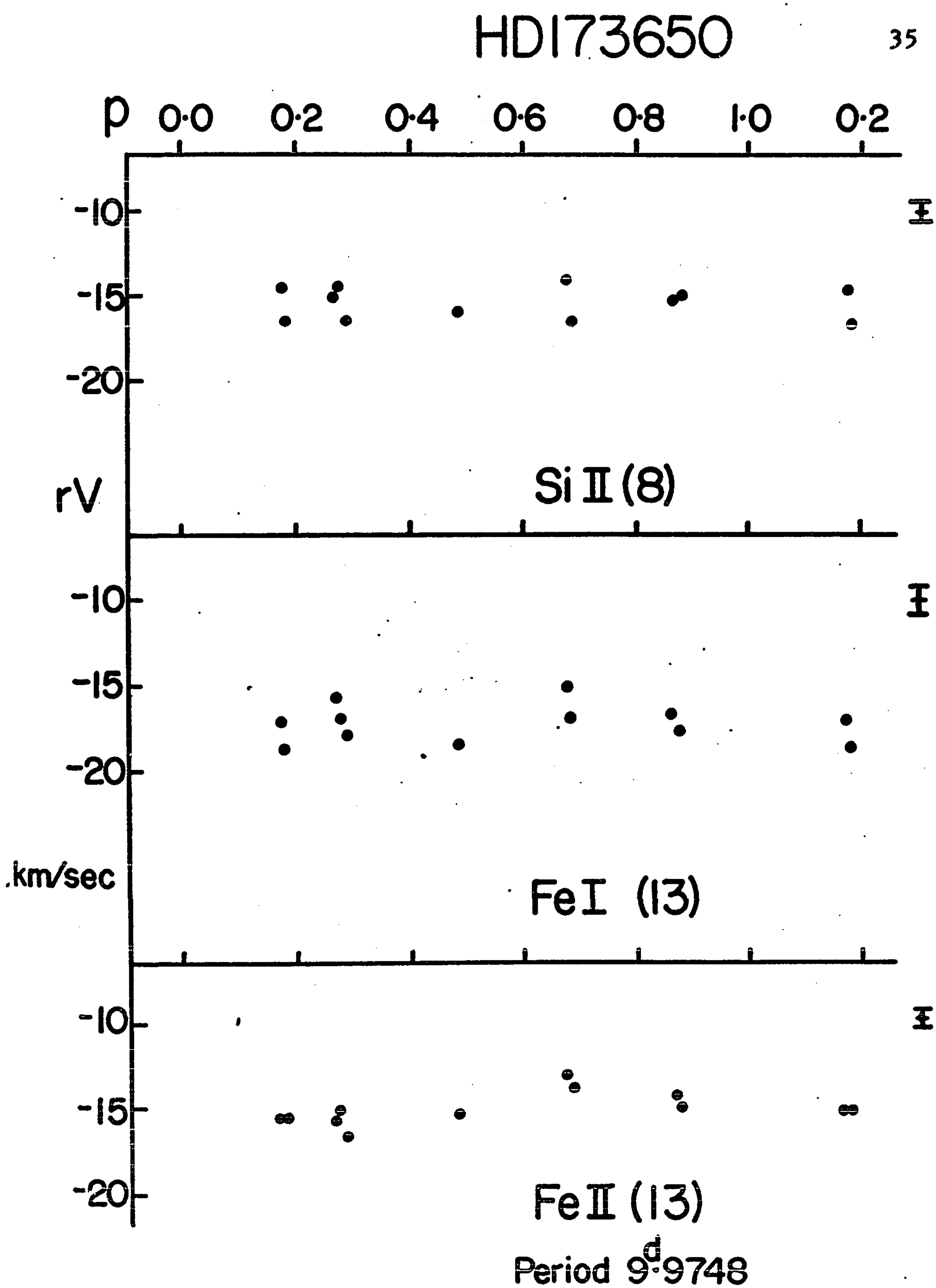
HD173650
p
0·0
0·2
0·4
0·6
0·8
1·0
0·2
-10
-15
-20
Si II (8)
rV
-10
-15
-20
.km/sec
Fe I (13)
-10
-15
-20
Fe II (13)
Period 9ᵈ9748

FIGURE V,3

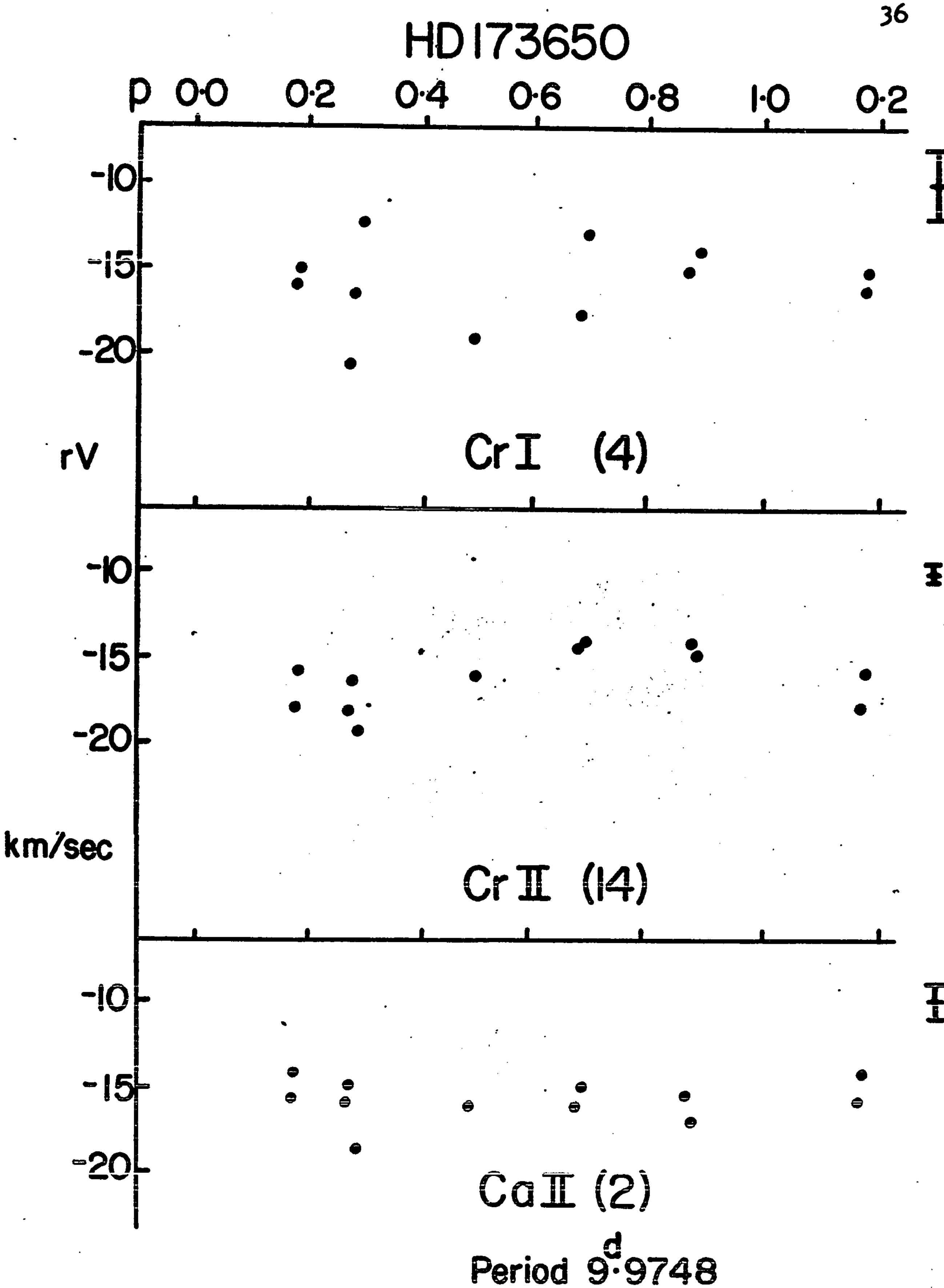
HD173650
p 0·0 0·2 0·4 0·6 0·8 1·0 0·2
-10
-15
-20
rV
Cr I (4)
-10
-15
-20
km/sec
Cr II (14)
-10
-15
-20
Ca II (2)
Period 9^d·9748

FIGURE V,4

Another point of note is the systematic difference in velocity between the Fe I and Fe II values. The wavelength values from C. Moore are not necessarily good values for radial velocity work, particularly as they are gathered from many sources and are in many cases only given to two decimal figures of an Angstrom. This is probably not a sufficiently large source of error to explain a systematic difference of from 1½ to 2 km/sec. An unknown factor that would be sufficiently large to explain this is the possibility of a certain amount of weak blending in the lines selected for Fe I and Fe II and the presence of some blending could easily produce a systematic difference of this magnitude even when restricted to a few lines. An inspection of the velocity residuals for each line helps to rid the observations of the worst of this source of error.

The maximum of the V_r curve would appear to occur around phase 0.80 which is one quarter phase after the maximum of both the light curve and the line intensity variation curves. This is precisely what one would expect from the oblique rotator model of the A_p stars. One would also expect that elements such as SrII and MnII, which show more pronounced line strength variations, would show stronger radial velocity variations than say Fe II which has a reduced line strength variation. This effect appears to be present as the variation of Mn II and Cr II is greater than that of Ti II, and Ti II varies more than Fe II. This is the same order in which one would put the elements if he were ordering them according to decreasing equivalent width variation from Figures IX,1 and 2.

CHAPTER VI

CURVE OF GROWTH

There is much discussion in the literature over the advantages and disadvantages of the various curve of growth procedures. While a complete review of the errors involved in curve of growth is not appropriate here since an absolute abundance analysis is not the principal aim of the thesis, the problem of the choice of procedure must be given some consideration.

In general, the sources of error in abundance analysis are, in order of decreasing significance, the equivalent widths, the log gf values, and the theoretical curve of growth that is adopted. Once one has done his best in measuring the equivalent widths and has selected the best available log gf values for the observed lines, he has then to choose the method of analysis. Normally one is concerned, when examining the various procedures for abundance analysis, with the accuracy of the model assumed for the atmosphere. With the simpler curve of growth procedures one assumes an isothermal atmosphere, an assumption which is clearly not correct; with the more sophisticated techniques one attempts to use an accurate relation of temperature with optical depth. When application of these procedures to an A_p spectrum variable is contemplated a much more serious problem appears. All abundance analysis procedures assume an atmosphere that may vary with depth but not with position on the surface of the star, and this assumption is believed not to apply to the spectrum variables which, under the oblique rotator hypothesis, have variations in abundances and atmospheric parameters over the stellar surface. At first glance it would appear that the situation with regard to curve of growth analysis is rendered completely hopeless. It would seem though that the region on the surface of the star that is responsible for the line strength variability must occupy a very large percentage of the visible surface at line strength maximum, or at the very least contribute a very large percentage of the observed light, otherwise line strength variations by a factor greater than two in this case would be impossible in lines such as λ4077 SrII that are already quite strong lines. Furthermore if the regions were quite small in general in spectrum variable A_p stars then one would expect some stars at least to have a "squared" appearance to their line strength cycle. If, as I have just argued and as the harmonic analysis reported at the end of the thesis indicates, the variations across the visible disc of the star are fairly regular and there are not isolated regions of quite extreme conditions, then it can be hoped that a curve of growth analysis at all phases will provide some information about the differences between the areas of minimum line strength and those of maximum. Since it is impossible to obtain the distribution of line strength over the surface of the star for each line that could be used in an abundance analysis then we must be content with this situation. Quite clearly though there is little point to using a conventionally refined model of the atmosphere of the star if the conditions in the atmosphere vary from point to point on the star. Even if the star were uniform one would not be allowing a serious error in the abundance determination by using an isothermal model since Aller and Ross (1967) find that "the Milne-Eddington model, interpreted with the Wrubel curve of growth, gives results that agree surprisingly well, for most elements, with those found by the more elaborate methods, whenever we have made comparisons". With a non-uniform star such as HD173650 the simpler procedures will serve as well as the more complicated.

This raises the question of which of the Shuster-Schwarzschild (pure scattering or absorption) or Milne-Eddington (pure scattering or absorption) models is to be adopted. Aller (1956) has compared the Shuster-Schwartzschild (Ünsold 1938) and both Milne-Eddington models. He finds that one obtains substantially the same temperature and ionization equilibrium results for all models. The abundances for the M-E scattering curve and the Ünsold curve compared quite well and the M-E absorption would appear from a table to run perhaps -0.10 dex different, on the average, from the mean of the former two. There was a substantial difference in microturbulent velocity between the three models, however, since the vertical shift was 0.20, in the log, for the M-E scattering, 0.35 for the Unsold curve and 0.60 for the M-E absorption model. This suggests that as far as the abundance, temperature and log Pe results are concerned, there is little difference between the methods. With this in mind it was decided, because much published work has been based on the Wrubel (1949) curves, that the Milne-Eddington pure scattering model should be used. The advantage to be gained was that it would provide ease of comparison to other published results.

a) Procedure and Results

The references for log gf values were used in the following manner. For neutral elements the values were taken from the Corliss and Bozman (1962) monograph and the FeI values were supplemented by the Corliss and Warner (1963) reference. Warner (1967) points out that the Corliss and Bozman log gf values for once ionized elements are in error by a considerable factor. He has compiled a large catalogue of values for singly ionized elements, and he has been careful to keep his results on the same absolute scale as the values of Corliss and Bozman. The very extensive table of log gf values by Corliss and Warner are a review of the best values for FeI. The remainder of the values were obtained from the references in the bibliography for log gf values and the references are arranged in order of preference.

Wrubel (1949) has computed the variation of $\log\left(\frac{W}{\lambda}\frac{c}{V}\right)$ with $\log \eta_c$ using Chandrasekhar's solution, on the pure scattering hypothesis and in a Milne-Eddington model, of the transfer equations. In this model, η_c is the ratio at the centre of the line of the opacity due to the line to the continuum opacity. Its value is given by:

$$\log \eta_c = \log N_r - \theta\chi - 1.824 + \log gf\lambda - \log Vu(t) - \log \kappa + \Delta \log \eta$$

When one has estimated $\log N_r$, θ and V correctly, the observed variation of $\log \left(\frac{wc}{\lambda v}\right)$ with $\log \eta_c$ should "fit" the theoretical curve as closely as possible(Aller 1963).

The procedure followed here was to estimate the values of θ , V and log Pe and to compute from these the opacity in the continuum κ, the partition function u(t) and $\Delta \log \eta$. $\Delta \log \eta$ is a small correction given by Wrubel as a function of $\log \left(\frac{wc}{\lambda v}\right)$ and T_o, the boundary temperature of the star (assumed to be 7500°K here). These values allow one to compute a value of $\log \eta_c - \log N_r + \Delta\theta\chi$ which is plotted against $\log \left(\frac{wc}{\lambda v}\right)$ and the vertical shift in the plot required to fit it to the theoretical curve of growth provides the correction factor for $\left(\frac{c}{v}\right)$. When the fit to the theoretical curve of growth is accomplished, the horizontal shifts between each line and the theoretical curve $\Delta\theta\chi$ can be established, and the slope of a plot of these shifts against χ provides the correction to the estimated excitation temperature. One follows this procedure iteratively until satisfied with the result, and at that point the horizontal shift to fit the curve of growth is used to determine $\log N_r$. When one has evaluated $\log N_r$ for two ionization levels of a given element, usually FeI and FeII, by assuming the excitation temperature and ionization temperature are equal, the electron pressure can be obtained from the Saha equation. With the corrected electron pressure, the curve of growth procedure is repeated for FeI and FeII and continued for all other elements. The value of log Pe provided by this method was 2.88. For this work, plates of the same phase were grouped together and an average equivalent width was used for each line. One plate (0.685) was exempted from this procedure because it had apparently consistently higher equivalent widths than its co-phase partners and it was analysed separately. The results of the analysis are given in figures VI,2(a) and 2(b) where N_r is the number of atoms per gram of stellar material. Some representative curves of growth for average phase (0.68) are given in figures VI,1(a), 1(b), 1(c). While the plate at phase 0.685 was singled out for separate attention, it will be noticed that the curve of growth results derived from this one plate do not deviate markedly from the results obtained from the mean line strengths of the other two plates at this phase. For the curves of growth of FeI, FeII and CrII, estimates of the error involved in fitting to the theoretical curve can be made with some confidence, but errors are hard to assess for the other curves of growth. As a result of this situation, one should be careful in drawing conclusions about the oblique rotator model from the curve of growth unless the results of the analysis of FeI, FeII and CrII support these conclusions. The other elements should only be used for the overall abundance analysis of the star and perhaps to support any conclusion drawn from the better results.

It would appear from the curve of growth that the line strength change for CrII and perhaps SrII is caused primarily by an apparent change of about a factor of two in abundance and a fairly strong change in microturbulent velocity. For FeI and FeII there is a much smaller change in abundance if any change at all, but there is still the variation in microturbulence. The results for MnII and CrI exhibit considerable scatter, but CrI still shows a strong microturbulent velocity variation. TiII would appear to have quite a constant abundance but shows again a pronounced variation in microturbulent velocity. These values bear a striking resemblance to the ones derived for CrII and FeII in α^2CVn by the Burbidges (1955). For α^2 C Vn it was found that the microturbulent velocity ranged from 2.2 km/sec for CrII at zero phase to 3.6 km/sec at phase 0.5 with a Δlog N of 0.22. For FeII the microturbulent velocity ranged from 2.9 km/sec to 3.8, and Δlog N was 0.15. These observations would indicate a fairly strong role for the phenomenon known as microturbulence in the cause of line strength variations in A_p stars.

The mean abundances over all phases, given on a log H = 12.0 scale to facilitate comparison with the other stars, are presented in table VI,1 along with the G.M.A. solar abundances and abundances for a selection of peculiar A stars of approximately the same temperature. The conversion to the log $H = 12.0$ scale was made by assuming $X = 0.65$ for HD173650. As can be seen from the values given in the table, Fe tends to be slightly more abundant than is typical for other A_p stars of about the same temperature and Cr is definitely more abundant in HD173650. There are nine stars of approximately the same temperature listed by Aller and Ross (1967) and in no case is the abundance relative to the sun for Cr greater than +1.05 which is significantly less than +1.52 in HD173650. Among the nine examples given by Aller and Ross there are two that display a greater abundance of Fe compared to the sun than HD173650 with the extreme case being HR6870 at +2.12.

It is very often assumed that the line strength variation is indicative of an abundance variation over the surface of a peculiar A star. An alternative to this was a suggestion put forward by Tai (1939) and revived by Bidelman (1967). This alternative suggests that in α^2 C Vn the rare earth elements such as Europium are primarily in the form EuIV and that temperature variations of a "few thousand degrees" and the accompanying variations of electron pressure will cause a significant variation in EuI and EuII. The lack of variation in SrII is explained by the fact that it has a much higher third ionization potential (43 ev) than most of the rare-earths. In the case of HD173650 this mechanism would seem to be very unlikely since both the curve of growth results for FeII and FeI, two of the best curves, and the lack of colour variation indicate little temperature change. In fact the FeI and FeII curve of growth determination of the temperature being constant to within $\Delta\theta = \pm 0.2$ is not as severe a requirement on the constancy of the temperature as the one which would be determined if one were to assume the brightness and colour variations were entirely due to temperature changes. The curves of growth also show little relative abundance variation for FeI and FeII and this would indicate very little electron pressure variation. What the curves of growth do show is that while there would appear to be an abundance variation for most elements of only about a factor two there is a pronounced microturbulent velocity variation apparent in all cases.

b) Transverse Field and Magnetic Intensification

Before an analysis of line profiles is performed for a magnetic star, it is useful to know to what extent the magnetic field could be distorting the profiles. In HD173650 the measured longitudinal field corresponds to a separation in the σ components of only about three hundredths of an Angstrom when the field is strongest. Any distortion due to this field would seem to be insignificant in lines of minimum half widths of 0.3 A but while the average field, as indicated by the displacement of the tips of the line profiles as seen on the spectrograms of the Zeeman analyser, may be sufficiently small that it would seemingly have little effect upon the profiles, there may be large field fluctuations over the star that could cause a distortion of the profiles but show little average field. There may also be large transverse fields in the star that would go undetected in Babcock's Zeeman analyser but that would again cause distortions of the line profiles. Fortunately, if field effects exist that are great enough to seriously distort the line profiles, one would expect to see an increase in equivalent width in those lines which fall on the saturated portion of the curve of growth. This Zeeman intensification can be used to test for possible effects of the magnetic field on the line profiles.

Any mechanism which broadens the line absorption coefficient of a line which falls on the saturated portion of the curve of growth will increase the equivalent width of that line. Two such broadening mechanisms are the total doppler broadening, made up of thermal and microturbulent motion, and the Zeeman splitting. For a magnetic field the important quantity is Z, the intensity-weighted mean displacement of the σ components of the lines in Lorentz units, i.e., if Z is multiplied by the Bohr magneton and magnetic field, it gives the mean energy separation of the σ components. Z is obtained, if one assumes L-S coupling, from the following expressions where 1 refers to the lower level and 2 to the upper. For a $\Delta M = -1$ transition, the displacement from the zero field position of the line in Lorentz units for each component is

$$\text{Displ}\ (1) = (G(1) - G(2)) * M + G(2)$$ where G is the Landé g factor.

The intensity weighting for each line of the pattern is given by one of the following equations.

For the case $J \rightarrow J$ the weighting is

$$\text{Int }(I) = (J(1) + M) \times (J(1) - (M-1)),$$

for the case $J \rightarrow J-1$ it is

$$\text{Int }(I) = (J(1) + M) \times (J(1) + (M-1)),$$

and for the case $J \rightarrow J+1$ it is

$$\text{Int }(I) = (J(1) - (M-1)) \times (J(1) - (M-2)),$$ where M is the M value of the lower level of the transition.

Z is now given by

$$Z = \frac{\sum \text{Int }(I) \times \text{Displ }(I)}{\sum \text{Int }(I)}$$

and the summations are taken over all permitted components of the $\sigma\,(\Delta M = -1)$ pattern. If the mean separation of the components is of the order of the broadening due to thermal and microturbulent velocities or greater , then the magnetic field will begin to increase the equivalent widths of those lines which fall on the saturated portion of the curve of growth. If this zeeman intensification occurs, the profile of the non-rotationally broadened line (i.e. the line that one would see if the star were not rotating) can be suspected of being affected by the magnetic field. Where there is no Zeeman intensification one can feel confident that the profiles are not significantly affected by the transverse component of the field.

To search for Zeeman intensification, those lines which were on the shoulder or saturated portion of the curves of growth for FeII and CrII were measured for vertical displacement from the curve of growth. This displacement was plotted against Z for each line at each phase of the star's cycle. The plots so created did not appear to deviate from a straight line for even the largest Z values, and this indicated that there was no observable Zeeman intensification and that the effect of magnetic broadening could be ignored. Figure VI,3 illustrates this for one phase of CrII and FeII.

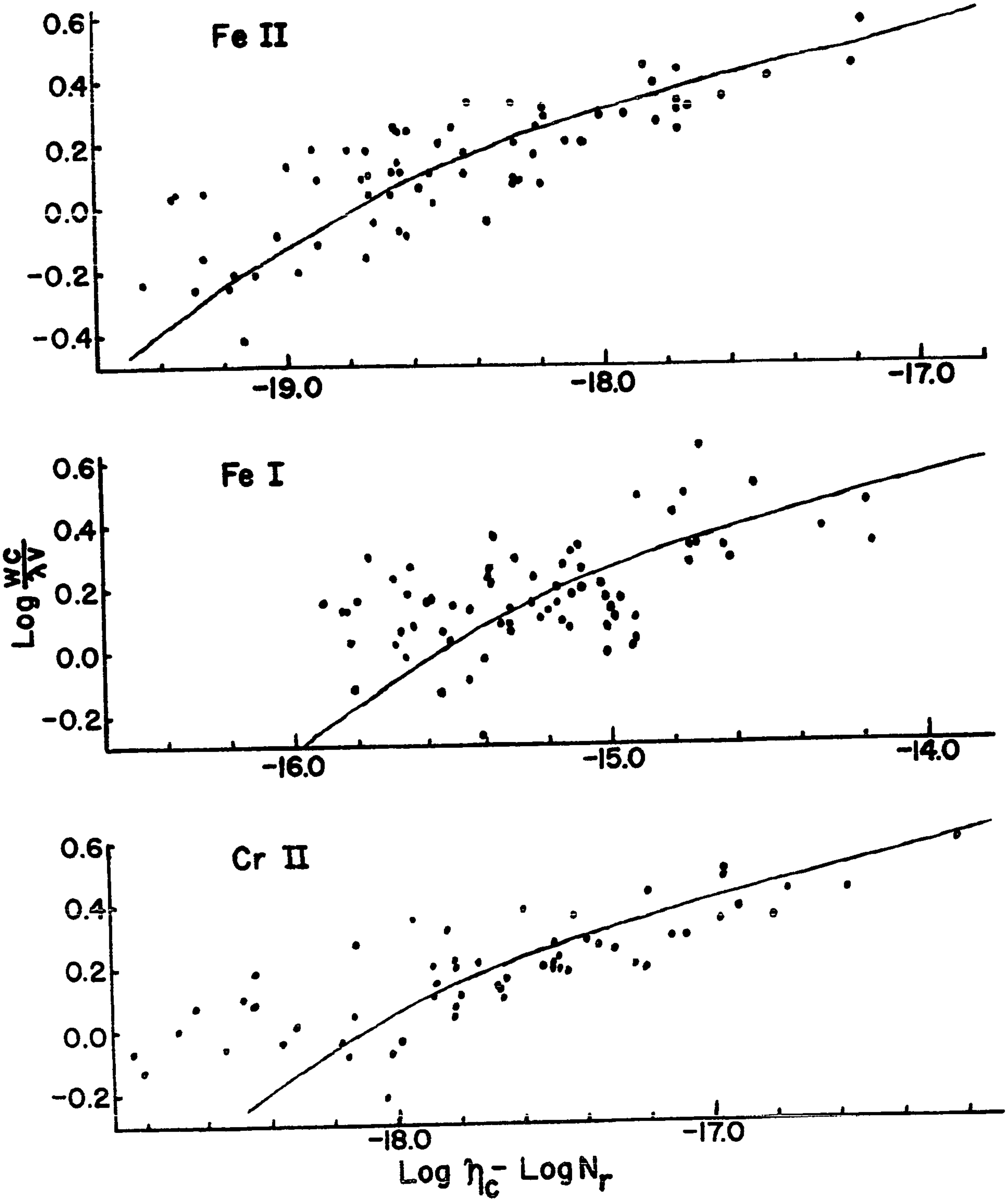

FIGURE VI, I (a) CURVES OF GROWTH PHASE=0.68
LOG a = -1.8

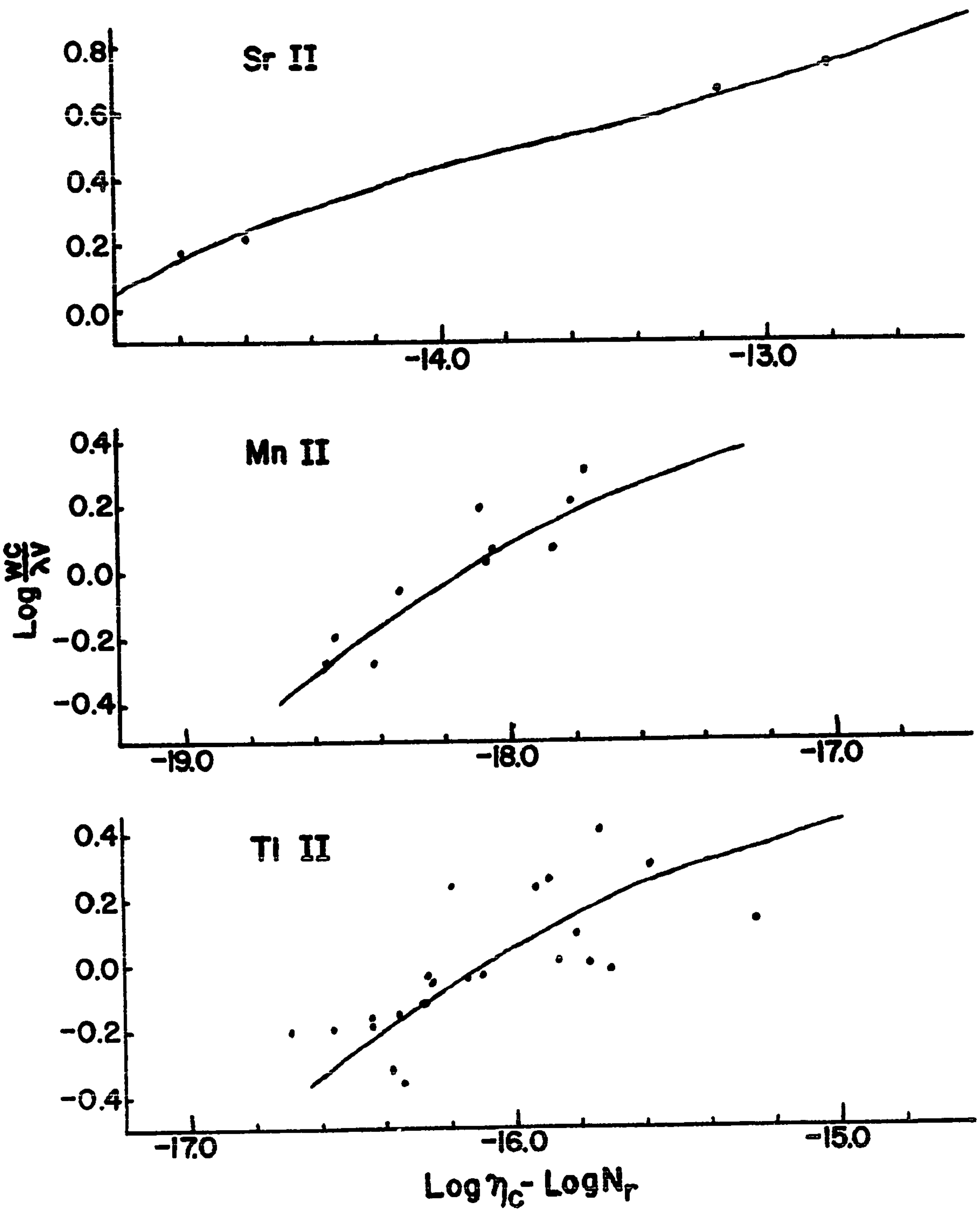

FIGURE VI,1(b) CURVES OF GROWTH PHASE=0.68
LOG a = -1.8

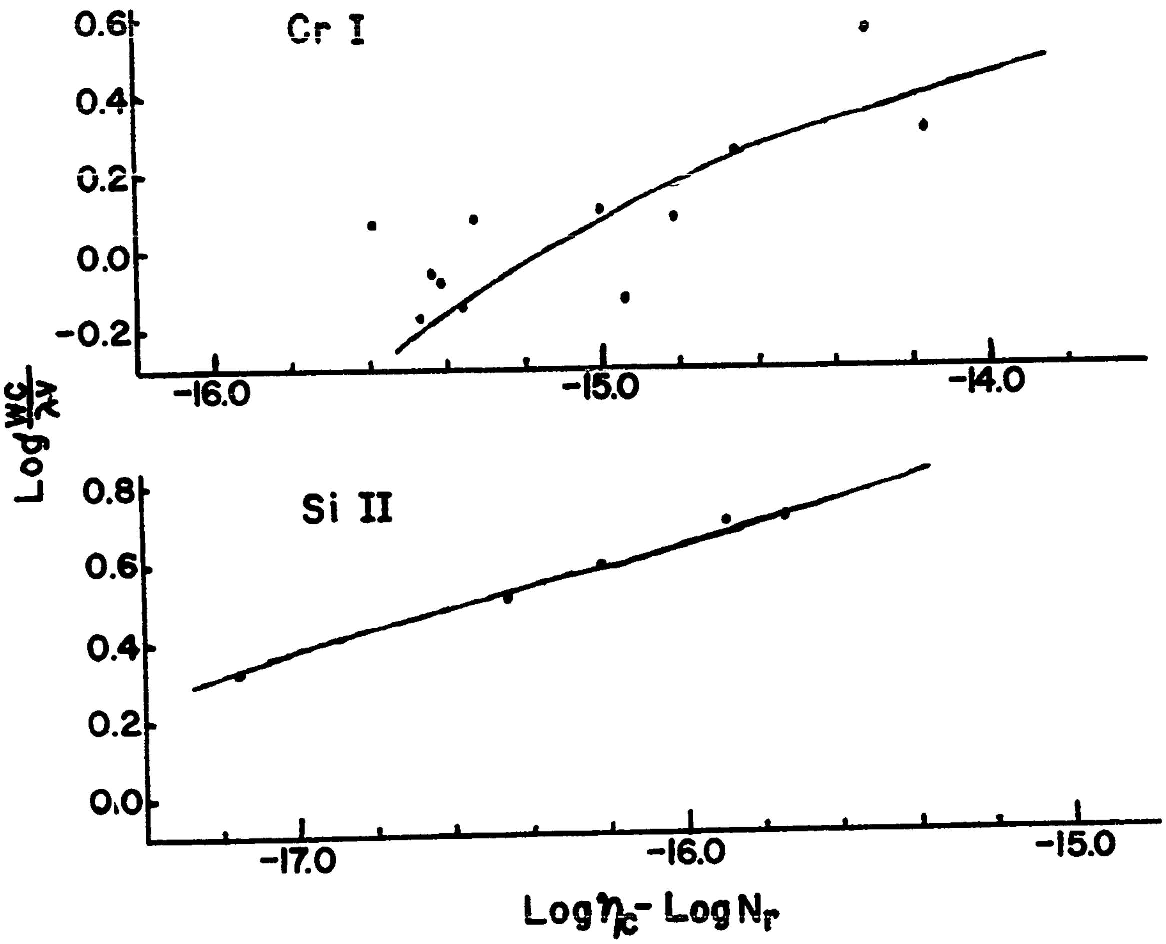

FIGURE VI, I (c) CURVES OF GROWTH PHASE=0.68
LOG a = -1.8

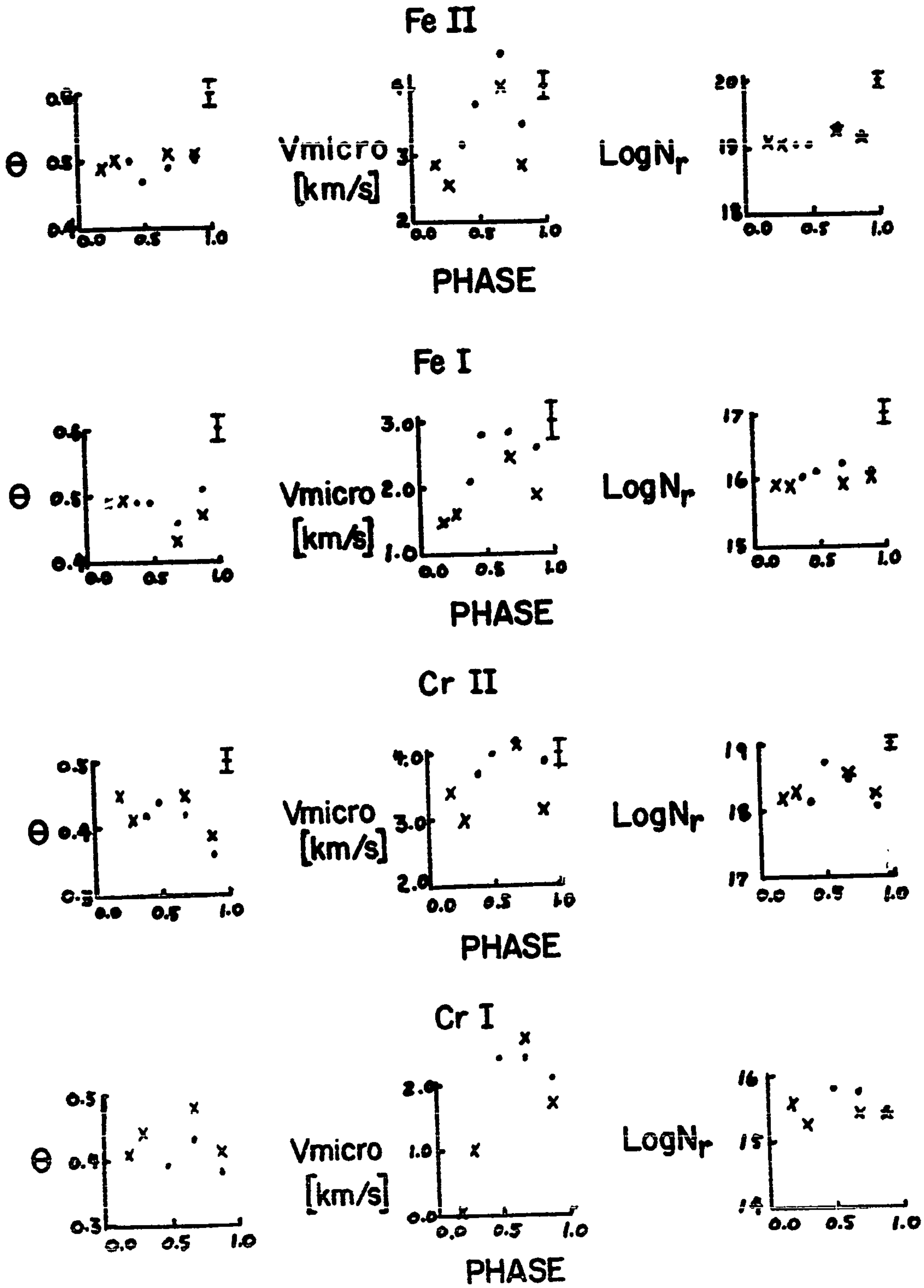

FIGURE VI, 2(a) X - curve of growth result obtained from mean equivalent widths of two or three plates.
• - curve of growth result obtained from equivalent widths of one plate.
errors are estimates.

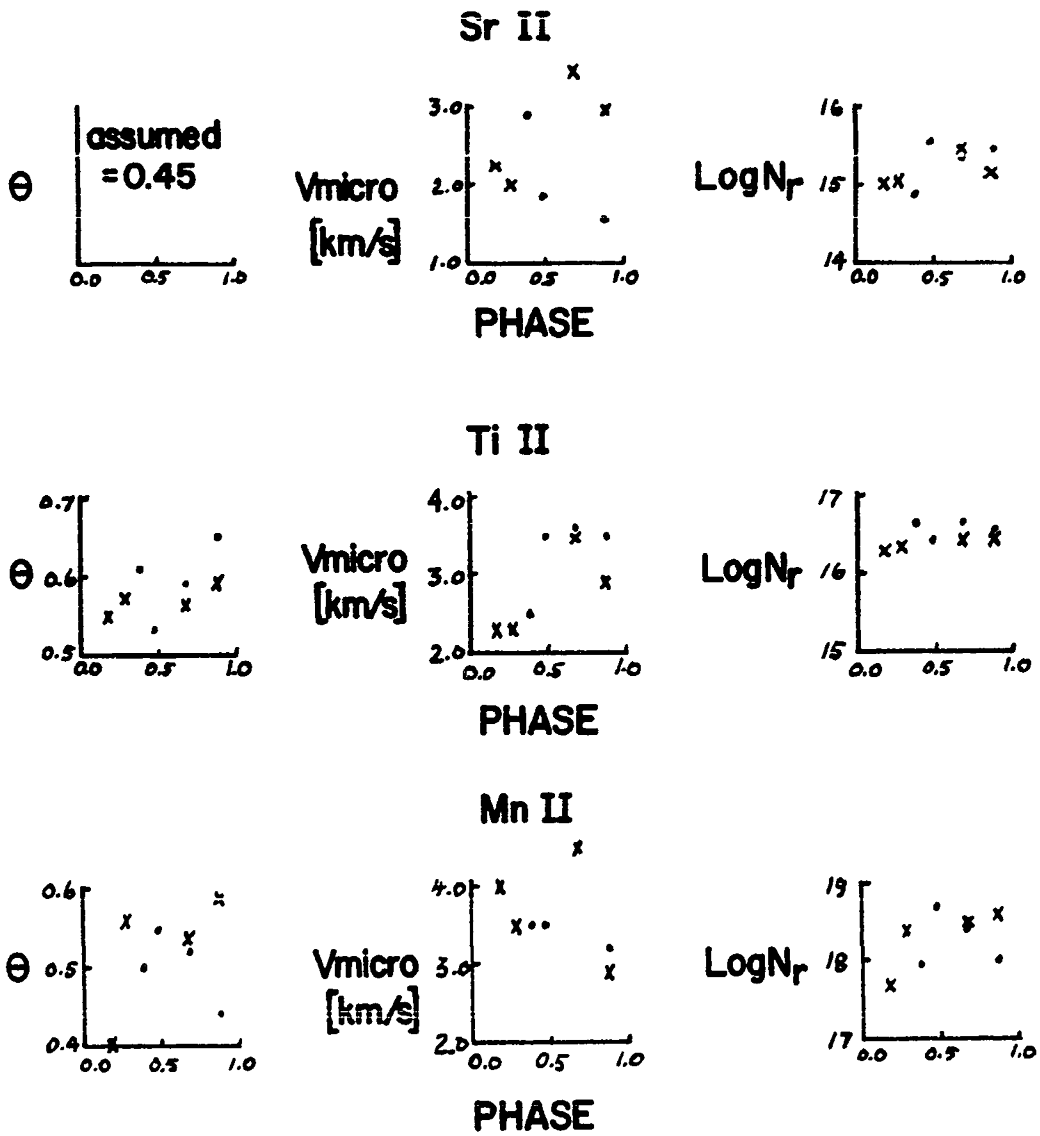

Sr II
Θ
assumed
=0.45
Vmicro
[km/s]
LogNr
PHASE
Ti II
Θ
Vmicro
[km/s]
LogNr
PHASE
Mn II
Θ
Vmicro
[km/s]
LogNr
PHASE

FIGURE VI, 2(b)

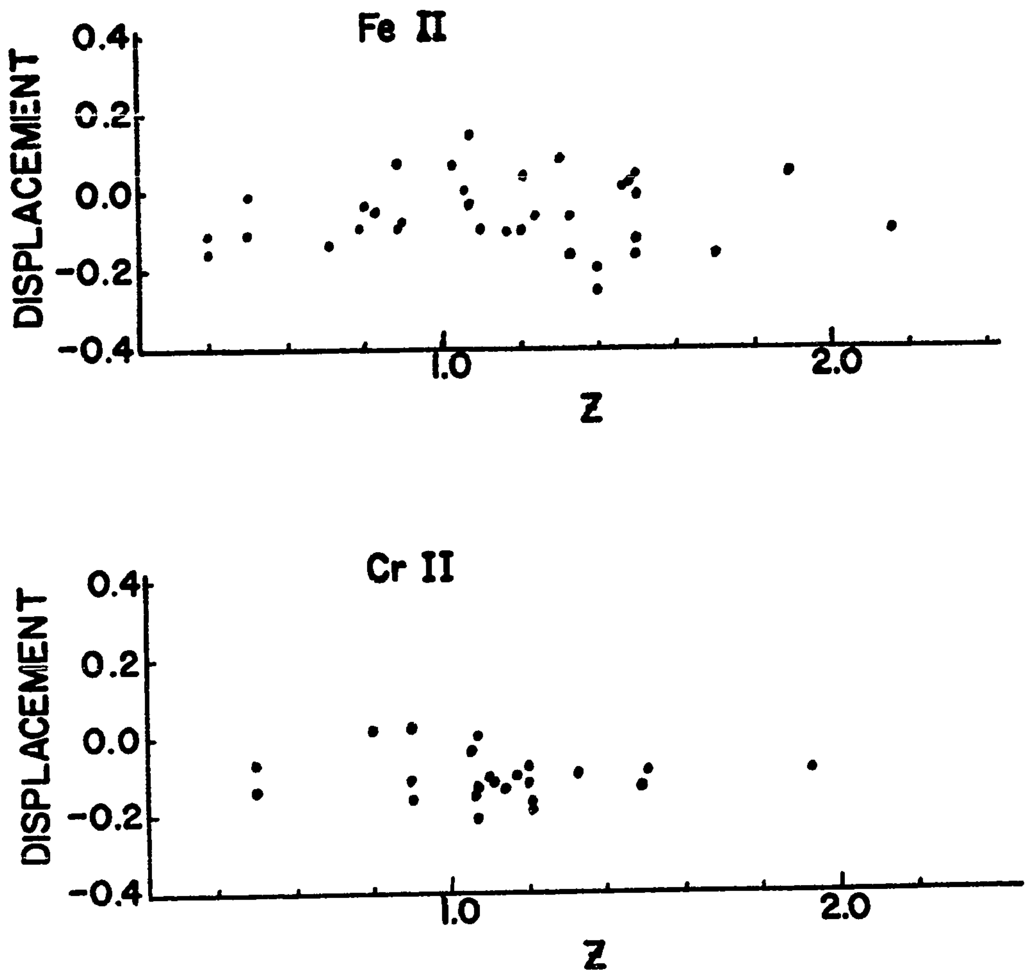

FIGURE VI,3 PHASE=0.68

Vertical displacement from curve of growth of lines of FeII and CrII plotted against Z.

TABLE VI,1

	HD173650		GMA	i Cr B	χ Lup	ϕ Her
Sp	A0p			A0Vp	B9p	B9p
Te (^{o}K)	12,500 estim.			12,500	11,080	11,450
Fe	7.58		6.57	+0.8	+ 0.62	+ 0.30
Cr	6.88		5.36	+0.6	+ 0.3?	+ 0.90
Sr	4.94		2.60	+2.0	+ 2.45	---
Mn	6.87		4.90	+1.70	---	+ 0.8 poor
Ti	5.14		4.68	+0.72	+ 0.45	+ 0.26
Si	6.97	± 0.15	7.50	0.0	-1?	0.0
Gd	$\lesssim$ 5.0	very poor				
Eu	$\approx$ 5.2	poor				

The mean abundances for HD173650 and the GMA solar abundances are on a log H = 12.0 scale and the abundances for the other stars are log N (star)/N(sun), again on the assumption of log H = 12.0 for each object. Comparison abundances are taken from Aller and Ross (1967). Note that a suspected helium deficiency in the hotter A_p stars may require that the values for HD173650 be revised slightly downward. If the value for X were 0.90 (as has been determined for 53 Tauri) the revision would be to reduce all values by 0.14.

CHAPTER VII

INCLINATION OF THE ROTATIONAL AND MAGNETIC AXES

The oblique-rotator model is premised on the assumption that the spectrum and magnetic variability is due to rotation, and consequently the period of the spectral and magnetic variations is the same as the rotational period. Since one can determine the value of Ve sin i from the profiles of the lines in the spectrum and if the photoelectric results are used to determine the radius of the star, one can then directly obtain Ve from the period and radius, and then sin i. For a preview of the final model of the star a simple model consisting of one patch at one magnetic pole of the star may be assumed. To determine the appropriate latitude for the spot one may estimate from the radial velocity amplitudes and from the range of line strength variation of each element, the velocity of the patch where that element is concentrated as it comes around the limb of the star. The velocity of the patch divided by Ve sin i gives the value of sinβ where β is the co-latitude of the centre of the patch and the presumed inclination of the magnetic axis.

a) The Rotational Velocity Ve sini

As a preliminary step, the curve of line depth was used to estimate the value of Ve sin i and to assess possible variations of profile with phase. The curve of line depth is a procedure developed by Huang and Struve (1955) to derive Ve sin i from the slope of the line depth versus equivalent width relation at the point of zero equivalent width and zero line depth. As it turns out, the procedure did not work very well for this star since a study of the mean profiles, which will be reported in the following sections, showed that the author has a tendency when drawing in the weakest lines on the traces to make them slightly deeper and narrower than they should be. This means that the value for Ve sin i of 13.1 km/sec, which is a mean value of the curve of line depth results of all plates for the lines of FeII and for CrII (each element done separately), is not reliable and is probably too low. There is some value in the results though and the value is that they suggest there is little, if any, change in the line profiles of the star during its cycle. If the spot of line strength concentration on the star is sufficiently small that it occupies only a small portion of the visible disc at the phase of line strength maximum say, then one would expect that the rotational broadening of the lines would be reduced and the lines would be deeper and narrower at this phase than at other phases. This should be true for only variable lines and one would expect that the effect might be more pronounced in some elements than in others. One must be assured then, if the line profiles are to be analysed for the rotational broadening, that the profiles used as standards are not characteristic of a phase in the star's cycle when the lines are narrower as a result of the above mechanism than would be predicted by a uniform line strength distribution. It was found when doing the curve of line depth that the separate values for Ve sin i for CrII deviated from the mean value of 13.1 km/sec by more than 1 km/sec at only two phases, 0.28 and 0.68, and those for FeII deviated by more than 1 km/sec at phase 0.68. At phase 0.68 the value for Ve sin i for CrII was 15.0 km/sec and that for FeII was 11.4 km/sec for an average of 13.2 km/sec so that these deviations are regarded as insignificant. This result suggests that the area or areas of line strength maximum are sufficiently extensive that they cause little variation of the line profiles of the variable lines. The result also shows that the mean profiles, developed for the measurement of equivalent widths, can be used as standards for the profile analysis which follows and which is intended to give a value for Ve sin i.

For the purposes of obtaining a more accurate estimate of the value of Ve sin i, a computer programme was created to produce theoretical profiles of stellar lines using as input the parameters of the atmosphere derived from the curve of growth and a variety of values of Ve sin i. The programme was also designed to compute rotationally broadened line profiles arising from stars with rotationally symmetric line strength distributions on the stellar surface. These distributions were represented by the expression

$$W_\lambda = 1 + A_2^0 P_2 = 1 + A_2^0 \left(3/2 \cos^2\theta - \tfrac{1}{2}\right)$$

where θ is co-latitude on the star and A_2^0 an arbitrary parameter. Such a distribution gives a belt of line strengthening around the rotational equator if A_2^0 is negative and line strengthening at the poles if A_2^0 is positive. This distribution or component of a distribution is not detectable by an analysis of line strength or radial velocity variations.

The mean profiles of lines in the star that were determined for the measurement of equivalent widths were the profiles that were required to be reproduced by the computer programme for the evaluation of Ve sin i. The instrumental broadening was removed from these profiles by an iterative procedure consisting of storing the observed and instrumental profiles in the computer along with an approximation to the true profile. A convolution of the approximate and instrumental profiles was performed according to the following expression:

$$O(\lambda) = \int T(\lambda - \lambda') * I(\lambda') \, d\lambda'$$

and the result compared with the observed profile. If the convolution was insufficiently close to the observed profile, the approximation to the true profile was adjusted and the procedure repeated. The instrumental profile used for this purpose was obtained by taking a tracing of the comparison lines on plate 3280 using the same calibration curve that had been used for the stellar spectrum. A comparison line whose central density on the plate was approximately the same as the stellar continuum was used as the standard for the instrumental profile. Since the source for the comparison spectrum was a hollow cathode iron-argon tube that has a low operating temperature, it was not necessary to correct the profile of the comparison line for the thermal broadening of the source. Since the stellar lines had, at their narrowest, a half width of three times the half width of the instrumental profile, the effect of instrumental broadening was quite small. The two sets of stellar profiles, with the instrumental broadening removed, and the instrumental profile itself are given in figure VII,1.

The programme for the theoretical profiles used the empirical formula

$$R_\nu = R_c * \frac{N \alpha_\nu}{1 + N\alpha_\nu}$$

where R_ν is the line depth and R_c is the central line depth for strong lines in the stellar spectrum. This formula was suggested by Munch (1958) as appropriate for stars at the hotter end of the spectral range. R_c must be determined empirically and the curve of line depth relations had already suggested a value in the neighbourhood of 0.60 which seemed at first appearance to be rather small. Values of R_c as small as 0.50 can be found in the literature though (eg. Aller 1956) so the value 0.60 would appear to create no problems. There were two subroutines to the main programme, one of which supplied α_ν to the programme as computed from the classical expression for the line absorption coefficient assuming the damping constant from the curve of growth. The other subroutine supplied the rotational profile $A(\Delta\lambda)$ using the integral

$$A(\Delta\lambda) = \int_{-1}^{+1} \int_{x=-\sqrt{1-y^2}}^{x=\sqrt{1-y^2}} f(x, y, i)\, dx\, dy$$

where the X axis is defined on the apparent disc of the star as being along the projected rotational axis and having its origin at the centre of the disc. The disc is taken to have unit radius.

We also define

$$y = \frac{c \quad \Delta\lambda}{\lambda \; (V_e \sin i)}$$

and f(x,y,i) is the product of limb darkening and the line strength distribution assumed for the star. In this case the limb darkening was assumed to be u = 0.48 in the expression $I = 1 + u - u\cos\theta$ and the line strength distribution was assumed to be, as discussed earlier, $w_2 = 1 + A_2^0 P_2$, which is a function of $\cos\psi$ (ψ being the rotational co-latitude) and must now be converted to a function of x, y and i where i is the rotational inclination.

The computing procedure required first the calling of the two subroutines to provide the line absorption coefficient and the rotational profile. A trial value of R_c was adopted and the Munch formula was used with successive approximations to N until the equivalent width of the profile matched the true equivalent width. A convolution was then conducted with the rotational profile and the one achieved with the Munch formula to give the observed profile. This procedure was followed iteratively, each time with improved input values, until the computed profiles matched, as well as possible, the observed profiles.

The profiles that seemed to fit the observations best are shown in figures VII,2 and 3. For the profiles at λ 4450 the parameters for the theoretical profiles were $A_2^0 = 0.0$ or -1.0 with V sin i $= 15.0$ km/sec., $i = 80^o$ and log a $= -1.4$. The central part of the line profile would appear to be the most sensitive to changes in A_2^0 and for these profiles the slope of this region is best reproduced for $A_2^0 \approx +1.0$ and V_e sin i $= 15.5$ km/sec. As can be seen though, any judgement about the non-uniformity based on these profiles can at best be quite crude. For the profiles at λ4000 the best overall fit is achieved with $A_2^0 \approx -1.0$, V sin i ≈ 15.5 and $i \approx 80^o$ although the weaker lines are very well represented by the profiles corresponding to $A_2^0 = 0.0$, V sin i $= 15.5$ and $i = 80^o$. Again the value of log a was -1.4 which deviates somewhat from the value (-1.8) assessed from the curve of growth. The value of -1.4 is on the larger end of the range of values that the curve of growth would apparently allow one to use for log a. A slightly larger value yet of log a would produce a better fit to the second and third strongest profiles but the author was reluctant to stray too far from the values consistent with the curve of growth. The profiles numbered in order of increasing equivalent width, two, three and four, were considered to be the most important for the purposes of determining Ve sin i since the stronger profiles are primarily determined by the values of log a and microturbulent velocity in this case and the weakest profile probably has a poorly determined shape since the noise on the micro-photometer tracing is a significant proportion of its depth. It would appear in fact from the computed profiles that the observed shape of this profile is badly biased by the author's pre-conception of its shape as it is far too narrow and deep to be consistent with the remainder of the profiles. The bias in drawing these profiles for the weaker lines would also account for the curve of line depth indication of a somewhat smaller rotational velocity than that required by the computed profiles, since a method which depends on the slope of the depth vs. equivalent width relation as the equivalent width goes to zero, will be sensitive to errors in the weakest lines. The value of R_c required for these profiles was 0.58 for the wavelength region λ4000 and 0.54 for λ4450. A set of profiles with $R_c = 1$ are given to indicate the drastic difference between the profiles with the above values for R_c and those if you assume $R_c = 1.0$.

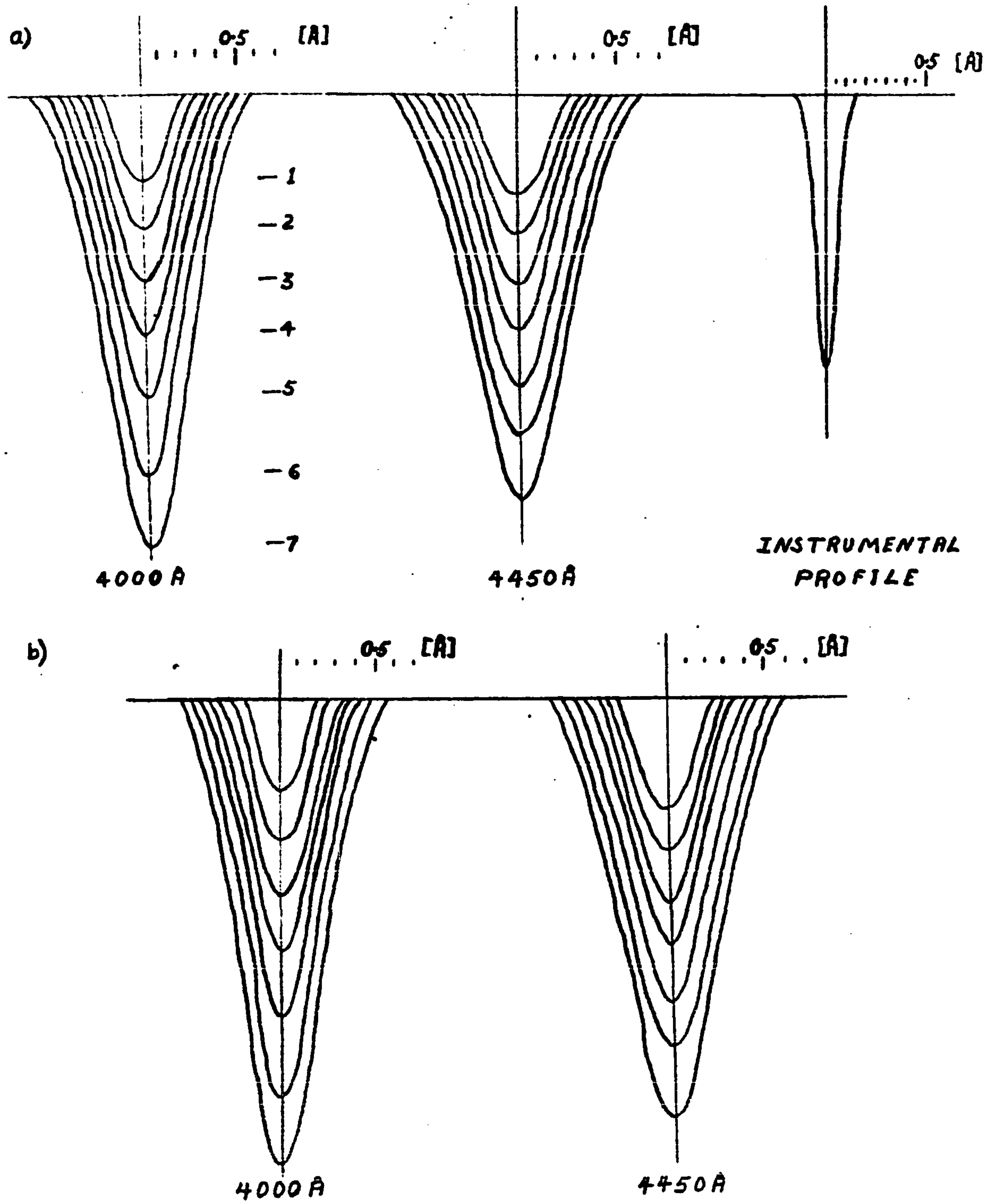

a) OBSERVED PROFILES - CONTINUUM HEIGHT IS FIVE INCHES

b) PROFILES WITH INSTRUMENTAL BROADENING REMOVED

FIGURE VII, 1 OBSERVED PROFILES

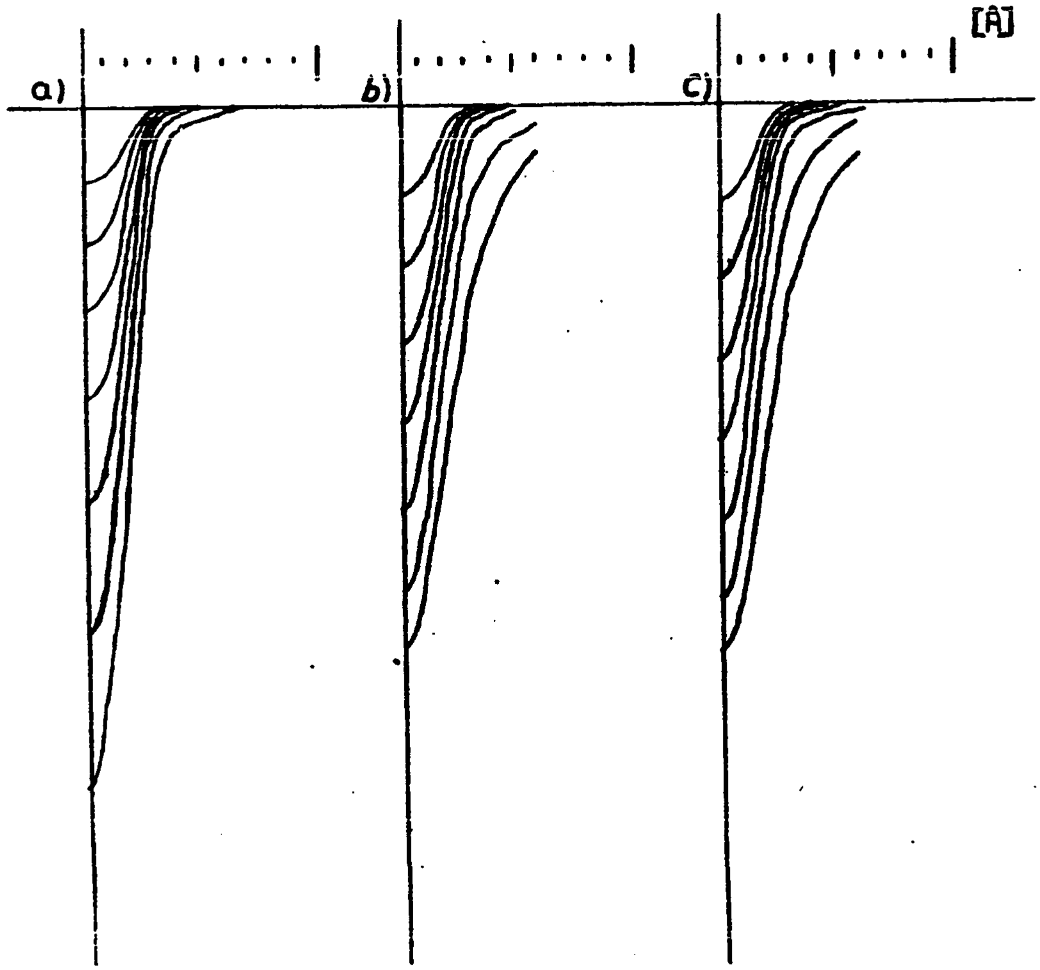

	WAVE-LENGTH	LIMB DARK-ENING	MICRO TURBU-LENCE	LOG a	V_e SIN i	R_c	A_2°	INCLIN-ATION i
a)	4000 Å	0.48	4.8 KM/S	−1.8	17.0 KM/S	1.0	−1.0	80°
b)	4000	0.48	4.8	−1.4	15.5	0.58	−1.0	80°
c)	4000	0.48	4.8	−1.4	15.5	0.58	0.0	80°

FIGURE VII, 2 COMPUTED PROFILES

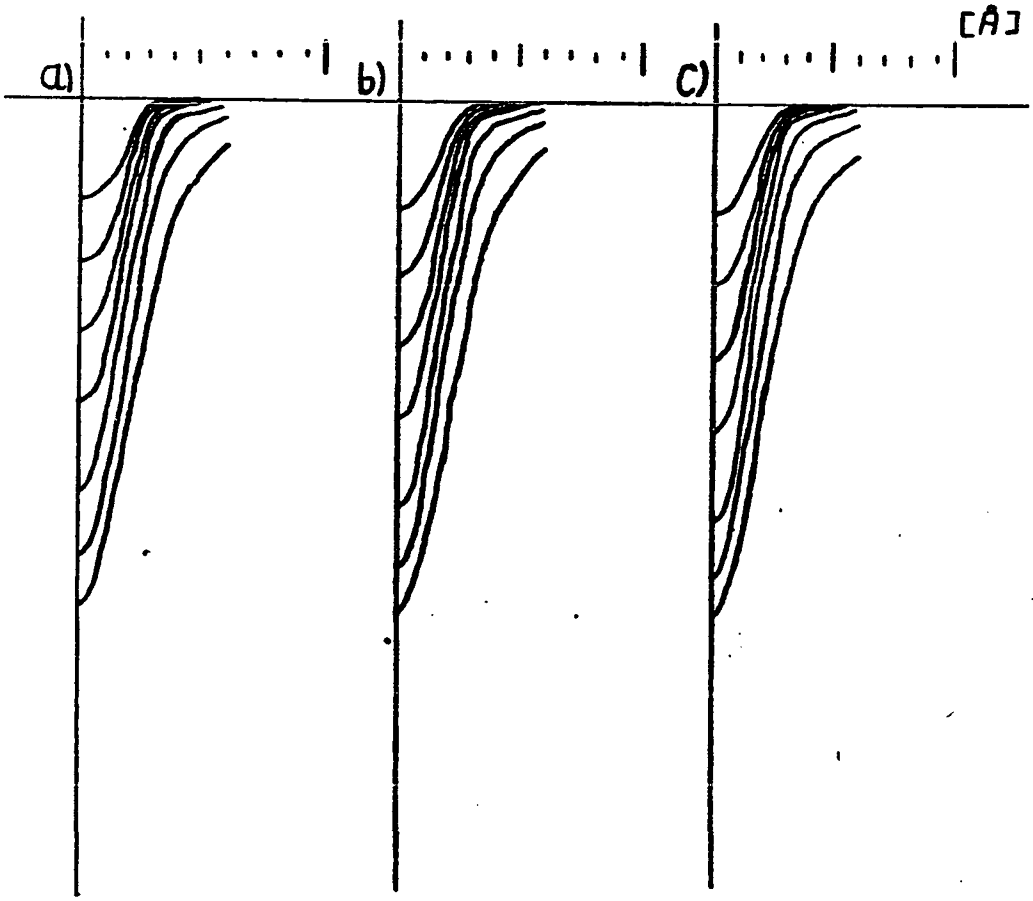

	WAVE-LENGTH	LIMB DARK-ENING	MICRO TURBU-LENCE	LOG a	$V_e \sin i$	R_c	A_2^0	INCLIN-ATION i
a)	4450A	0·48	4·8 KM/S	-1·4	15·0 KM/S	0·54	-1·0	80°
b)	4450	0·48	4·8 KM/S	-1·4	15·0	0·54	0·0	80°
c)	4450	0·48	4·8 KM/S	-1·4	15·5	0·54	+1·0	80°

FIGURE VII,3 COMPUTED PROFILES

It can be argued that a fairly large share of the broadening here attributed to rotational broadening, could be due to macro-turbulence. While no argument based on the profiles themselves can be made to support the contention that the broadening is all due to rotation, the observed radial velocity variations do lend some support to this view. As will be seen later, the radial velocity variations suggest a velocity of the 'spot' when it is on the limb of the star of 10 to 11 km/sec. This then puts a lower limit on the value of Ve sin i of about 11 km/sec. One cannot defend the contention that there is no contribution from macro-turbulence to the large scale broadening but this assumption must be made in order to make progress in evaluating Ve sin i.

The profiles computed for the present analysis would suggest that there is little tendency to the drastic surface distribution suggested by a value of $A_2^0 = -1.0$ i.e. zero line strength at the poles and a strong concentration of line strength to the rotational equator, but whatever deviation from $A_2^0 = 0$ there is probably tends in this direction. The value of V_e sin i would appear to fall between 15.0 and 15.5 km/sec with a slight preference for 15.5 km/sec. The value adopted is 15.4 km/sec with an estimated probable error of about 0.5 km/sec.

b) The Inclination of the Rotational Axis

The determination of the inclination of the rotational axis depends upon a determination of the radius of the star and the radius must be estimated from either the U.B.V. or the spectral classification of the star. In this class of stars the spectral types appear to be systematically two spectral subclasses later than the B-V colour would suggest. The U.B.V. magnitudes of the A_p stars give a colour-colour diagram that reproduces the main sequence relationship and the colour-magnitude diagram for A_p stars falls along the normal main sequence. With the consistency of the U.B.V. photometry of A_p stars with normal main sequence stars in mind and noting that spectral classification is much more strongly influenced by the profusion of weaker lines that occur in most of these stars (and in particular in HD173650) than wide band photometry, the best estimate of the radius must be derived from the relationship of the radii of main sequence objects to their unreddened colour.

Eggen (1967) gives the following values for HD173650

(B-V) apparent = +0.015 , M_V = -0.3 ,

(U-B) apparent = -0.09 , E(B-V) = 0.10

The colour excess is derived from the displacement of HD173650 from the colour-colour relation of nearby A_p stars, most of which are presumably unreddened. The excess is larger than one would expect for such a close star and must indicate fairly strong obscuration in this direction. These observations provide an unreddened B-V of -0.085 for the star and this is consistent with a main sequence spectral type of B7.5.

A number of papers provide evaluations of the radius corresponding to observed spectral types and colours. The following were used to obtain the best estimate of the radius.

1.D.McNamara I.A.U. Symposium #24 p.202

A range of radii from about 2 to 4 solar radii is obtained from eclipsing binary observations for stars around B7.5 with a mean result of 2.9 solar radii.

2.A.Underhill Vistas in Astronomy 8 , 48

Extrapolation on estimates of the radii of early B stars by Underhill gives a radius for B7.5 of 2.8 to 3.0 solar radii. These estimates are based on the absolute magnitudes of B stars and her own values of effective temperature. The results are checked against the radii obtained from values of g obtained from model atmosphere calculations combined with the masses obtained from eclipsing systems.

3. D.Popper Annual Review of Astronomy and Astrophysics 1967 p.101 Eclipsing binary results give a mean radius for B7.5V of 2.7 solar radii with scatter from 2.0 to 3.2.

4. D.Gray - unpublished

Photometric results with model atmosphere calculations give, with a slight extrapolation, a radius of 2.8 solar radii ±10% for a B7.5V.

5. D.Gray A.J. 73 ,769, 1968.

Gray's formula $\log R = -0.541\ (B-V) + 0.405$ gives a value of 0.454 for $B-V = -0.90$. This corresponds to a value of 2.84 solar radii ±10%.

The value taken for the radius was 3.0 solar radii with a presumed probable error of about ±10%. This value is slightly higher than the average of the above estimates but this is to take account of the fact that the log radius-colour relation curves up around (B-V) = 0.0 and earlier. Since several of the estimates amount to linear extrapolation from either earlier, in the case of Underhill, or, in the case of Gray, later stars, it must be assumed that these values for the radius will be inclined to be slightly low and consequently the adopted value was taken to be 3.0 instead of around 2.8 to 2.9 solar radii.

A radius of 3.0 solar radii combined with a rotational period of 10 days gives an equatorial velocity of rotation of 15.2 km/sec with 10% probable error estimated. Combined with a value of Ve sin i of 15.4 km/sec this value of Ve and the associated error implies a lower limit for the inclination of the rotational axis of about 65°.

c) The Co-Latitude of the "Spot"

The radial velocity variations observed do not represent the actual line-of-sight velocity of the "spot" as the star rotates. If the observations did represent the velocity of the spot, then as it came around the limb of the star its radial velocity would be the same as the amplitude of the radial velocity curve. The real situation though, is that there are contributions from areas of the star, other than the 'Spot', that have the effect of reducing the apparent radial velocity. A very crude approximation to a correction for this effect will be derived here but the radial velocity and line strength variations will be treated more correctly in the harmonic analysis section.

Suppose, very simply, that the star is made up of two line forming regions, the "spot" with a radial velocity displacement χ , and the rest of the star with weaker lines and an oppositeradial velocity displacement $-\chi$. Further, assume that the "spot" is quite large in area and when its centre is on the limb, it contributes equally with the rest of the stellar surface to the luminosity of the star. If the central line depth in the "spot" is B and that in the rest of the star is A, and if we assume that in measuring radial velocities that one bisects the area under the intensity profile with the cross hair, then from figure VII,4 we reach the following conclusions. With the two lines of central depths A and B displaced a distance χ on either side of the zero velocity position, the difference in area between the two areas on each side of this zero velocity position in the resultant profile is $2A\chi(R-1)$, where $R = B/A$. If one moves the cross hair to balance the areas it must be moved a distance y

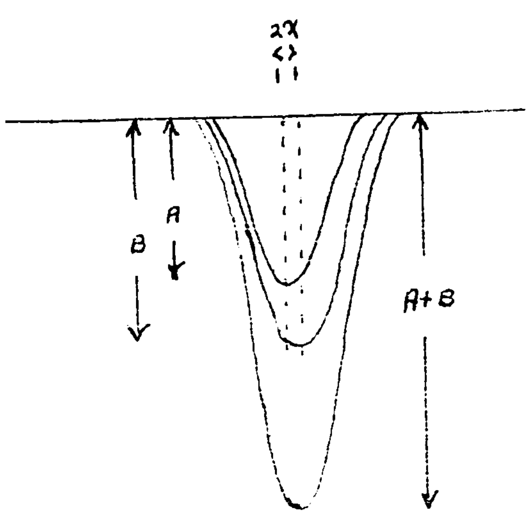

FIGURE VII,4

so that 2yA (R+1), which represents the change in the difference in area between the two sides caused by moving the cross hair a distance y, is equal to the initial imbalance 2Aχ(R-1). That is, χ , the true radial velocity at the limb, equals (R+1)/(R-1) times the observed radial velocity y. The value R can be approximated by the ratio of the line depths at maximum and minimum line strengths and y is the amplitude of the radial velocity curve. Since one is not measuring direct intensities but is instead measuring on a plate whose density varies as the log of the intensity, a testcase of a profile made up of the sum of the intensities of two displaced lines of unequal strength was created. The log of the resultant profile was plotted and a planimeter used to find the location of the point where equal areas under the profile were found on either side. This point, as it turned out for this test case of R = 3 was related to the displacement of the original profiles by a factor only 10% different from the value of (R+1)/(R-1). This correction should give a good approximation to the radial velocity of the spot as it appears at the limb of the star. Table VII,1 gives the amplitude of a least squares fit of a sin curve to the radial velocities of the various elements, the factor R and the corrected velocity for each element that had a substantial V_r variation.

TABLE VII,1

Element	Amplitude of Vr curve	R	Corrected Amplitude	Number of Lines
CrII	1.87 km/sec.	1.46	10.0	14
MnII	2.10	1.50	10.5	11
EuII	4.17	1.92	13.3	3
GdII	2.68	1.67	10.7	4
ZrII	3.21	1.41	18.9	5
SrII	1.49	1.68	5.9	4

The corrected amplitudes (velocity of the spot at the limb) are consistent with an angle β, the co-latitude of the spot, of between 40° and 50°. As pointed out earlier, the velocities also imply a lower limit to the possible values of Ve sin i of approximately 11 to 12 km/sec and lend credence to the suggestion that the line broadening (which was earlier used to evaluate Ve sin i) is in fact little affected by macroturbulence and that the assigned value of Ve sin i of 15.4 km/sec is very near the true value. The lower limit to the value of i is about 50° as assessed from the radial velocity information.

The result of this preliminary analysis is that whatever model is adopted for this star it should be consistent with a rotational axis inclination of at least 65° and an angle for β of approximately 40° to 50°.

CHAPTER VIII

THE MAGNETIC FIELD

The question of the apparent variation of the magnetic field under the oblique rotator hypothesis has been examined by a number of authors, most recently by Bohm-Vitense (1966, 1967). A variety of divergence-free cylindrically symmetric fields were investigated but particular attention was paid to a dipole field and to a field designated H3. The general field description used by Vitense was that given by Lust and Schluter (1954),

$$B = \begin{Bmatrix} B_z \\ B_\rho \\ B_\varphi \end{Bmatrix} = \begin{Bmatrix} -\left(\frac{\partial p}{\partial \rho} + \frac{p}{\rho}\right) \\ \frac{\partial p}{\partial z} \\ 0 \end{Bmatrix}$$

where p is any function of the cylinder coordinates ρ and z. The function used by Vitense was $p = \frac{\rho}{(az^2 - \rho^2)^{\delta/2}}$ so that a dipole field was obtained if $a = 1, \delta = 3$ and the H3 field resulted if $a = 3, \delta = 3$. The characteristic of the H3 field is that instead of decreasing in field strength as one goes from the pole to the magnetic equator, as does the dipole field, it increases in strength to a maximum at a latitude of about 20^o and then decreases to the equator. The maximum value of the field strength is about 4.5 times the polar value and the strength at the equator is down to approximately 3.0 times the polar strength.

Bohm-Vitense explains the line intensity variations in the following way. If one looks at a large selection of curves depicting the expected magnetic variation for a star with an H3 field, it will be noticed that a broad extremum occurs whenever the magnetic polar region is most nearly pointed toward the observer. Noting that the maximum of the EuII lines is always associated with the broadest extremum of the magnetic field, she suggests that the line strength maximum on the stellar surface must be at the magnetic poles for EuII. Those elements whose variation is in anti-phase to EuII would be concentrated around the magnetic equator in a belt corresponding to maximum field strength. This model gives a curve for the line strength variation that has a single maximum if the sum of i and β is less than 90° but if this sum should be of the order of 90° or slightly larger, then a secondary maximum will occur in the line strength curve. The magnetic field, on the other hand, will show no change in polarity during the stars cycle if the sum of i and β is less than 90°. For the magnetic field of HD173650 the positive extremum is approximately half the negative, so that $i + \beta$ must be substantially larger than 90°. As a consequence, such a very symmetric model cannot explain the star HD173650, since, from figure IX,3, it is clear that no significant secondary maximum is present in the line strength variation. It is apparent that a more complicated, non-symmetric surface distribution is required.

A programme to compute the apparent variation of effective magnetic field with phase was developed using the formulae given by Bohm-Vitense. Allowance was made for the effect of a non-uniform line strength distribution over the surface of the star by weighting the magnetic field predicted by the above expression for each point on the star by the local equivalent width. For illustrative purposes, the magnetic field variation for a uniform line strength distribution and rotational inclination angle of 80° with a β angle of 40° is given in figure VIII,5. The line strength variations that would be expected for several distributions that are cylindrically symmetric about the magnetic axis are given in figures VIII,2,3,and 4. The distributions assumed for line strength were

a) $W = 1 + E(|\cos\psi|)^{\gamma}$

b) $W = 1 + E(|\cos\psi \sin\psi|)^{\gamma}$

c) $W = 1 + E(\sin\psi)^{\gamma}$

where ψ is co-latitude in a spherical coordinate system (Figure VIII,1) whose z axis is coincident with the magnetic axis, γ and E are arbitrary parameters.

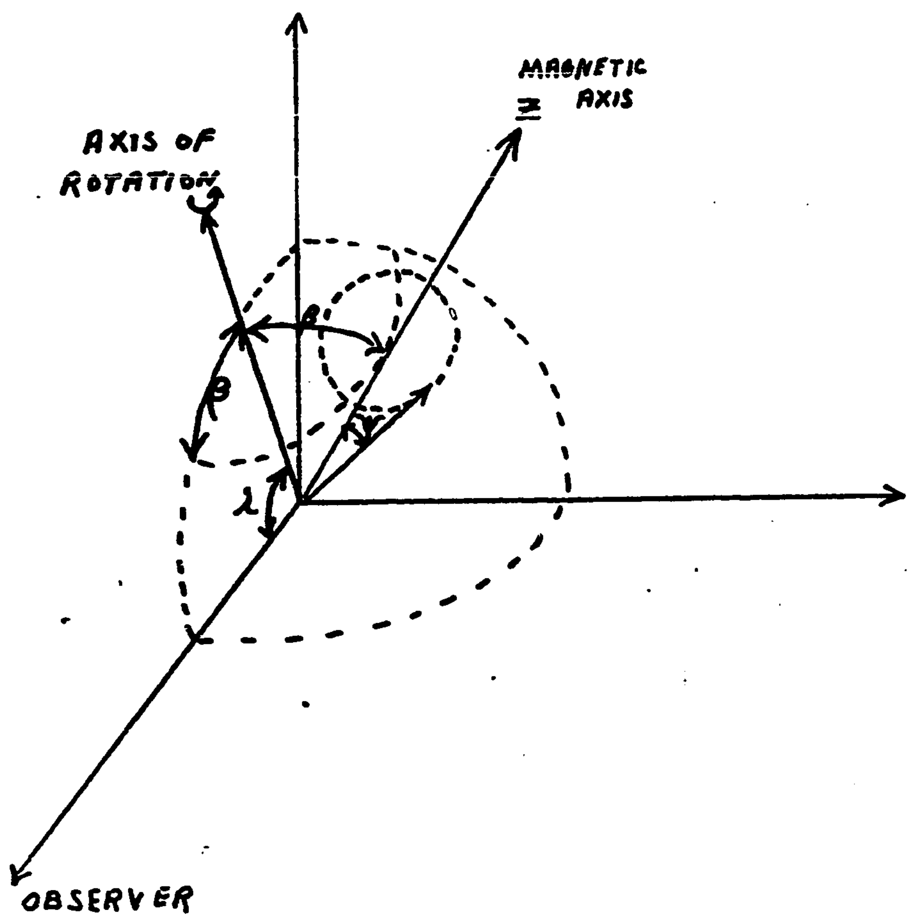

FIGURE VIII,1

ILLUSTRATION OF ANGLES USED TO DESCRIBE ORIENTATION OF MAGNETIC FIELD

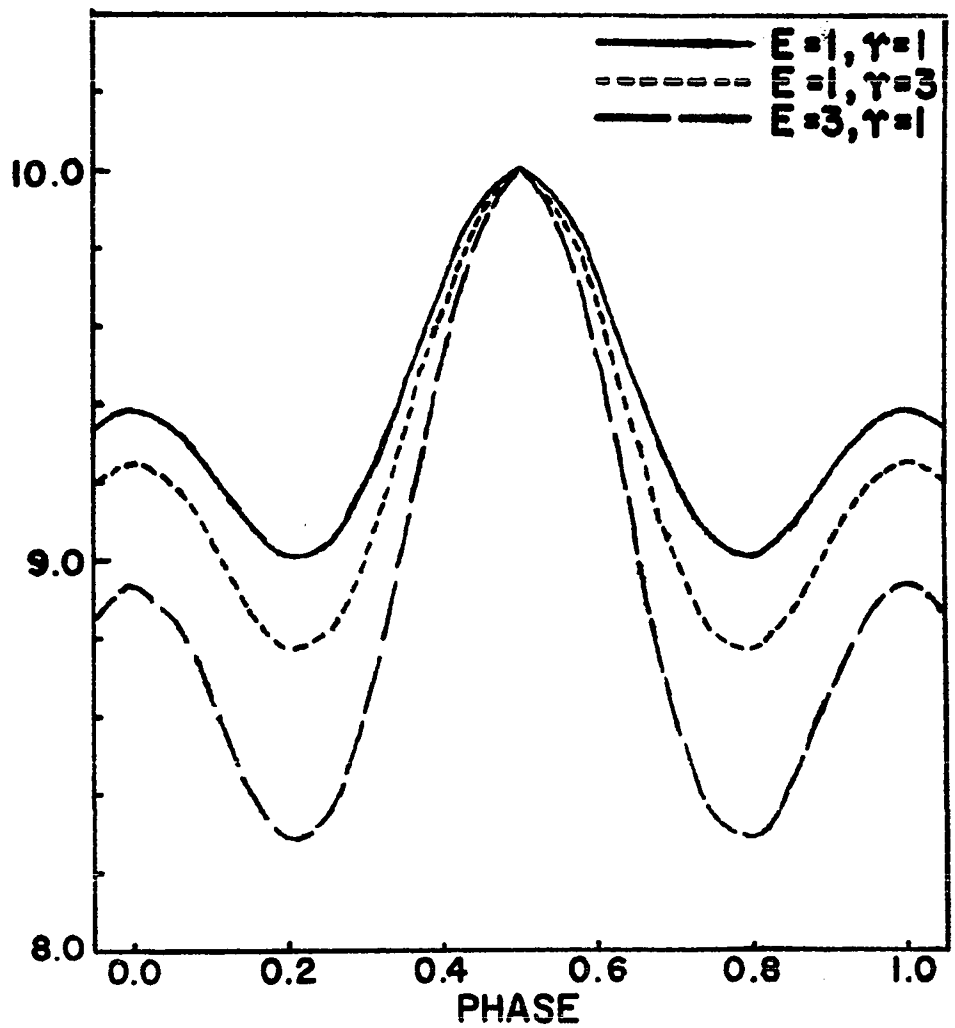

FIGURE VIII,2

Variation of equivalent width with phase if the cylindrically symmetric distribution $W = 1 + E\,(|\cos\psi|)^{\gamma}$ represents the distribution of local equivalent width on the star and $i = 80^{\circ}, \beta = 40^{\circ}$.

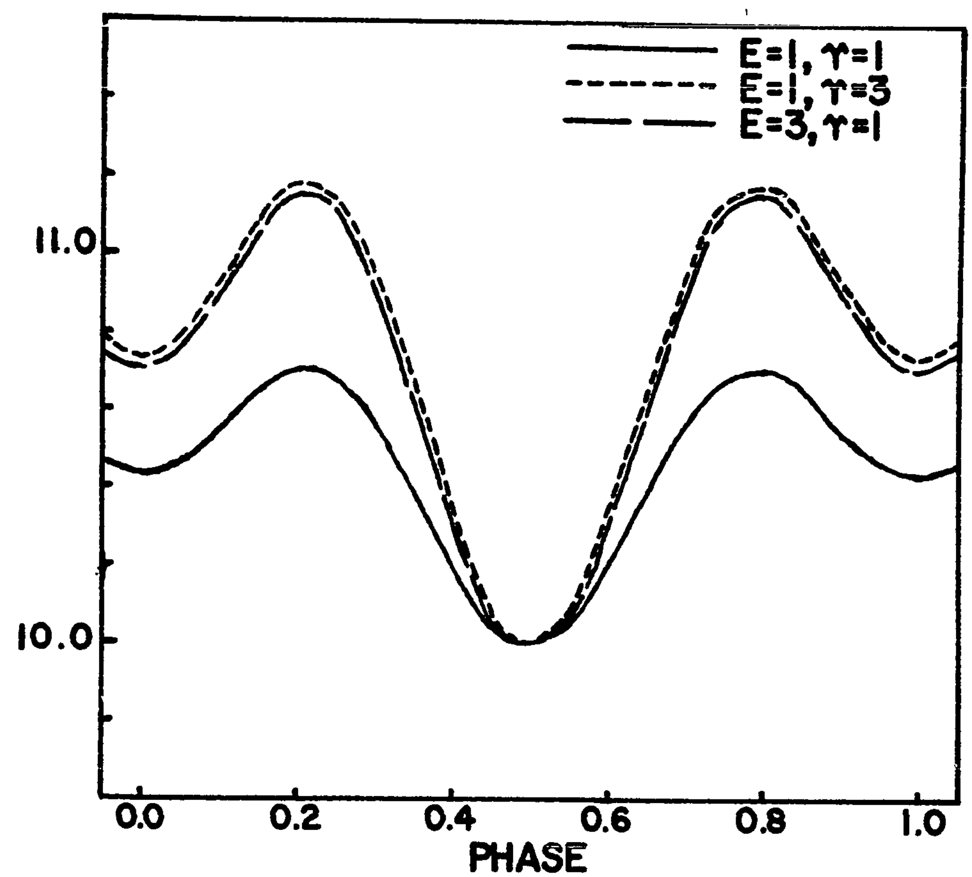

FIGURE VII,3

Variation of equivalent width with phase if the cylindrically symmetric distribution $W = 1 + E\ (\sin\psi)^{\gamma}$ represents the distribution of local equivalent width on the star and $i = 80^{\circ}$, $\beta = 40^{\circ}$.

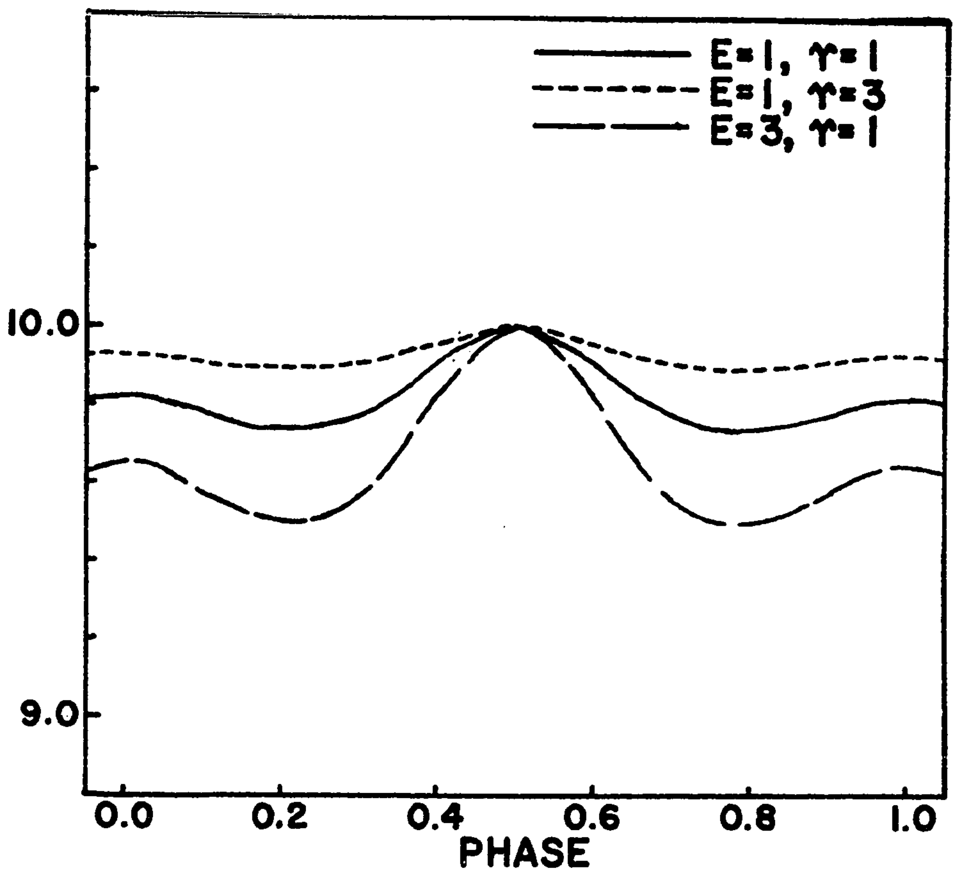

FIGURE VIII,4

Variation of equivalent width with phase if the cylindrically symmetric distribution $W = 1 + E\ (|\cos\psi \sin\psi|)^{\gamma}$ represents the distribution of local equivalent width on the star and $i = 80^{o}$, $\beta = 40^{o}$.

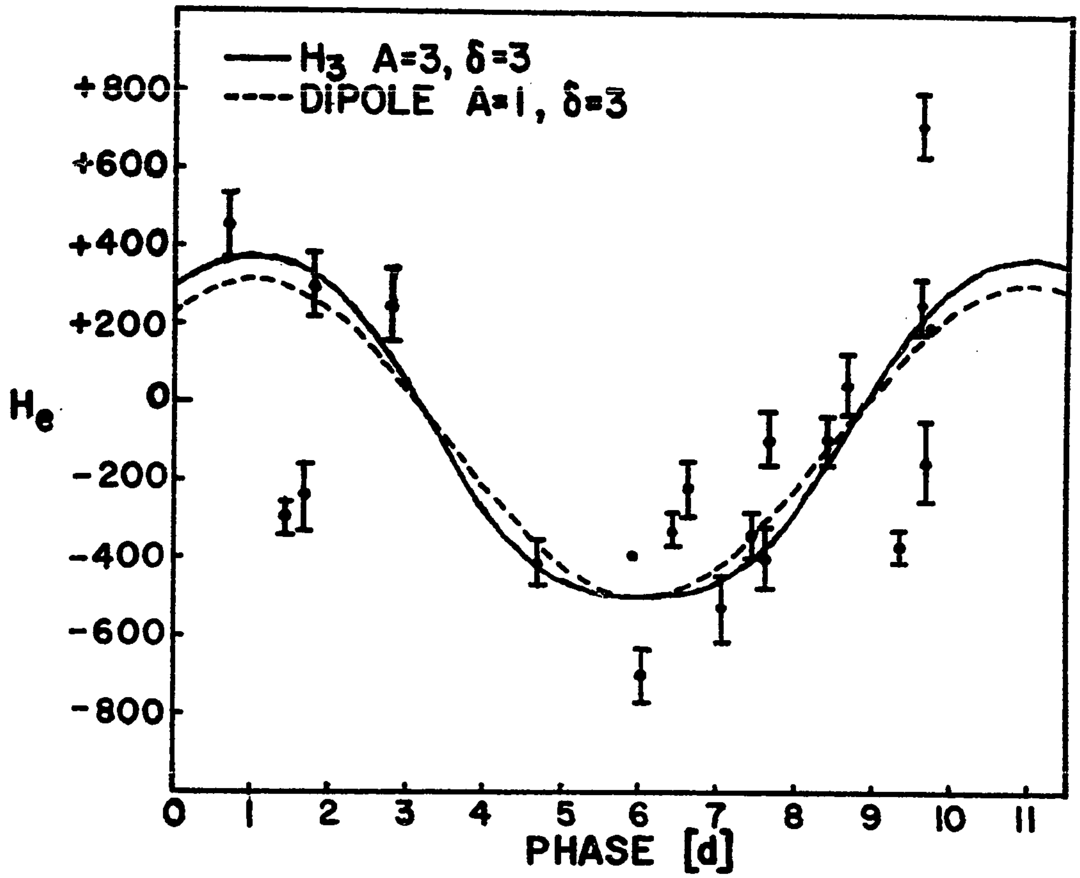

FIGURE VIII,5

Magnetic field variation with phase, $i=80^{\circ}$, $\beta=40^{\circ}$. Uniform line strength distribution. Plotted points are observed magnetic field for HD173650.

CHAPTER IX

THE HARMONIC ANALYSIS

A representation of the local equivalent width on the surface of the star can be developed in spherical harmonics and the coefficients of this development can be related to the Fourier coefficients of the equivalent width and radial velocity curves of the star. If one also includes the magnetic field the Laplace coefficients up to second order are completely determined by this procedure as is shown by Deutsch (1958). The results achieved by including the magnetic field did not appear to be completely satisfactory and since the magnetic variation in HD173650 is very poorly determined it was decided to change the approach to use only the equivalent width and radial velocity curves plus the condition that the inclination of the rotational axis be in the neighbourhood of 65° to 90° and that the local equivalent widths be everywhere positive. After determining a distribution of local equivalent widths that reproduces the line strength and radial velocity variations and that is consistent with the line widths, then the magnetic fields of the previous chapter will be used with the non-uniform line strength distribution to make the best possible fit to the magnetic cycle.

a) Theory

Let

$$\Xi(\psi,\nu)=\sum_{n=0}^{\infty}\left(A_n^0 P_n^0(\cos\psi)+\sum_{m=1}^{n}\left(A_n^m e^{im\nu}+A_n^{-m}e^{-im\nu}\right)P_n^m(\cos\psi)\right)$$

be the expression for the local equivalent widths on the surface of the star where ψ is the co-latitude and ν the longitude in a spherical coordinate system whose z axis is the rotational axis of the star. If only the real part represents the local equivalent widths, we have for the line strength at any point (ψ,ν) on the stellar surface;

$$\xi(\psi,\nu)=\sum_{n=0}^{\infty}\left(a_n^0 P_n^0(\cos\psi)+\sum_{m=1}^{n}\left[\left(a_n^m\cos m\nu+\alpha_n^m\sin m\nu\right)P_n^m(\cos\psi)\right]\right)$$

where the terms in -m have been dropped (because the expansion is made no more general by retaining them, if we look only at the real part) and where $A_n^m = a_n^m - i\alpha_n^m$ relates the first and second expressions. Sâto (1950) discusses the transformations that are necessary to convert this expansion to one in terms of the a's and α's in a (θ,φ) coordinate system whose z axis is in the direction of the observer as shown in figure IX,7. In the notation of Sâto, after the transformation $(\Phi,X,0)$ the function $\xi(\psi,\nu)$ to second order becomes;

$$\xi(\theta,\varphi)=\Big[\Big[\Big[a_0^0+a_1^0\left[\cos\theta\cos X-\sin\theta\cos\varphi\sin X\right]$$

$$+a_1^1\left[-\sin\Phi\left[\sin\theta\sin\varphi\right]+\cos\Phi\left[\cos\theta\sin X+\sin\theta\cos\varphi\cos X\right]\right]$$

$$+ a_2^0 \Big[(0.25 + 0.75 \cos 2\theta)(0.25 + 0.75 \cos 2\chi) - 0.75 \sin 2\theta \cos\varphi \sin 2\chi$$

$$- 1.5 (\cos 2\theta - 1) \cos 2\varphi (0.125 - 0.125 \cos 2\chi) \Big] - a_2^1 \Big[\sin\Phi \big[1.5 \sin 2\theta$$

$$\sin\varphi \cos\chi + 0.75 (\cos 2\theta - 1) \sin 2\varphi \sin\chi \big] + \cos\Phi \big[-1.5 (0.75 \cos 2\theta$$

$$+ 0.25) \sin 2\chi - 1.5 \sin 2\theta \cos\varphi \cos 2\chi + 0.375 (1 - \cos 2\theta)$$

$$\cos 2\varphi \sin 2\chi \big] \Big] + a_2^2 \Big[\sin 2\Phi \big[-3.0 \sin 2\theta \sin\varphi \sin\chi$$

$$- 1.5 (1 - \cos 2\theta) \sin 2\varphi \cos\chi \big] - \cos 2\Phi \big[(0.75 \cos 2\theta + 0.25)$$

$$(1.5 \cos 2\chi - 1.5) - 1.5 \sin 2\theta \cos\varphi \sin 2\chi - 1.5 (1 - \cos 2\theta)$$

$$\cos 2\varphi (0.75 + 0.25 \cos 2\chi) \big] \Big] \Big] + \Big[\alpha_1^1 \big[\sin\Phi \big[\cos\theta \sin\chi$$

$$+ \sin\theta \cos\varphi \cos\chi \big] + \cos\Phi \big[\sin\theta \sin\varphi \big] \big] + \alpha_2^1 \big[-\sin\Phi$$

$$\big[-(1.125 \cos 2\theta + 0.375) \sin 2\chi - 1.5 \sin 2\theta \cos\varphi \cos 2\chi$$

$$+ 0.375 (1 - \cos 2\theta) \cos 2\varphi \sin 2\chi \big] + \cos\Phi \big[1.5 \sin 2\theta$$

$$\sin\varphi \cos\chi - 0.75 (1 - \cos 2\theta) \sin 2\varphi \sin\chi \big] \big]$$

$$+ \alpha_2^2 \big[\cos 2\Phi \big[3 \sin 2\theta \sin\varphi \sin\chi + 1.5 (1 - \cos 2\theta)$$

$$\sin 2\varphi \cos\chi \big] - \sin 2\Phi \big[1.5 (0.75 \cos 2\theta + 0.25)(\cos 2\chi - 1)$$

$$- 1.5 \sin 2\theta \cos\varphi \sin 2\chi - 0.375 (1 - \cos 2\theta) \cos 2\varphi$$

$$(3 + \cos 2\chi) \big] \big] \Big]$$

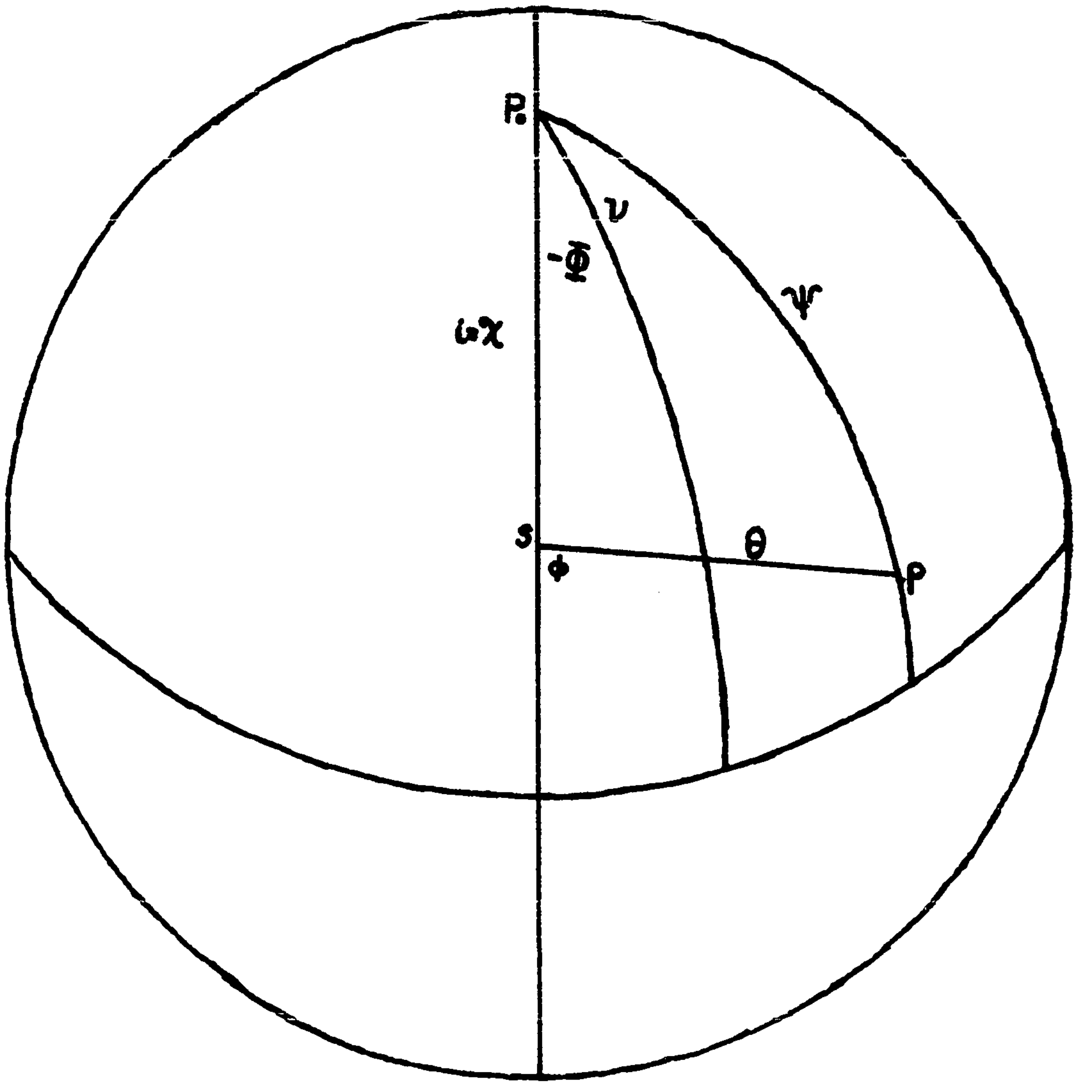

FIGURE IX,7

Illustration of the angles used for the transformation. Po is the rotational pole, S the sub-solar point and χ the inclination of the rotational axis.

The observed equivalent width W is found from the integral

$$W = \frac{\int_0^{\pi/2}\int_0^{2\pi} \xi(\theta,\varphi)\Delta \sin\theta\cos\theta \, d\varphi\, d\theta}{\int_0^{\pi/2}\int_0^{2\pi} \Delta \sin\theta\cos\theta\, d\varphi\, d\theta}$$

where $\Delta = 1-u+u\cos\theta$ = limb darkening and the line weakening to the limb is ignored because it is considered negligable at this level of approximation. While the darkening to the limb might amount to 20% for moderately strong lines, in the sun the very weak lines actually show a strengthening to the limb. Consequently, in this first approximation study of lines whose mean strength is around 80 mA, we do not expect the results to be seriously affected by assuming zero weakening to the limb. The result of the above integration is

$$W = \frac{1}{(1+u/3)}\Big[\Big[a_0^0(1-u/3) + a_1^0\, {}^2\!/_3 \cos\chi(1-u/4) + a_2^0\, {}^1\!/_{16}(1+3\cos 2\chi)(1+\tfrac{u}{15})\Big]$$
$$+ \cos\Phi\big[a_1^1\, {}^2\!/_3 \sin\chi(1-u/4) + a_2^1\, {}^3\!/_8 \sin 2\chi(1+u/15)\big]$$
$$+ \cos 2\Phi\big[-a_2^2\, {}^3\!/_8 (\cos 2\chi - 1)(1+u/15)\big]$$
$$+ \sin\Phi\big[{}^2\!/_3\, \alpha_1^1 \sin\chi(1-u/4) + \alpha_2^1\, {}^3\!/_8 \sin 2\chi(1+\tfrac{1}{15}u)\big]$$
$$+ \sin 2\Phi\big[-{}^3\!/_8\, \alpha_2^2 (\cos 2\chi - 1)(1+u/15)\big]\Big]$$

which is a Fourier expansion in terms of the phase Φ. Equating these coefficients to those given by the Fourier analysis of the observed equivalent width variations provides expressions relating the coefficients a_n^m and α_n^m to the empirically determined values. The notation for the observed curve will be

$$W = \alpha_0 + \alpha_1 \cos\Phi + \delta_1 \sin\Phi + \alpha_2 \cos 2\Phi + \delta_2 \sin 2\Phi$$

The radial velocity V caused by the rotation is

$$V = \frac{\int_0^{\pi/2}\int_0^{2\pi} (-V_e \sin\chi \sin\theta \sin\varphi)\, \rho \Delta \sin\theta \cos\theta \, d\varphi \, d\theta}{\int_0^{\pi/2}\int_0^{2\pi} \rho \Delta \sin\theta \cos\theta \, d\varphi \, d\theta}$$

Since the denominator equals $W\pi(1 - \frac{u}{3})$ where W is the observed equivalent width value at a given phase, then one obtains

$$WV = -\frac{V_e \sin\chi}{(1-u/3)}\Big[\sin\Phi\big[a_1^1(-\tfrac{1}{4} + \tfrac{7}{60}u) + a_2^1 \cos\chi(\tfrac{2}{5} - \tfrac{3}{20}u)\big]$$

$$+ \sin 2\Phi\big[-a_2^2 \sin\chi[\tfrac{4}{5} - \tfrac{3}{10}u]\big]$$

$$+ \cos\Phi\big[\alpha_1^1(\tfrac{1}{4} - \tfrac{7}{60}u) + \alpha_2^1 \cos\chi(\tfrac{2}{5} - \tfrac{3}{20}u)\big]$$

$$+ \cos 2\Phi\big[\alpha_2^2 \sin\chi\,(\tfrac{4}{5} - \tfrac{3}{10}u)\big]\Big]$$

This expression will be equated coefficient by coefficient to the Fourier expansion of WV with the notation as follows:

$$WV = -V_e \sin\chi\big[e_0 + e_1 \cos\Phi + \varepsilon_1 \sin\Phi + e_2 \cos 2\Phi + \varepsilon_2 \sin 2\Phi \cdots\big]$$

It can be seen that the coefficients a_2^2 and α_2^2 are over determined and that a_0^0, a_1^0 and a_2^0 can only be determined if two more relations can be found. By trying solutions with various values of the inclination of the rotational axis, within the allowed limits, and adjusting the relative values of a_0^0, a_1^0 and a_2^0, a solution will be found that satisfies the condition that ρ be positive everywhere on the surface of the star. The adjustment of a_1^o and a_2^o does not affect the predicted radial velocity and line strength curve of the solution since they are the coefficients of the rotationally symmetric components of the expansion.

b) The Equivalent Width and Radial Velocity Curves

All of the elements that show a variation in line strength in HD173650 exhibit that variation in phase with one another and with the light curve. It would require a very large number of spectrograms to determine accurately the shape of the equivalent width variation for each element since only a small number of lines that can be definitely identified and declared blend free are on each exposure. In an attempt to determine more precisely the shape of the variation, all of the lines of the elements that showed a large radial velocity variation had an average of both their radial velocities and equivalent widths taken for each plate and these averages were plotted versus phase. The elements chosen for this averaging were CrII, MnII, EuII, GdII, ZrII, SrII and TiII with the lines selected for radial velocity measurement being used for the equivalent width average. The theoretical objection to this procedure is that if each element is distributed differently over the surface then the surface distribution derived from the average curves of equivalent width and radial velocity variation will not be physically meaningful. The procedure appeared more plausible when it was noticed that the light curve (V), if converted to intensity and multiplied by a scale factor to give it the correct amplitude, was an exceedingly good fit to the mean equivalent width points. The representation is so good that it leads one to believe that the distribution of local brightness must be the same, except for a scale factor of course, as the distribution of local equivalent widths. It was then noticed that if the various elements contributing to the mean were taken separately, the intensity curve, with different multiplicative factors, fitted each individually. This is illustrated by figures IX, 1,2 and 3 which show the light intensity curve fitted to the mean equivalent widths, and to the means of FeII, TiII, MnII and CrII. Only one plate, at phase 0.180, gave equivalent widths that deviated systematically from the intensity curve and from the equivalent widths of the plates of similar phase. No apparent reason, such as an incorrectly placed continuum, could be found for this deviation on the traces of plate 2749 but it is possible that an error was made in determining the calibration when the plate was micro-photometered. FeII did not contribute to the mean curve that was used for the harmonic analysis. This apparent uniformity of shape in the equivalent width variation with phase suggests that the shape of the distribution of local equivalent widths is the same for all elements showing variation in this star. It is interesting to note that Deutsch discovered in HD125248 that those elements which varied in phase all appeared to have the same shape to their curve of variation with phase and he too made the assumption that these elements had the same distribution of local equivalent widths.

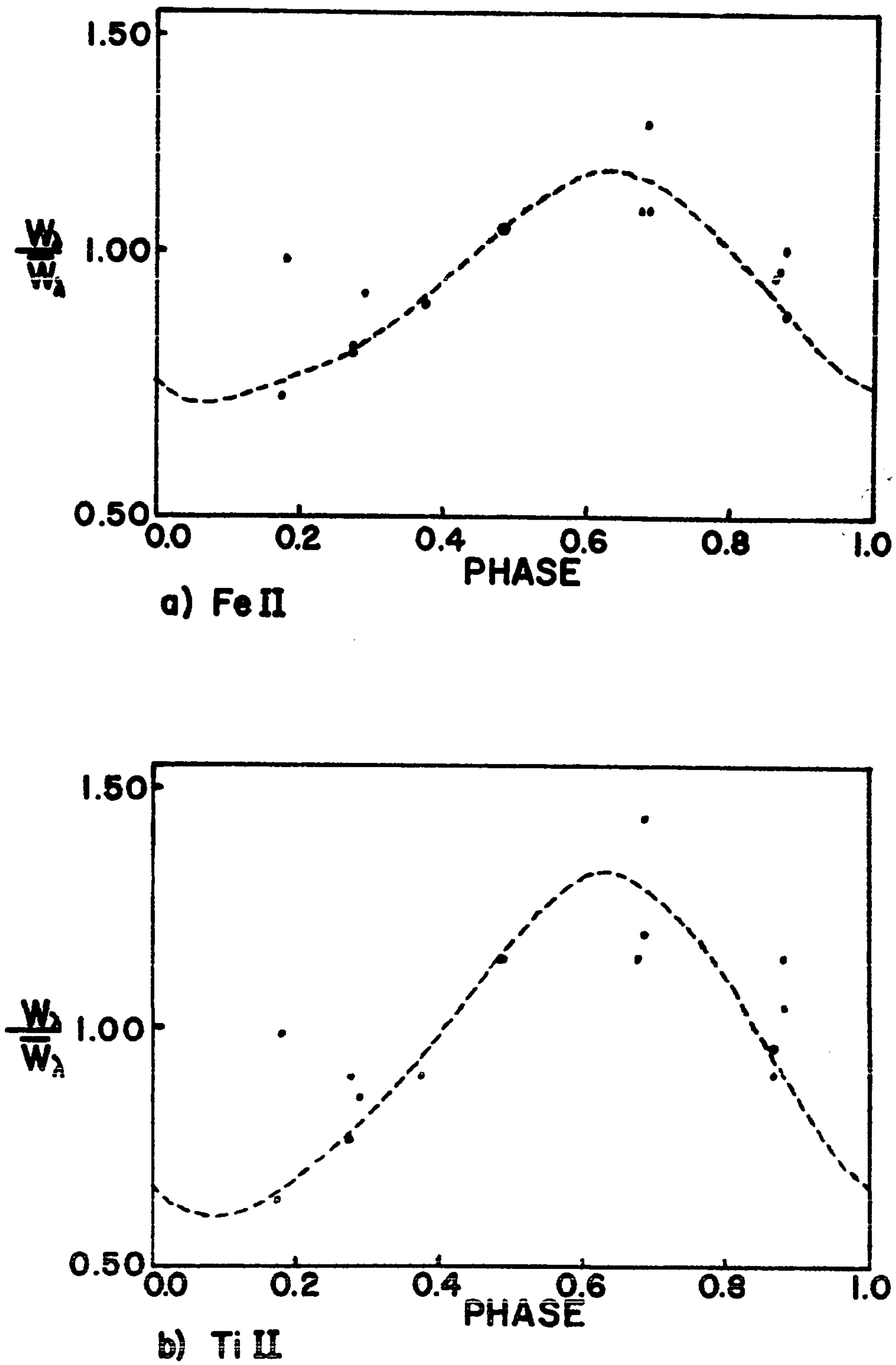

FIGURE IX, 1

Light intensity curve fitted to plot of mean equivalent widths versus phase for various elements.

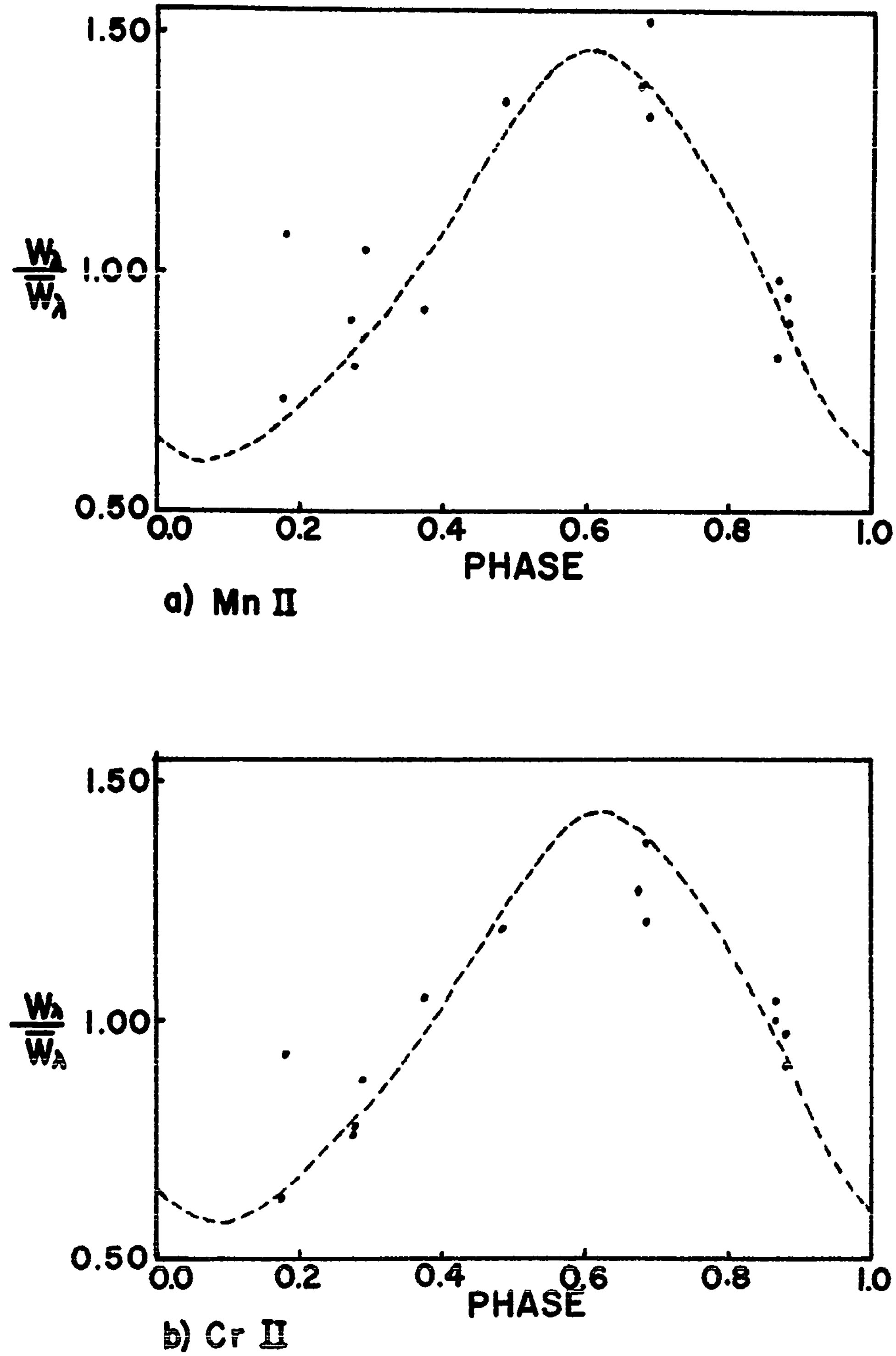

FIGURE IX, 2

Light intensity curve fitted to plot of mean equivalent widths versus phase for various elements.

The problem of insufficient data to define the shape of the curve to the desired precision was also apparent in the radial velocity results. Upon checking Babcock's (1958) catalogue it was discovered that while the lines used for the Zeeman and radial velocity measures were not identified, the number of lines used for each species was given for many of the plates. It would appear in general that the elements that were the major contributors to the mean radial velocities determined here were also the major contributors to Babcock's radial velocities and with the numbers of lines of each species being relatively the same (with the exception of FeII). Even though FeII wasn't used for the mean radial velocities computed here, it should not cause the radial velocity variations measured by Babcock to deviate significantly from the mean radial velocity curve expected to correspond to the mean equivalent width curve used for this analysis. The shape of the FeII distribution of local equivalent widths must be the same as the other elements used for the mean (figure IX,1) so that any effect it would have upon the radial velocity curve would be only to adjust its amplitude but not change its shape. Upon plotting Babcock's radial velocities and the means of the observations reported here (see figure IX,3) it appeared that no correction would have to be applied to Babcock's observations in order to use them as a device to indicate the true shape of the radial velocity curve.

c) The Solution

A series of four solutions corresponding to angles of inclination of the rotational axis (i) of 80°, 65°, 60° and 45° were computed from the equivalent width and radial velocity variation. Two of these solutions, for $i=65^\circ$ and $i=45^\circ$ are shown in figure IX,4 along with the Laplace coefficients of the solutions a_n^m and α_n^m. The Fourier coefficients (d_m) of the equivalent width curve and (e_m) those of the curve corresponding to W ($V - V_o$) are given in table IX,1. V_o is the radial velocity of the whole star. Of the four solutions, the one for $i = 65^\circ$ appears to be the one most consistent with the observations of line width and the requirement that the local equivalent widths be positive everywhere on the surface of the star.

TABLE IX,1

$d_o = 80.74$

$d_1 = 29.33$ $e_1 = -25.62$ /Ve sini $\delta_1 = 2.94$ $\epsilon_1 = -168.81$/Ve sini

$d_2 = 1.46$ $e_2 = -5.43$ /Ve sini $\delta_2 = 2.83$ $\epsilon_2 = -39.36$/Ve sini

The following discussion of the four solutions, and of the degree of agreement that each solution can achieve with the observed magnetic field variations, is intended to clarify the statement that the solution corresponding to $i = 65^\circ$ is in the best agreement with the observations and the requirements on the solution.

The second order Fourier expansion of both the equivalent width and the multiplied equivalent width by radial velocity curves is quite a good representation in each case. The second order representation of the equivalent width curve deviates from the observed values by never more than 1.1 milliangstroms and the radial velocity by equivalent width curve is represented to within 9.0/Ve sin i milliangstroms. This implies that the third and higher order coefficients of the Fourier analysis will be small compared with the first and second order coefficients. The equations from which the coefficients of the distribution on the surface of the star a_n^m and α_n^m are determined relate the sums of either the a's or α's of a given m to the Fourier coefficient of order m, It is therefore suggested, but not proved, by the fact that the third and higher order terms are relatively small that the Laplace coefficients a and α are small for m equal three and greater. This leaves us with no knowledge of the coefficients a_n^1 , a_n^2 , α_n^1 , and α_n^2 where n is equal to three and larger and one must accept as a reasonable assumption that they are small relative to the first and second order coefficients in N. One bases this assumption on the expectation that there should be no abrupt changes in conditions on the surface of the star (at least none which contribute to the observed variations) and consequently the higher order terms should be of decreased importance. If these assumptions are reasonable then the second order representation of the equivalent width distribution should be a close approximation to the true situation.

Predicted field strength variations are given for the two solutions at $i = 65^\circ$ and at $i = 45^\circ$ using parameters of the field and of its location that give some correlation of local field strength with local equivalent width and that show the best fit to the observed points of the magnetic cycle. Because of the known relation of the phase of the magnetic to the phase of the line strength variations, only one or two locations of the pole of the magnetic field appear, for each line strength distribution, to give a reasonable representation of the magnetic observations. The location of the magnetic pole as given in the diagrams is not critical and any position within 10° of the quoted position would give very nearly the same variation of the apparent field. Because all possible locations for the pole of the magnetic field were not tried and the author relied on personal judgement to select the positions that were most likely to produce results that agreed with the magnetic observations, there is the possibility that there are other locations for the pole that would give good agreement with observation. The determination of the predicted apparent field was accomplished by computing at each visible point of the surface the component of the field in the line of sight and weighting it according to its limb darkening (given by $u = 0.48$ in the expression $1 - u + u \cos\theta$), the projected area of the region, and the local equivalent width and then integrating over the visible surface. The integration is performed for twenty aspects of the star corresponding to successive steps in phase of the star's rotational cycle and for the various fields and orientations that might fit the observations. The best results of these computations for the solutions corresponding to $i = 45^{\circ}$ and $i = 65^{\circ}$ are given and the significance of the closeness of the fit to the observations is discussed for each of these solutions.

The solution corresponding to $i = 80^{\circ}$ gives line intensities that are highly negative at two extended regions on the star's surface. The maximum negative value reached by the solution is -115 mA and no adjustment of the coefficients of the rotationally symmetric terms would improve this situation to the point where it could even be considered to be approaching a physically reasonable solution.

The solutions for $i = 65^{\circ}$ and $i = 60^{\circ}$ are naturally quite close to one another in appearance. Both solutions become negative over two quite restricted regions of the star and the maximum negative value for the $i = 65^{\circ}$ solution (coefficients given in figure IX,4) was 30 mA and that for the $i = 60^{\circ}$ solution (with $A_1^0 = -\frac{1}{2} A_0^0$) was 20 mA. The value of $A_1^0 = -\frac{1}{2}A_0^0$ was chosen for each of these two solutions so that they would remain as uniformly positive as possible. The value of A_2^0 was left at zero since adjusting it would do very little to reduce the areas where the solutions became negative and furthermore the line profiles had not indicated that the value of this coefficient deviated to any great extent from zero. As can be seen from figure IX,3, if the solution at $i = 65^{\circ}$ is used and wherever the local equivalent width becomes less than 15mA it is set equal to 15mA, then the representation of the equivalent width (light) and radial velocity variations remains quite good. Clearly the solution in terms of second order spherical harmonics can only be an approximation to the real solution since the second order harmonics cannot represent all conceivable distributions. If one were to adjust the approximation achieved with the second order harmonics more carefully, that is by not only setting those areas which were less than 15mA to 15mA but by reducing some values that were just outside these regions, then a solution which perfectly reproduced the observations and was at the same time never less than 15 mA could be achieved. The solution used here is very close to what must be the correct distribution for $i = 65^{\circ}$, and further adjustment of the distribution would not be worth while. This is the conclusion reached when one considers the accuracy of the observational material that is available and when one also considers that the changes called for will not adjust the major characteristics of the distribution.

Two magnetic field orientations were found to predict magnetic cycles that can be regarded as equally well representing the observed one. The prediction of figure IX,5(a) is derived from an H3 field whose negative pole is located at 0° longitude and 65° co-latitude and that of figure IX,6 is derived from a dipole field whose positive pole is located at longitude 115° and co-latitude 45°. An H3 field will not work near the latter location. The latter representation is the preferred one on the grounds that the magnetic field strength and the belt of line strength concentration around the star can be correlated. With a dipole field the magnetic field strength is a maximum at the magnetic poles and falls monotonically to a minimum at the magnetic equator. As can be seen from figure IX,4 (a) the line strength concentration would be around the magnetic equator(corresponding to minimum field strength) of a field which is oriented in the manner of the field of figure IX,6. This belt of greater line strength is not uniform though and has two maxima along it, the primary at longitude 70° co-latitude 135° and the secondary at longitude 300° and co-latitude 45°. These two regions are almost at opposite sides of the star but no cylindrically symmetric field could be found which, if its poles were located in these spots, fitted the observations even approximately.

The solutioh for $i = 45°$ corresponds to the case for Ve sin $i \simeq 12$ km/sec and forms, as a result of the radial velocity measurements and the crude analysis performed in chapter VII, a practical lower limit to the value of i. As might be expected, with the reduced value of Ve sin i, the region of line strength maximum concentrates more to the rotational equator. The overall appearance of the distribution bears a fairly strong resemblence to the solution at 65° but the belt effect of the maximum is broken and the maximum could be described more properly as a much elongated and quite extensive "spot". This solution is represented in figure IX,4(b).

No really adequate representation of the magnetic cycle could be produced with cylindrically symmetric fields that have a correlation in distribution of field strength with the line strength distribution. Placing the positive pole, as in the case of the 65° solution, at longitude 115° co-latitude

45° was a failure since the predicted field did not switch polarity during its cycle. An attempt to locate the pole near the maximum of the line strength distribution was not much more successful as can be seen in figure IX,5(b). Here the location of the negative pole was longitude 0° and co-latitude 90° with an H3 field. To achieve a fit in phase one would have to move to longitude 320° and any correlation with the line strength distribution would be completely lost. While a field orientation that would provide an acceptable fit to the magnetic observations can undoubtedly be found, it would appear that no field that can be correlated to the line strength distribution of figure IX,4(b) will produce such a fit.

Considering the fact that the line profile study resulted in a suggested range of angles for the inclination of the rotational axis from 65° to 90° , and also considering the degree to which the solutions in the neighbourhood of 80° become negative and the difficulty of reproducing the magnetic observations with solutions in the neighbourhood of 45°, the solution for 65° has been adopted for the star. The limits that one could put on the acceptable range of values for i would be from about 55° to 70° and in this range the major characteristics of the solution do not change.

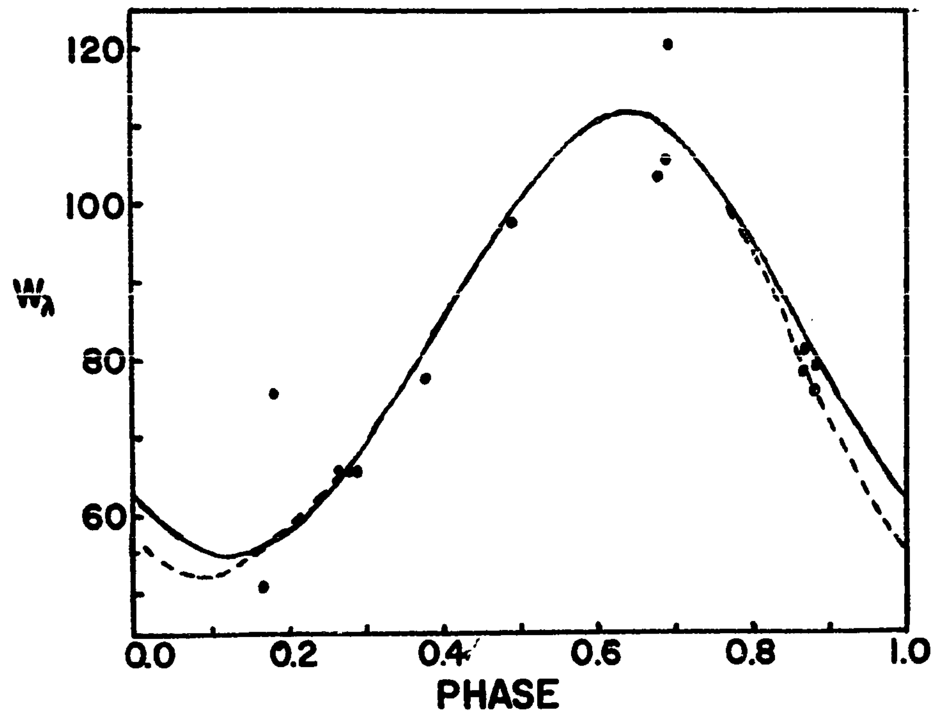

a) The dashed curve is the light intensity observed variation and the solid curve the predicted equivalent width variation using the 65° solution with a minimum of 15 m A.

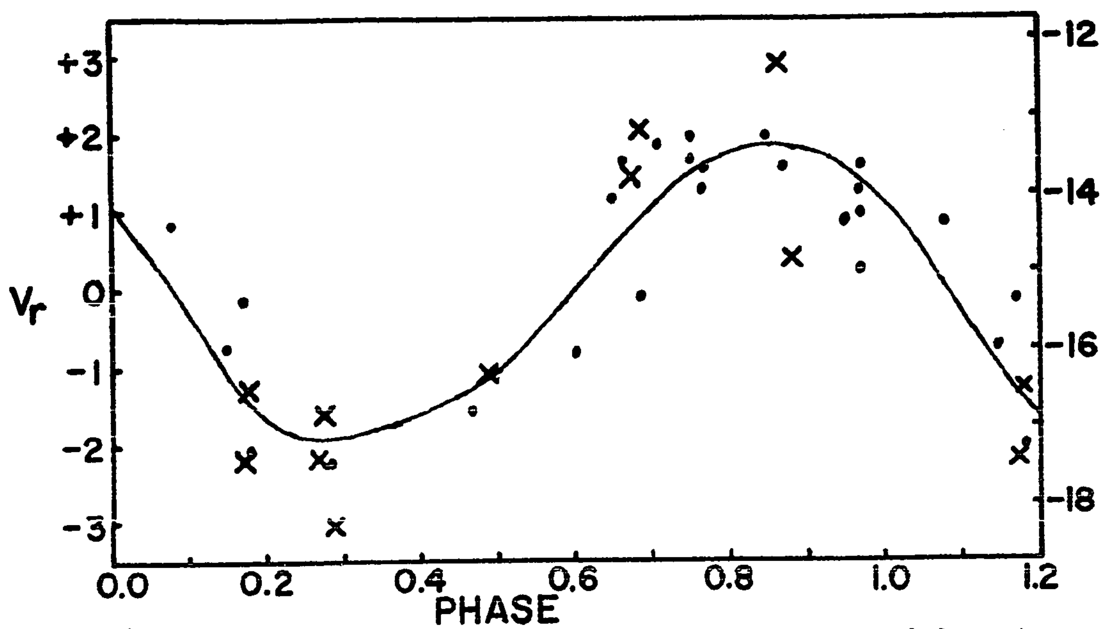

b) The radial velocity variation predicted by the 65° solution with a minimum local equivalent width of 15 m A.

FIGURE IX, 3

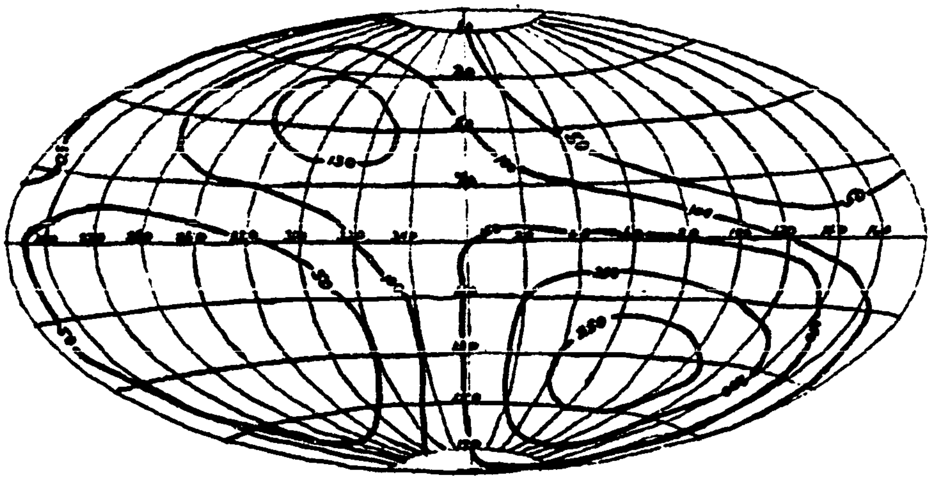

a) SOLUTION FOR $\chi = 65^\circ$ $a_0^0 = 92.7$ $a_1^1 = 46.8$ $a_2^1 = -0.9$ $a_2^2 = +2.8$

LIMB DARKENING $u = 0.48$ $a_1^0 = -48.9$ $\alpha_1^1 = 47.1$ $\alpha_2^1 = -76.0$ $\alpha_2^2 = +1.6$

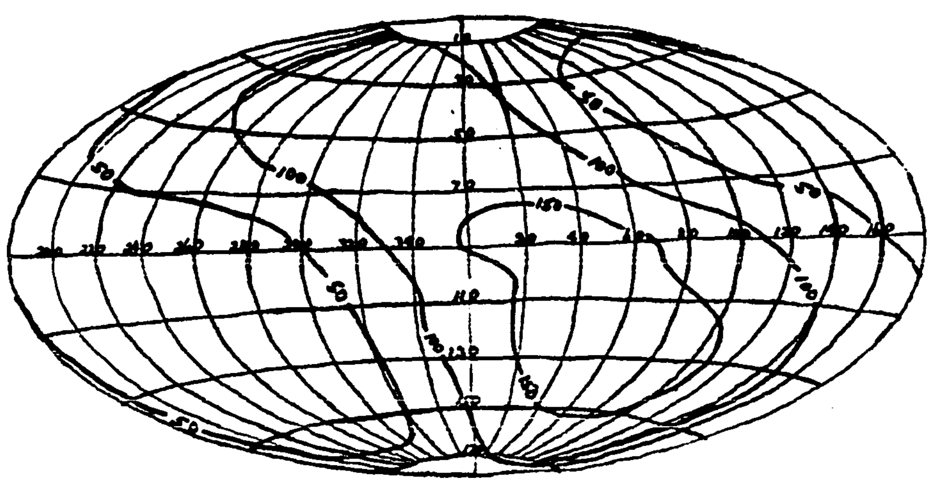

b) SOLUTION FOR $\chi = 45^\circ$ $a_0^0 = 80.7$ $a_1^1 = 60.0$ $a_2^1 = -0.7$ $a_2^2 = 4.6$

$\alpha_1^1 = 60.2$ $\alpha_2^1 = -58.1$ $\alpha_2^2 = 2.7$

LIMB DARKENING $u = 0.48$

FIGURE IX,4

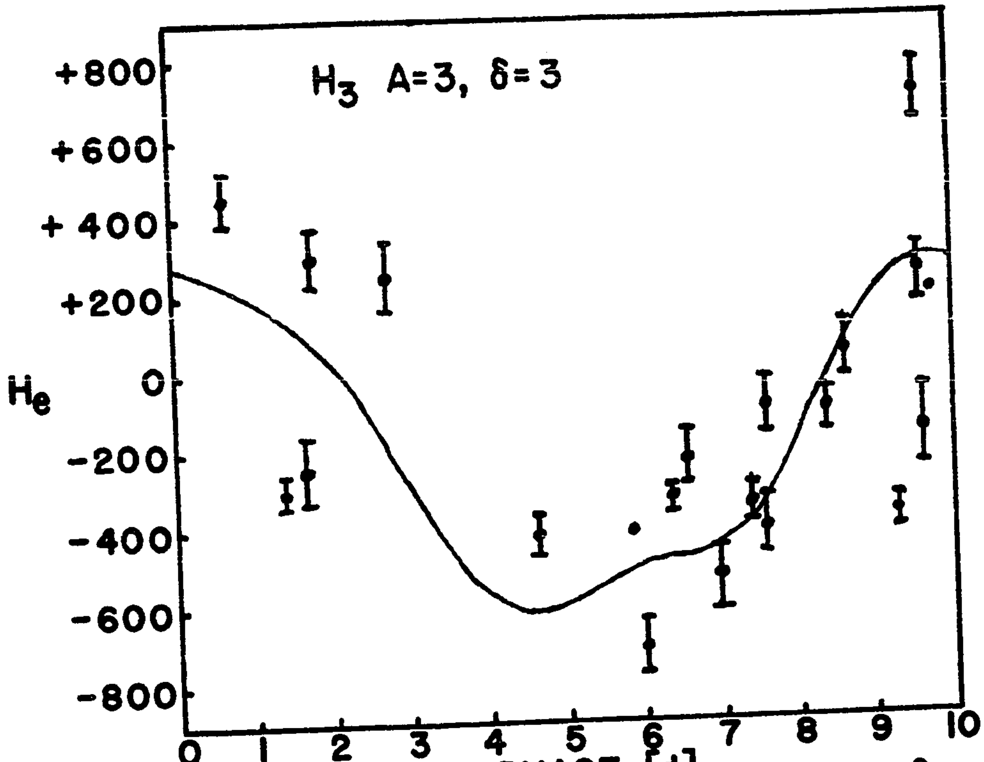

a) Magnetic variation H3 field and $i = 65^\circ$ solution, limb darkening u = 0.48. Co-latitude negative pole = 65°, longitude negative pole = 0°.

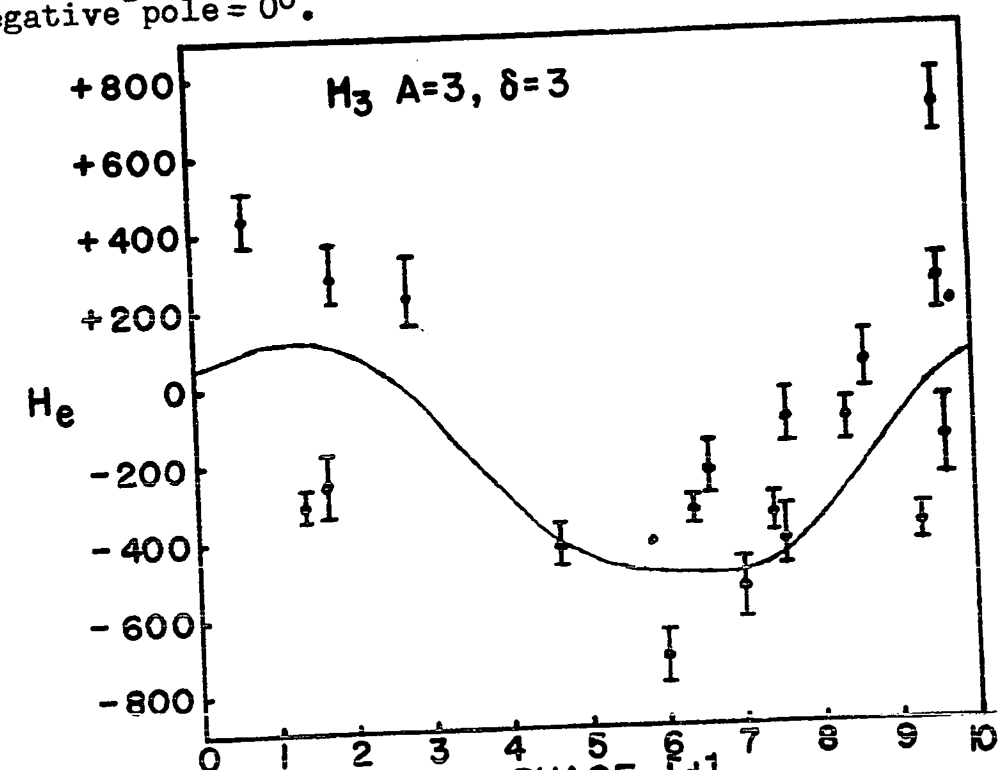

b) Magnetic variation H3 field and i = 45° solution, limb darkening u = 0.48. Co-latitude negative pole = 90°, longitude negative pole = 0°.

FIGURE IX,5

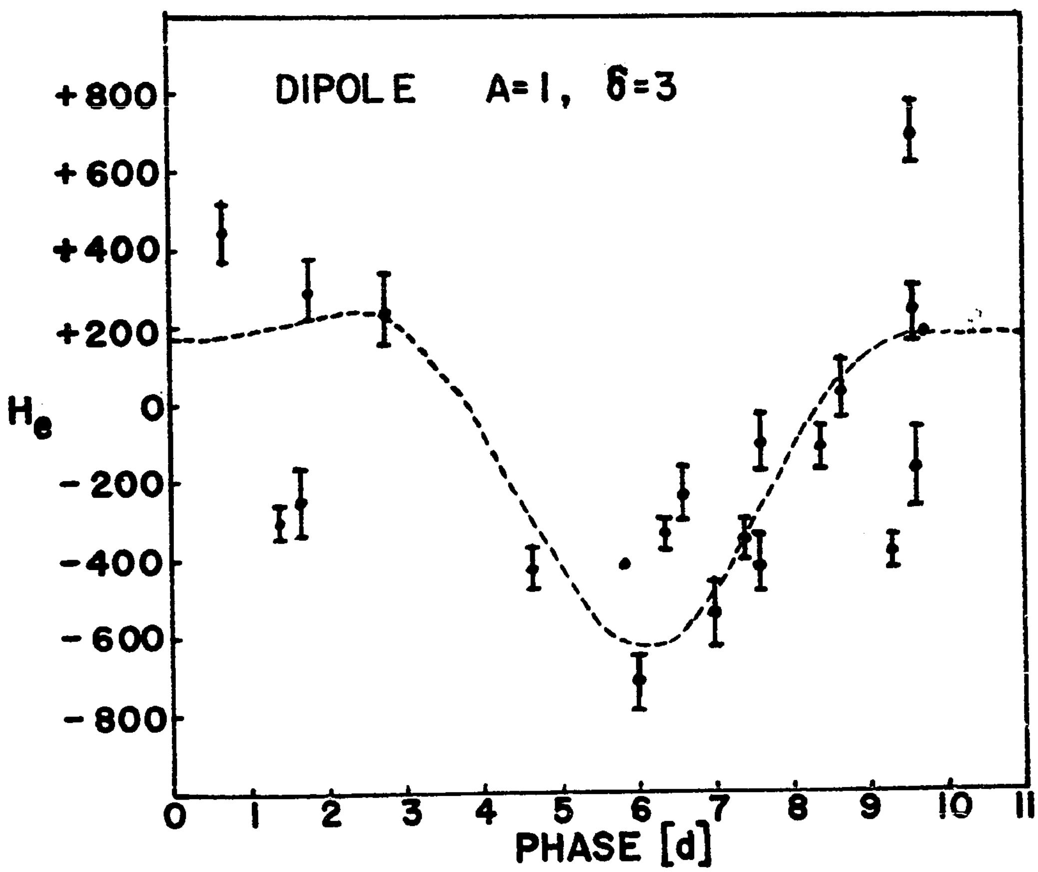

FIGURE IX, 6

Magnetic variation dipole field and $i = 65^{\circ}$ solution, limb darkening coefficient $u = 0.48$. Co-latitude of positive pole = 45° longitude positive pole = 115°.

Two questions can be asked to test this model for the star HD173650. First, suppose the model were viewed from some other orientation, then would the variations observed be far different from anything ever observed in a peculiar A star? To test this, the model was inverted so that the inclination of the axis of rotation is set at 115° instead of 65°. Then the predicted curves were computed and the ratio of maximum to minimum line strength became slightly greater than three instead of just over two. This is not an uncommon amplitude of variation and can be found for example in the star HD125248 for lines such as those of the elements CrII and SrII. The range of variation of the radial velocity curve was doubled to 8 km/sec and this again is commensurate with the radial velocity range of the star HD125248.

The other question that can be raised is that if there are elements observed in the star which have amplitudes of equivalent width variation much larger than that of the mean curve used for the analysis, then the distribution of line strength over the stellar surface will be, if one assumes that the shape of the distribution is the same for all elements, quite negative at the two areas of minimum. As it turns out, by the very method of choosing the lines used for the mean curves, the curve used for the solution is typical of the curves of greatest amplitude. That is, those elements which showed the greatest radial velocity variation were chosen for inclusion in the mean curve and the largest contribution came from lines of CrII and MnII which are among the elements of greatest line strength variation. The mean curve is about 5% smaller in amplitude than the curves of CrII and MnII and this causes no problem with the solution. Those elements which in other A_p stars show the greatest variation, the rare earths, could be a source of trouble in this respect though. The elements sbout which the greatest information is known among the rare earths in this star are EuII and GdII but as is typical of the hotter A_p stars, these lines are quite weak and only a few well identified and unblended lines of each element are available. The three lines of EuII and four lines of GdII that had been selected for use in the radial velocity measurements were used to create a mean curve for each element. While the resultant curves showed considerable scatter, it appeared that the GdII curve was actually of lesser amplitude than the mean curve used for the analysis but the EuII curve quite probably has an amplitude about 25% greater. The radial velocities observed for EuII, it should be noticed, show a correspondingly greater variation than the mean radial velocity curve. If the shape of the curve of line strength variation for EuII is the same as that of the curve of light intensity variation then the distribution of local equivalent widths must become quite negative at the two minima on the stellar surface. This situation would pose quite a problem for the oblique rotator model since it is hard to see how one could adjust the solution at $i = 65^{\circ}$ by the large amounts that would be required to make the local equivalent widths everywhere positive for EuII without seriously altering the shape of the predicted line strength observations. The minimum local equivalent width does not alter very quickly with a change in i so that adopting a somewhat smaller value for i doesn't get one out of the difficulties presented by this possibility. The alternative is that the shape of the EuII variation is somewhat different from that of the other elements, that is the curve may have, for example, a slightly flatter minimum than the other curves. This is quite possible since in many A_p stars the rare earth elements vary in anti-phase with the metals and the evidence in this star for the uniformity in the shape of the variation has been based on the metal lines since they are most common. The fact that the rare earths vary in antiphase to the metals in many stars suggests that the magnetic field, presuming it is responsible for the uneven distribution of local equivalent widths, affects these classes of elements differently. This, in fact, suggests that even though the line strengths of the various metals may be distributed in the same way over the surface of the star, it does not necessarily follow that the rare earths are also distributed in exactly the same way. An attempt should be made in the future to examine the variation of EuII to determine the shape of its equivalent width curve.

The stability of the solution with respect to a small error in Ve sin i is fairly good. The largest three components of the harmonic expansions vary by less than 10% for a 10% error in Ve sin i. It should be pointed out that an error in the scale of Babcock's radial velocities due to his use of some FeII lines causes the solution to behave in the same way as an error in Ve sin i so that any small error due to using Babcock's radial velocities as a device for indicating the shape of the radial velocity variation will not be great and will not substantially alter the appearance of the solutions.

d) The Distribution of Physical Parameters

A distribution of local equivalent widths has been computed for the star and it would now be worthwhile to determine from the curve of growth results that are available from the spectrograms of the entire visible disc of the star at various phases, what differences in the values of microturbulence and log abundance occur between the areas of minimum line strength on the star and the two areas of maximum line strength, the maximum in the north and the principal maximum in the south. A rough approximation to the microturbulent velocities at the areas of minimum line strength and at the primary and secondary maxima can be made by plotting the observed curve of growth result for log V (where V is the total micromotion) at the phases corresponding to minimum and maximum observed line strength against the log of the mean equivalent width used for the analysis of the line strength distribution at these phases and extrapolating linearly to the values of log W corresponding to the minima and maxima points on the distribution predicted by the harmonic analysis. The assumption made in scaling the micromotion in this way is that the change in the curve of growth with variation in the observed mean equivalent widths reflects the way the local curve of growth changes with the variation of local mean equivalent width. As mentioned in the curve of growth section, a more sophisticated treatment of this problem would be desirable but the present data does not make such a treatment possible. In order to determine the difference in log N between the minimum on the stellar surface and the two maximum points, it will be assumed that log N is also linearly related to log W and the treatment will be just as with the micromotion. The observed curve of growth results and the extension of these results to the surface of the star are given for FeII, FeI, CrII and SrII in Table IX,2. The assumed minimum value for the local equivalent width is 20 mA, a value which has been chosen on the basis that it is about the largest value that can be used as a minimum and still have the model give a good representation of the observed radial velocity and equivalent width curves. The reason for adopting as large a value of the local equivalent width for the minimum as possible is that the values given in the table should represent the minimum values in the variation of microturbulence and abundance over the stellar surface that one requires in order to explain the observations. Unfortunately, the computed values for the differences in the physical parameters on the stellar surface are most sensitive to uncertainties in the minimum. Representative errors corresponding to a 5 mA error in the minimum value of the local equivalent width are given for FeII in the table.

TABLE IX,2

a) Observed Curve of Growth Results

Element	logN	Vmax/Vmin microturbulent
FeII	0.25	4.3/2.6 km/sec
FeI	0.20	2.6/1.6
CrII	0.40	4.2/3.2
SrII	0.40	3.5/2.0

b) Extension to Oblique Rotator Model

Element	Nsecondary max / N minimum	Nprimary max / N minimum
FeII	4.2 ± 1	5.6 ± 1.5
FeI	3.2	4.1
CrII	10.0	15.9
SrII	10.0	15.9

Element	V microturbulent at secondary maximum	V micro at primary max	V micro at minimum
FeII	5.0 km/sec	6.7 km/sec	1.0±1 km/sec
FeI	2.9	3.8	0.1
CrII	4.6	5.8	2.1
SrII	4.1	5.9	0.4

A table comparing the observed curve of growth results for several species to the ranges in values for abundance and microturbulence that would be required over the surface of the $i = 65^0$ oblique rotator model of HD173650. The errors that correspond to a 5 mA error in the assumed (20 mA) minimum local equivalent width are given for FeII.

CHAPTER X

CONCLUSION

The star HD173650 has been investigated with respect to its light, line strength and radial velocity variations with the intention of determining whether the oblique rotator is an adequate model for this typical magnetic and spectrum variable. It has been shown first that the star is typical in that it is variable in all of the above aspects and the variability is of period $9^{d}.9748$. The light variation and line strength variations for all elements are in phase and the radial velocity curves for all species become most positive one quarter cycle following line strength maximum. It has also been shown that Babcock's magnetic observations are in anti-phase to the light variability.

The curve of growth analysis predicts that the line strength variation is primarily due, in each species, to an apparent change in microturbulent velocity and only secondarily to changes in abundance with phase. In fact for FeII, where the curve of growth result is well determined, the abundance change is very small, if present at all, and the variability is due almost entirely to microturbulence.

In the process of developing a model for the star it was first shown that no oblique rotator model can be formed with a cylindically symmetric local line strength distribution if its axis of symmetry is to be coincident with the magnetic axis of a cylindrically symmetric magnetic field distribution. The observation that in this star the curve of light intensity variation is the same shape as the line strength variation, assisted greatly in forming a more general non-symmetric oblique rotator model of the star by a method of harmonic analysis. This model of the star gives predictions of the line strength and radial velocity variations that are in good agreement with observation. The requirement of the model being consistent with an inclination of the rotational axis of 65° or greater as determined from the line profiles (V_e sin i), the period and the radius (determined from the photoelectric data) has been met.

The solution appears as an area of line strength maximum that forms a wide irregular belt around the star. By placing a dipole field on the star so that the irregular belt is coincident with the magnetic equator and the positive pole is located at the northern area of minimum line strength, negative pole in the southern minimum, a predicted magnetic variation has been obtained that fits the observations very well. The model is therefore complete and satisfactory in that it fits all the observations and that the line and dipole field strength distributions bear some resemblance to one another as one might hope if the current belief that the magnetic field is responsible for the spectroscopic anomalies is correct.

The important result of this investigation is that for HD173650, a typical A_p spectrum variable star, an oblique rotator model, that explains all the observations, can be formed in detail without complication, and in doing this, strong support has been supplied for the oblique rotator as a general model that explains the spectrum and magnetic variables. To complete the task, an effort has been made to assess from the curve of growth results the amount of variation in abundance and microturbulent velocity for which one must account in suggesting a physical process that might produce this oblique rotator model.

BIBLIOGRAPHY

Abt, H.A. 1967 The Magnetic and Related Stars, Mono Book Pub. p.173.

Abt, H.A. and Golson, J.C. 1962 Ap. J. 136, 35.

Aller, L.H. 1956 Ap. J. 123, 117.

Aller, L.H. 1963 Atmospheres of the sun and stars (Ronald).

Aller, L.H. and Ross, J. 1967 The Magnetic and Related Stars, Mono Book Pub. p.339.

Babcock, H.W. 1958 Ap. J. Suppl. 3, #30,141.

Babcock, H.W. 1960 Stellar Atmospheres ed. Greenstein p. 282 (Vol.VI Stars and Stellar Systems).

Bidelman, W. 1967 The Magnetic and Related Stars, Mono Book Pub. p.29.

Bohm-Vitense, E. 1966 Zt's f. Ap. 64, 326.

Bohm-Vitense, E. 1967 Zt's f. Ap. 67, 1.

Bohm-Vitense, E. 1967 Magnetism and the Cosmos, Ed. Hindmarsh, American Elsevier Pub. p.179.

Burbidge G. and Burbidge, M. 1955 Ap. J. Suppl.1, #11,431.

Deutsch, A.J. 1956 P.A.S.P. 68, 92.

Deutsch, A.J. 1958 I.A.U. Symposium #6 p.209.

Deutsch, A.J. 1958 Hdb. d. Phys. 51, 689.

Eggen, O. 1967 The Magnetic and Related Stars, Mono Book Pub. p.141.

Huang, S-S. and Struve, O. 1955 Ap. J. 121, 84.

Jaschek, M. and Jaschek, C. 1958 Zt's f. Ap. 45, 35.

Jaschek, M. and Garcia, Z.L. 1966 Zt's f. Ap. 64, 217.

Lust, R. and Schluter, A. 1954 Zt's f. Ap. 34, 263.

Moore, C.E. 1959 National Bureau of Standards, Technical Note #36.

Munch, G. 1958 Ap. J. 127, 642.

Preston, G. 1967 The Magnetic and Related Stars, Mono Book Pub. p.3.

Preston, G. 1968 Ap. J. 151, 583.

Preston, G. 1969 In Press

Sâto, Y. 1950 Bull. Earthq. Res. Inst. 28, 175.

Slettebak, A. 1954 Ap. J. 119, 146.

Steinitz, R. 1964 B.A.N. 17, 504.

Tai, W.S. 1939 M.N.R.A.S. 100, 94.

Wehlau, W. 1962 PASP 74, 137.

Wrubel, M.H. 1949 Ap. J. 109, 66.

log g f BIBLIOGRAPHY

Corliss, C. and Bozman, W. 1962 National Bureau of Standards Monograph #53.

Warner, B. 1967 Memoirs R.A.S. 70 pt.5.

Corliss, C. and Warner, B. 1963 Ap. J. Suppl. #8, 395.

Warner, B. 1966 M.N.R.A.S. 133, #4, 398.

Boyarchuk and Boyarchuk 1960 Pub. Crim. Astro.Obs. 22, 234.

Warner, B. 1968 M.N.R.A.S. 138, #2, 229.

King, R. B. 1941 Ap J. 94, 27.

Goldberg, Muller and Aller 1960 Ap. J. Suppl. 5, 1

Baschek, Kegel and Traving 1963 Zt's f. Ap. 56, 282

Penkin, N.P. 1964 J. Quant. Spect. Rad. Trans 4, 41.